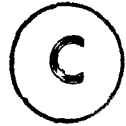


CHARACTERISTICS OF SEISMIC FLOOR MOTIONS

by



JOHN C. WILSON, B.Eng.

A Thesis

Submitted to the School of Graduate Studies

in Partial Fulfilment of the Requirements

for the Degree

Master of Engineering

McMaster University

June 1980

CHARACTERISTICS OF SEISMIC FLOOR MOTIONS

MASTER OF ENGINEERING (1980)
(Civil Engineering)

McMASTER UNIVERSITY
Hamilton, Ontario

TITLE: Characteristics of Seismic Floor Motions

AUTHOR: John C. Wilson, B.Eng. (McMaster University)

SUPERVISORS: Dr. A.C. Heidebrecht
Dr. W.K. Tso

NUMBER OF PAGES: xi, 171

ABSTRACT

The overall objective of this study is to obtain characteristics of seismic floor motions in a nuclear reactor structure in order to examine current procedures used in seismic qualification of nuclear power plant equipment.

The study incorporates seismic data from real earthquake events and uses these records as inputs to a mathematical model of a CANDU nuclear reactor building. Seismic floor responses at typical equipment locations are calculated by standard techniques of structural dynamic analysis.

Six mathematical techniques are applied to develop characterizations of each seismic floor response record. From this data a set of parameters are evolved to qualitatively and quantitatively describe the characteristics of the ensemble of floor motions.

Results of a theoretical study on sine beat, limited-duration sine, and decaying sinusoidal motions are compared to the characteristics of the seismic floor motions to evaluate the realism afforded by current single frequency seismic qualification test procedures.

It is concluded that single frequency test motions have a valid application in seismic qualification test programs and can realistically simulate many seismic floor motion characteristics provided that the specific type of test motion and the test procedures are well defined.

Recommendations are presented for the selection of single frequency test motions and for developing the test procedures.

ACKNOWLEDGEMENTS

I would like to express my sincere gratitude to my supervisors, Dr. A.C. Heidebrecht and Dr. W.K. Tso, for their advice and understanding during the preparation of this thesis and for their continual encouragement for me to freely explore many areas of research. I would also like to jointly thank my supervisors and McMaster University for supporting me in the position of Research Engineer over the past three years.

Special thanks must go to Betty Petro and Nancy Sine for patiently enduring the numerous typing drafts and in the end, for producing a very neat and presentable thesis. A large amount of credit is also due to Reg Woodruff and Ian Matheson for their capable work in producing the figures.

The financial support of this research by the Atomic Energy Control Board of Canada is gratefully acknowledged.

DEDICATION

I would like to dedicate this thesis to my parents in appreciation of the great interest and encouragement they have shown at every stage of my education.

TABLE OF CONTENTS

		PAGE
CHAPTER 1	INTRODUCTION	1
	1.1 Nuclear Power Plants in a Seismic Environment	1
	1.2 Seismic Qualification of Equipment	2
	1.3 Objectives and Scope of the Research Program	4
CHAPTER 2	SELECTION OF EARTHQUAKE GROUND MOTIONS AND STRUCTURAL MODELS	6
	2.1 Introduction	6
	2.2 Earthquake Records	7
	2.3 Dynamic Model of CANDU	13
	2.4 Single-Degree-of-Freedom Models	23
	2.5 Summary	26
CHAPTER 3	PARAMETERS FOR SEISMIC MOTION CHARACTERIZATION	28
	3.1 Introduction	28
	3.2 Maximum Acceleration	29
	3.3 Response Spectrum	31
	3.4 Cumulative Damage Process	33
	3.5 Root-Mean-Square Acceleration	43
	3.6 Cumulative RMS Function	46
	3.7 Duration of Strong Seismic Motion	48
	3.8 Summary	52

TABLE OF CONTENTS (cont'd)

	PAGE	
CHAPTER 4	CHARACTERIZATION OF HARMONIC MOTIONS	54
	4.1 Introduction	54
	4.2 Constant Amplitude Sinusoidal Motion	54
	4.3 Sine-Beat Motion	66
	4.4 Decaying Sinusoidal Motion	94
	4.5 Summary	111
CHAPTER 5	RESULTS AND DISCUSSIONS	113
	5.1 Introduction	113
	5.2 Floor Motion Time-Histories	113
	5.3 Response Spectra	119
	5.4 Comments on Modelling Time and Frequency Domain Responses	126
	5.5 Maximum Floor Accelerations	127
	5.6 Duration of Strong Motion	130
	5.7 RMS Accelerations	136
	5.8 Cumulative Damage Process	139
	5.9 Summary	144
CHAPTER 6	SEISMIC QUALIFICATION TESTING	145
	6.1 Introduction	145
	6.2 Recommendations for Single Frequency Testing	147
	6.3 Equivalency in Single Frequency Tests	158
CHAPTER 7	SUMMARY AND CONCLUSIONS	164
REFERENCES		169

LIST OF TABLES

TABLE		PAGE
2.1	Earthquake Records	14
2.2	Physical Properties of CANDU Model	19
2.3	Structural Elements in the CANDU Model	20
2.4	Summary of Dynamic Analysis	21
2.5	SDOF Models of CANDU Structures	25
4.1	Maximum Values of Sine Beats	71
4.2	Durations of Strong Motion for Sine Beats	90
4.3	Characteristics of Harmonic Motions	112
5.1	Maximum FRS Values for CANDU Mass 4 and 5.83 Hz SDOF Model	122
5.2	Maximum FRS Values for CANDU Mass 12 and 10 Hz SDOF Model	125
5.3	Structural Amplifications	128
5.4	Durations of Strong Motion in Seconds	131
5.5	Site Dependent Durations of Strong Motion	132
5.6	Ratios of A_{rms}/A_m	137
5.7	Site Dependent Ratios A_{rms}/A_m	138
5.8	Cumulative Damage Parameter N_{eq} with $\beta = 2$	141
5.9	Site Dependent \bar{N}_{eq} Normalized to 1 g with $\beta = 2$	142
6.1	Frequency Characteristics	146
6.2	Examples of Equivalent Motions	163

LIST OF FIGURES

FIGURE		PAGE
2.1	Mean Acceleration Spectra for Different Site Conditions	8
2.2	Comparison of Ground Surface Accelerations	11
2.3	Dynamic Model of CANDU Reactor Building	15
2.4	Location of Dynamic Model Masses in CANDU Reactor Building	16
2.5	Typical Structural Plan of CANDU Reactor Building	17
2.6a	Internal Structure Mode at 5.83 Hz	22
2.6b	Vault Mode at 10 Hz	22
2.7	Single-Degree-of-Freedom System Subjected to Ground Acceleration $\ddot{z}(t)$	24
3.1	Development of a Floor Response Spectrum	32
3.2	Logarithmic Relationship for Cumulative Damage	36
3.3	Influence of the Exponent β	38
3.4	Two Versions of a Hypothetical Time History	40
3.5	Cumulative RMS Function	47
3.6	Determining Duration of Strong Motion for Eureka N79E Ground Motion	50
4.1	SDOF Response to a Constant Amplitude Sinusoidal Motion	58
4.2	Quasi-Resonant Response for Limited Duration Sine Motions	60

LIST OF FIGURES (cont'd)

FIGURE		PAGE
4.3	CRF and D(CRF) for a Sine Motion	63
4.4	Sine Beat Pulse	67
4.5	SDOF Response to a Sine Beat	76
4.6	Quasi-Resonant Amplifications for Sine Beat Motions	81
4.7	Cycles of Cumulative Damage for a Sine Beat	83
4.8	CRF and D(CRF) for a Sine Beat	85
4.9	Determining the Phase of Strong Beat Motion	86
4.10	Cycles of Strong Motion for a Sine Beat	91
4.11	Decaying Sinusoid	95
4.12	SDOF Response to a Decaying Sinusoid	99
4.13	Quasi-Resonant Amplifications for Decaying Sinusoidal Motions	102
4.14	Comparisons of Cumulative Damage Process for Harmonic Motions	104
4.15	RMS Functions of a Decaying Sinusoid	106
4.16	Duration of Strong Motion for a Decaying Sinusoid	110
5.1a	CANDU Mass 4 Floor Response to Caltech Seismological Lab Record, N-S Component	115
5.1b	CANDU Mass 4 Floor Response to Orion Record, E-W Component	116
5.2	Lankershim N-S Ground Motion Scaled to 1g	117
5.3	Comparison of CANDU and SDOF Responses for the Internal Structure	118

LIST OF FIGURES (cont'd)

FIGURE		PAGE
5.4	Comparison of CANDU and SDOF Model Responses for the Reactor Vault	120
5.5	Comparison of CANDU and SDOF Model Floor Response Spectra	123
5.6	Interpreting Calculations of Strong Motion Duration	134
6.1	Enveloping the Floor Response Spectrum	154
6.2	Cumulative RMS Functions of Single Frequency Motions	157

CHAPTER 1

INTRODUCTION

1.1 Nuclear Power Plants in a Seismic Environment

Nuclear reactor technology has presented engineers and scientists with a great stimulus to rapidly develop solutions to a multitude of structural and mechanical engineering problems. These problems have arisen from the necessity to expose new materials, new equipment systems and innovative structural designs to severe operational and environmental conditions and postulated loadings. The impetus to face these problems has stemmed from a desire to achieve a safe, reliable and economic exploitation of nuclear power.

One of the more complex of these problems is to provide a realistic evaluation and protective design for the effects of earthquake ground shaking at a nuclear power plant (NPP) site. For most structures which man creates the economic evaluation of earthquake resistant design is based on the reasoning that in the long term it is less costly to repair or rebuild some damaged structures than to make all structures highly resistant. However, concerns for public and environmental safety make this an unacceptable philosophy for the design and operation of nuclear power generating stations. During and after an earthquake a NPP must be functional at least to the extent that radioactive material is prevented from escaping from the plant. This can be accomplished only if the operational capabilities of certain safety-related systems are

not impaired by the effects of the earthquake shaking.

The stringent requirements set by regulatory agencies for functional integrity and operational capability present new problems to engineers who must assess the postulated seismic motions within the reactor structures, and to equipment designers and manufacturers who must provide safety-related equipment assemblies which will function in a seismic environment. The overall problem then is one of providing an assurance that the reactor safety systems and equipment will have a proven seismic withstand capability. This is accomplished by demonstrating through testing and/or analysis that each equipment component will perform its intended function under the loads imposed during the anticipated levels of earthquake shaking. This procedure is referred to as seismic qualification.

1.2 Seismic Qualification of Equipment

The seismic response of electrical and mechanical equipment is usually a secondary response to the overall NPP response. Consequently, the reactor structure is often described as the primary system and equipment as secondary systems. During an earthquake the primary system responds to the broad-band random ground motions and, by using an appropriate mathematical model, the time-history response at a given floor location within the structure can be evaluated. This motion can then be subjected to a further analysis to produce a floor response spectrum which is generally an amplified and narrow-banded version of the ground motion spectrum, emphasizing the structure's natural

frequencies. Larger amplifications are generally observed at floor elevations higher in the reactor structure with the result that equipment mounted at these levels may experience accelerations several times that of the earthquake ground motion. Compounding the problem of large amplifications, the floor motion may tend to a quasi-harmonic state at one of the structural natural frequencies. Thus, the seismic environment at higher floor levels will usually impose more severe loading conditions on floor-mounted equipment than on equipment installed at ground level.

The development of a valid seismic qualification program whether by test, analysis, or a combination of both depends upon a realistic evaluation of the seismic environment which the equipment would be expected to experience in a NPP installation. For analysis purposes the environment is described mathematically or numerically. In test applications, the simulated seismic environment is defined by displacement and acceleration levels of a shake table motion which requires a practical consideration of how appropriate excitations can be defined and applied to the equipment.

At present, a wide variety of single frequency and multi-frequency test motions are in use. Single frequency motions involve various forms of amplitude-modulated sinusoids while multi-frequency waveforms consist of either a real or artificially created time-history. Both of these methods may be used to test equipment to either a proof level (exposure to a specified level of shaking) or to a fragility level (taking the test specimen to failure,

to evaluate the ultimate seismic capability (26). In most cases, the expense involved in failing a specimen in a fragility test is usually unwarranted as there may not always be a significant gain of information above that of the proof-level test. Consequently, most seismic qualification relies upon the proof test method.

The present measure of the acceptability of a particular form of test motion is primarily the extent to which it envelopes a specified response spectrum. This single measure alone provides only a limited amount of information about the earthquake environment. When the spectrum concept was used primarily to evaluate peak elastic structural responses for the purpose of strength evaluation, then this limitation did not seriously detract from the usefulness of the results. However, when the more complex considerations of equipment seismic qualification are concerned, there is a necessity that developed test motions be described by parameters which more closely characterize real seismic motions(14). Only in this way will it be possible to develop test procedures which provide realistic simulations of the actual seismic conditions at equipment locations.

1.3 Objectives and Scope of the Research Program

The objectives of this research investigation are to determine valid parameters for characterizing seismic floor motions and to apply these parameters to seismic qualification test procedures.

The first stage of the study involves the assembly of basic earthquake and structural information. A modest number of real

earthquake records are selected to be representative of the seismic ground motions which could occur during a 6.5 Richter magnitude earthquake on a wide range of soil conditions. Incorporating one of the mathematical models actually used in the seismic design of CANDU nuclear power plants, an ensemble of floor motion time-histories are obtained for two floor levels in the reactor building by subjecting the model to each earthquake record.

The second major phase of investigation considers several possible techniques for characterizing a time-series record, based upon a consideration of those aspects of seismic motion which could have an influence on equipment response and functionality. Theoretical analyses are performed to characterize some simple types of harmonic motions to gain a clear understanding of the characterization techniques and also to develop a basis for referencing the more complex real seismic motions. Subsequently, the characterization techniques are applied to the seismic ground and floor motions to develop a set of parameters describing real seismic input motions and structural floor responses.

The final stage of study combines the theoretical aspects with the characteristics of real seismic motions to make recommendations concerning single frequency motions appropriate for use in seismic qualification and to critically examine and make recommendations on single frequency test procedures.

CHAPTER 2
SELECTION OF EARTHQUAKE GROUND MOTIONS
AND STRUCTURAL MODELS

2.1 Introduction

Seismic qualification testing procedures for nuclear power plant (NPP) equipment require a description of the seismically induced floor motions at equipment mounting locations. Often, these descriptions are the outcome of seismic response studies using complex analytical models of the NPP. Their validity and applicability to real reactor systems depends upon three factors, (1) consideration of a sufficient number of real or hypothesized earthquake events to serve as a statistically meaningful set of inputs, (2) selection of appropriate mathematical models to represent the NPP structure and equipment systems, (3) selection of appropriate techniques of dynamic analysis. The first two areas are the focus of attention in this chapter. The criteria used to select a set of representative earthquake ground motion records is presented, then the dynamic model of the CANDU* system used in the analytical stages is discussed. The third area, techniques of dynamic analysis, is not treated in this investigation but an outline of the method used is given in a later section.

*CANadian Deuterium Uranium

2.2 Earthquake Records

At the outset of this investigation a list of criteria was established for selecting an ensemble of strong ground-motion records which would be used as inputs to the CANDU model. The overall objective was to select a modest number of real earthquake records which would be broadly representative of seismic ground motions associated with possible earthquakes affecting a nuclear power plant site. The selection process considered several factors which could influence the seismic ground motion at a given site. However, at an early stage it became apparent that to rigorously impose each criterion would likely lead to few, if any, records which would be considered acceptable in the end. This was due to the fact that the criteria were attempting to describe an average earthquake. A real earthquake however, is a single event having its own unique attributes and consequently few, if any, real records could be expected to simultaneously satisfy all the criteria. In the final selection a certain degree of engineering judgement was used to overrule some of the less rigorous criteria to include records which, in most respects were suitable.

2.2.1 Local Site Conditions

Statistical analysis of the spectral shapes of a moderate number of earthquake ground motions have shown that "clear differences exist in spectral shapes for different soil and geological conditions", and that spectral shapes are site-dependent (28). Figure 2.1 (from ref. 28) compares the mean spectral shapes of ground motions for different site

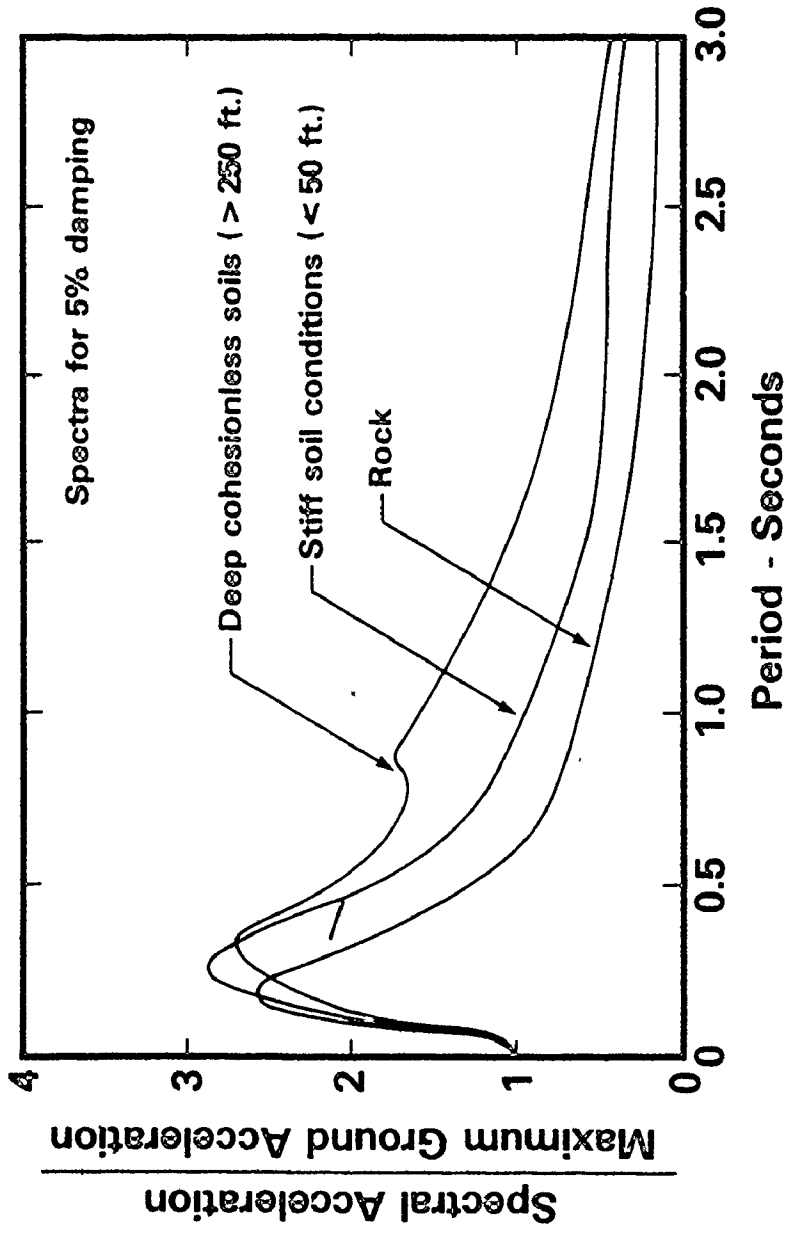


FIG. 2.1 MEAN ACCELERATION SPECTRA FOR DIFFERENT SITE CONDITIONS

conditions. For periods greater than about 0.4 sec. (frequencies less than 2.5 Hz) there are significant differences in the spectral shapes depending upon the local soil conditions. In this region of the spectrum, soft soils and deep cohesionless deposits show larger amplifications than stiff soils or rock sites. At low periods (\leq 0.4 sec) rock, stiff soils and deep cohesionless soils all result in approximately the same spectral response. Recognition that spectra are site-dependent and that there is a need for consideration of these effects in selecting design criteria is also made in the ATC-3 provisions (1).

The classification categories used to describe local site conditions were selected as follows:

- (i) Rock Sites - sites having a shear-wave velocity greater than about 2500 feet per second and where rock was considered to be shale-like or of sounder quality.
- (ii) Stiff Soil Sites - rock as defined above overlain by less than 150 feet of stiff clay, sand or gravel.
- (iii) Deep Cohesionless Soil Sites - rock overlain by at least 250 feet of cohesionless soil.

The categorization of site records into the above three groups is based on geological and geotechnical studies which are available in the literature (27,28). In this study it was decided that two sets of earthquake records would be selected in each of the above three site

categories. This would provide twelve ground-motion records (two horizontal components for each earthquake) on a wide range of soil deposits. Envisioning the variations to be considered later in the structural systems, twelve records would allow for a sizeable number of floor motion time-histories.

2.2.2 Magnitude, Maximum Acceleration and Duration

It was desirable that events of at least a 6M (Richter magnitude) and preferably in the range 6.5-7M be included. Trifunac and Brady (30) indicate the average maxima of each of acceleration, velocity and displacement seem to be achieved in the 6.5-7M range. Comparisons of the maximum ground surface accelerations for such an event are shown in Fig. 2.2 This indicates that for close epicentral distances (≤ 10 km), rock and stiff soil sites might be expected to experience surface accelerations of about 0.5 g., and deep cohesionless sites somewhat less at around 0.3 to 0.4 g. It was decided that at least one of the horizontal components in each record should have a maximum acceleration greater than 0.1 g and that all records would be of 30 second duration. The final selection produced maximum accelerations from 0.089 g to 0.348 g. Additionally, each acceleration time-history was visually examined to screen out any shock type (impulse loading) earthquakes or other anomolous effects.

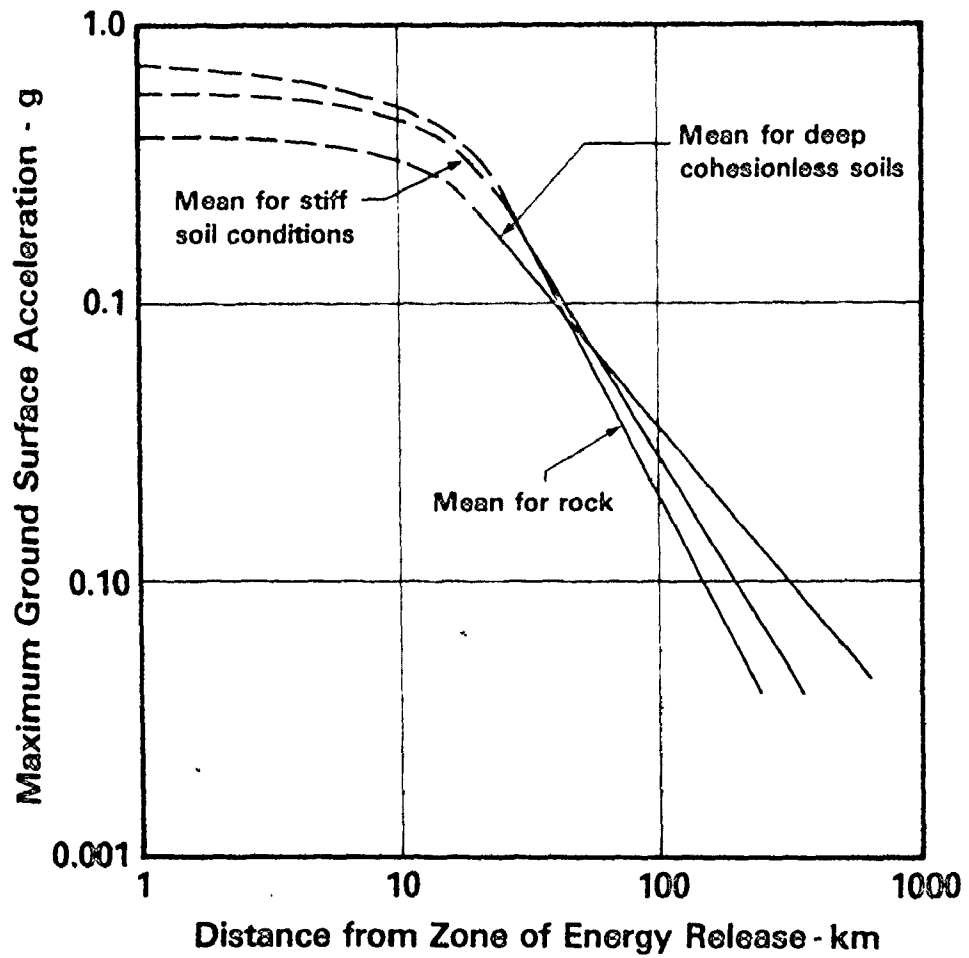


FIG. 2.2 COMPARISON OF GROUND SURFACE ACCELERATIONS

2.2.3 Source Distance

The characteristics of the earthquake ground shaking at a site may be substantially influenced by the path seismic waves follow through different geological regions, soil structures, and by the length of these pathways. This is in addition to effects of local site geology. The result is that ground motions at two nearby sites may often show striking dissimilarities even though the shaking originated from a single fault rupture. Differences in frequency content and amplitudes are two possible dissimilarities with high frequency components attenuating along the length of the transmission path causing more distant sites to receive predominately long period waves. Peak accelerations are also attenuated at increasing source distances, as shown in the comparisons of Fig. 2.2.

Source distance, as a factor in the selection criteria was considered in a fairly broad sense by trying to obtain a range of "near" and "far" events in the ensemble. This was not entirely successful however, owing to the fact that in many cases, suitable near station records just did not exist. If both a near and a more distant record could be obtained for a given soil condition this was done but it was not imposed as a mandatory condition. The 12 selected records had source distance variations from approximately 8 km to 37 km.

Strong-motion earthquake data from the western United States was reviewed using the above criteria to select the 12 records of horizontal ground motions, and baseline corrected accelerograms were obtained from the strong-motion data published by the California Institute of

Technology (17). Listings of the records and particular details on each are presented in Table 2.1. Soil data and approximate source distances were obtained from references 27 and 28. All other data was available through Caltech sources (16). In all computational phases each record was scaled to a 1 g maximum acceleration.

2.3 Dynamic Model of CANDU

The mathematical model used in this study, as provided by AECL* was a lumped mass representation of a 600 MeW CANDU nuclear power plant. Illustrated in Fig. 2.3, the model consists of four major groups of structural components; foundation base slab, containment structure, internal structure and reactor vault. To gain an appreciation for the manner in which the model is intended to represent the real NPP structure, a cut-away view of a typical 600 MeW CANDU unit in Fig. 2.4 is superimposed with the model mass numbers.

This study examines only planar response in the A-C direction (parallel to the calandria pressure tubes, see Fig. 2.4 and Fig. 2.5) but more complex analyses are possible with other versions of the model (e.g., coupled lateral-torsional responses (19)). Soil-structure interaction may be taken into account by adding flexible soil-springs to the base slab. In this study, a rigid foundation base was used ($K_y = K_\theta = K_\phi = \infty$) and consequently the containment wall is an independent system from the internal structure and vault areas. They are shown here together for the sake of model completeness and must be considered as a single system if soil flexibility is permitted.

TABLE 2.1 EARTHQUAKE RECORDS

RECORD	COMPONENT	DATE	MAGNITUDE	SOIL TYPE	MAX. ACCEL (g)	APPROX. SOURCE DIST. (km)	EARTHQUAKE EVENT	CALTECH REFERENCE
3838 Lankershim Blvd. L.A. (Bsmt)	N-S	2.9.71	6.4	Rock	.167	24	San Fernando	L166
3838 Lankershim Blvd. L.A. (Bsmt)	E-W	2.9.71	6.4	Rock	.150	24	San Fernando	L166
Caltech Seismological Laboratory	E-W	2.9.71	6.4	Rock	.192	37	San Fernando	G106
Caltech Seismological Laboratory	N-S	2.9.71	6.4	Rock	.089	37	San Fernando	G106
El Centro	N-S	5.18.40	6.7	Stiff Soil	.348	8	Imperial Valley	A001
El Centro	E-W	5.18.40	6.7	Stiff Soil	.214	8	Imperial Valley	A001
Hollywood Storage P.E. Lot. L.A.	E-W	2.9.71	6.4	Stiff Soil	.211	35	San Fernando	D058
Hollywood Storage P.E. Lot. L.A.	N-S	2.9.71	6.4	Stiff Soil	.170	35	San Fernando	D058
Eureka Federal Bldg. (Bsmt)	N79E	12.21.54	6.5	Deep Cohesionless	.258	25	Eureka	A008
Eureka Federal Bldg. (Bsmt)	N11W	12.21.54	6.5	Deep Cohesionless	.168	25	Eureka	A008
8244 Orion Blvd. L.A.	N-S	2.9.71	6.4	Deep Cohesionless	.255	20	San Fernando	G048
8244 Orion Blvd. L.A.	E-W	2.9.71	6.4	Deep Cohesionless	.134	20	San Fernando	C048

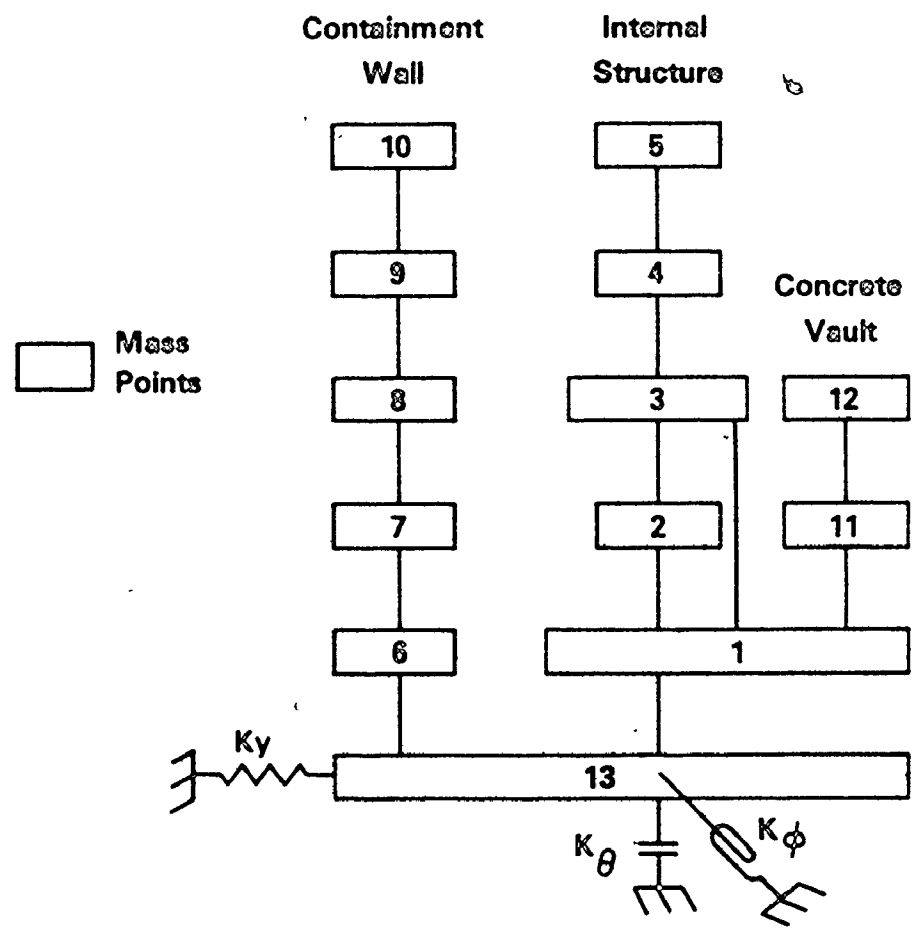


FIG. 2.3 DYNAMIC MODEL OF CANDU REACTOR BUILDING

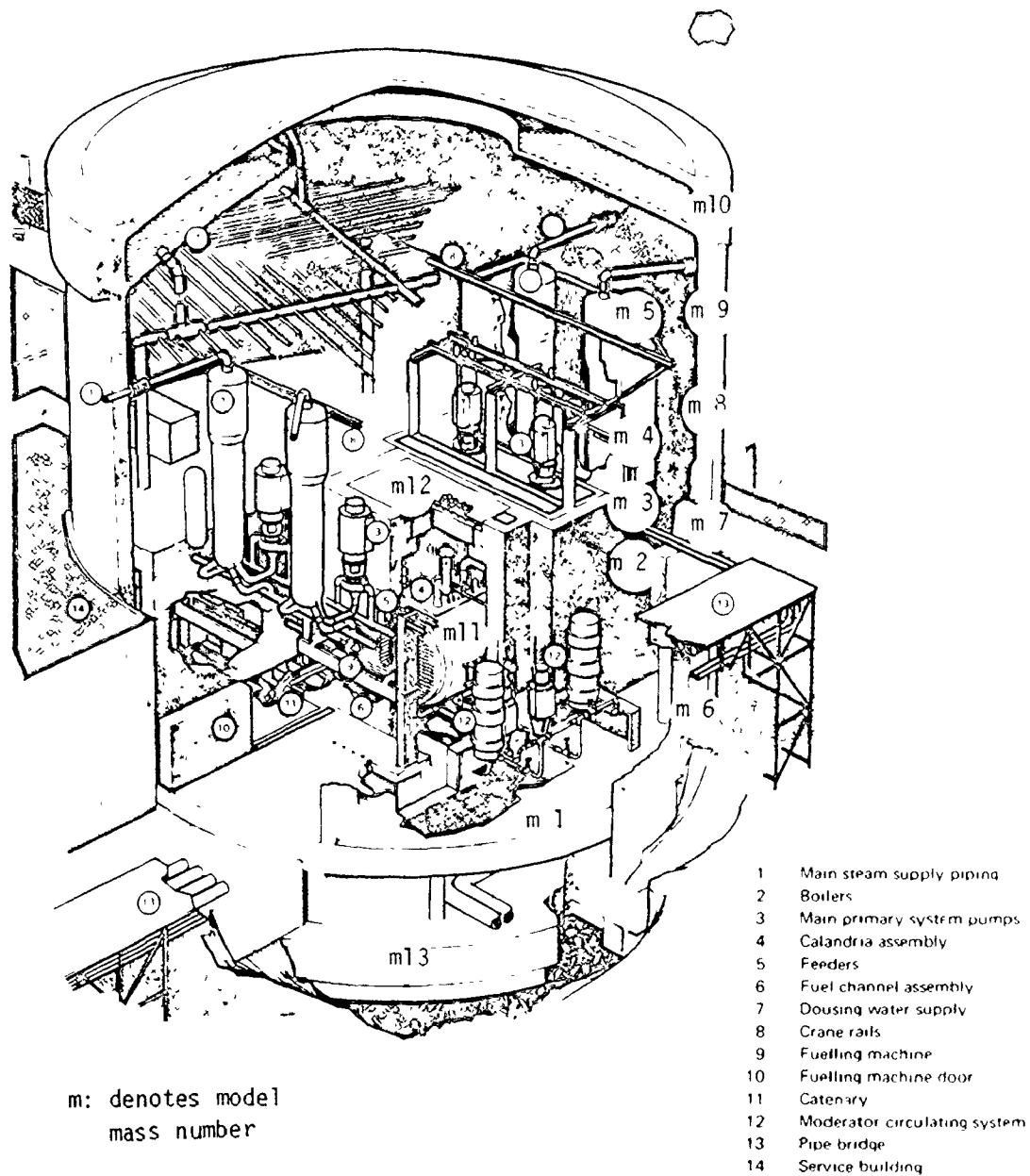


FIG. 2.4 LOCATION OF DYNAMIC MODEL MASSES IN CANDU REACTOR BUILDING

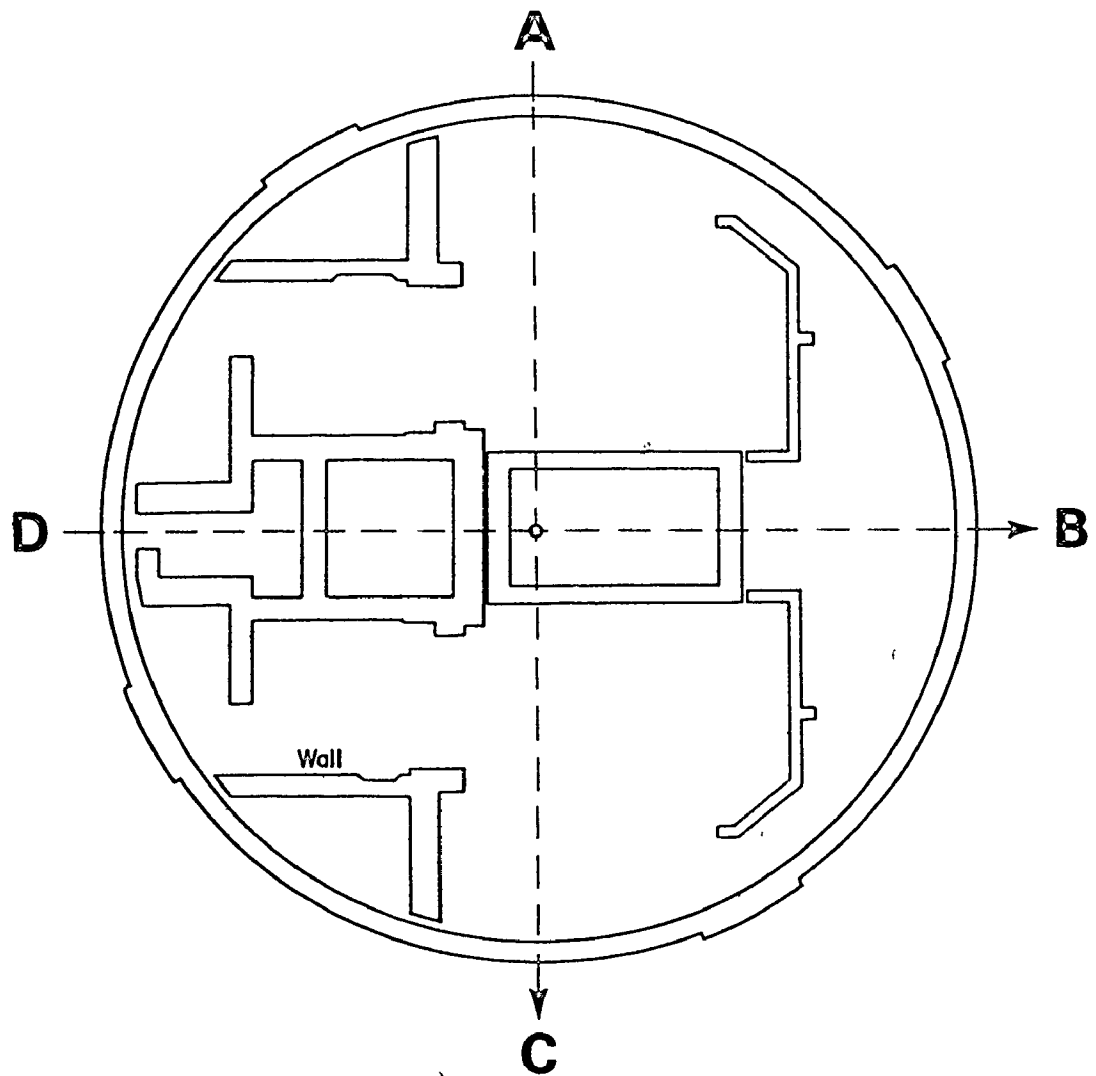


FIG. 2.5 TYPICAL STRUCTURAL PLAN OF CANDU REACTOR BUILDING

Owing to the extreme rigidity and thickness of floors in a NPP, both floor mass and floor stiffness must be incorporated into a realistic NPP model. At a given floor level, mass is lumped at a single node point and short, rigid elements above and below the node account for the high floor rigidity. Physical properties of the model are given in Table 2.2 and geometrical properties of the structural elements connecting the masses are given in Table 2.3.

A dynamic analysis of the complete model shown in Fig. 2.3, for the case of a rigid foundation was performed using the computer program SAP IV, (3) and a brief summary is given in Table 2.4. The modal frequency at 4.94 Hz is the fundamental mode of the containment structure, however owing to the rigid base assumption, containment modes do not influence the internal structure and vault motions. It is presented here for general information only. Mode 2 (5.83 Hz) and mode 3 (10.00 Hz) were found to be the first dominant modes of the internal structure and reactor vault, respectively, and their mode shapes are shown in Figs. 2.6a and 2.6b.

The earthquake records selected in section 2.2 were each used as inputs at the base slab level to obtain an ensemble of seismic floor acceleration responses at mass 4 and mass 12. Mass 4 of the internal structure represents the level of the boiler room floor, and mass 12 represents the reactivity deck level within the reactor vault area (ref. Fig. 2.4). Some equipment components and installations on both levels 4 and 12 are required to be seismically qualified and hence, descriptions of the seismic environments at these locations must be available.

TABLE 2.2 PHYSICAL PROPERTIES OF CANDU MODEL

STRUCTURE	MASS	LOCATION	ELEVATION (ft-inch)	WEIGHT (kips)	ROCKING INERTIA ₂ (kip-ft ²)
Vault	12	reactivity deck	99'-9"	2170	--
	11	calandria assembly	64'-9"	4126	--
	5	top of boiler box	128'	4765	1.02x10 ⁶
Internal	4	boiler room floor	102'-3"	7949	4.65x10 ⁶
Structure	3	intermediate floor	86'	4457	10.69x10 ⁶
	2	intermediate floor	71'	7875	2.64x10 ⁶
	1	grade floor	45'0"	21968	28.66x10 ⁶
Containment Wall	10	top of containment & dousing water supply	165'	23080	27x10 ⁶
	9	containment wall	135'	6728	--
	8	containment wall	105'	6278	--
	7	containment wall	75'	6728	--
	6	containment wall	45'	5606	--
	13	base slab	25'	29822	66x10 ⁶

TABLE 2.3 STRUCTURAL ELEMENTS IN THE CANDU MODEL

LOCATION	STRUCTURAL ELEMENT	AREA (ft ²)	INERTIA (ABOUT ₄ BD AXIS) (ft ⁴)
Vault	13	211	37,990
	12	211	31,510
	6	564	34,253
Internal Structure	5	1293	1,220,760
	4	221	3,070
	3	952	1,749,520
	2	1447	193,300
	1	2485	482,050
	11	1534	3,733,600
	10	1534	3,733,600
Containment Wall	9	1534	3,733,600
	8	1534	3,733,600
	7	1534	3,733,600

Elastic properties: $E = 5.76 \times 10^5$ ksf

$\nu = 0.15$

TABLE 2.4 SUMMARY OF DYNAMIC ANALYSIS

MODE	MODAL FREQUENCY (Hz)	DOMINANT STRUCTURAL FIRST MODE RESPONSES†
1	4.94	CW
2	5.83	IS
3	10.00	RV
4	16.29	*
5	18.24	*
6	23.88	*
7	27.89	*
8	28.69	*
9	29.46	*

† CW = containment wall

IS = internal structure

RV = reactor vault

* = higher modes

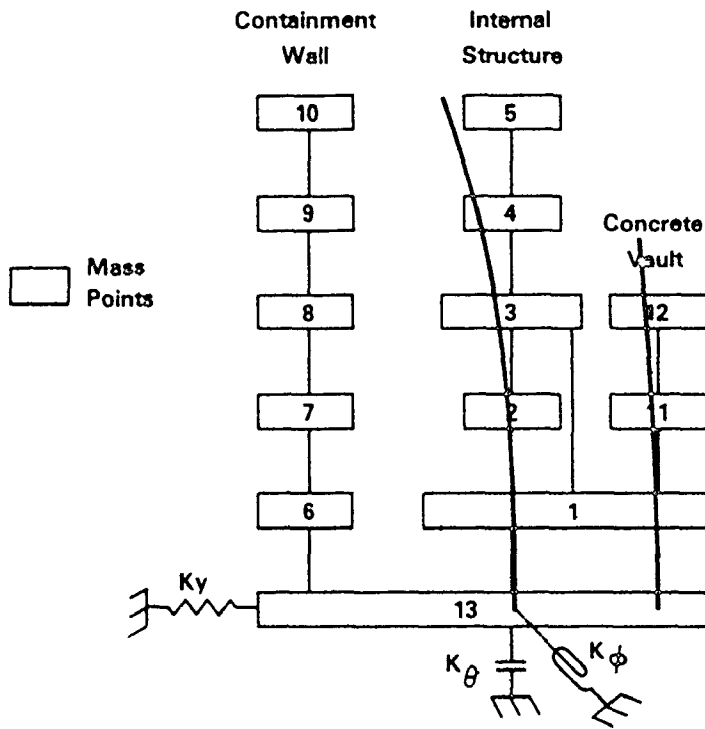


FIG. 2.6a INTERNAL STRUCTURE MODE AT 5.83 Hz

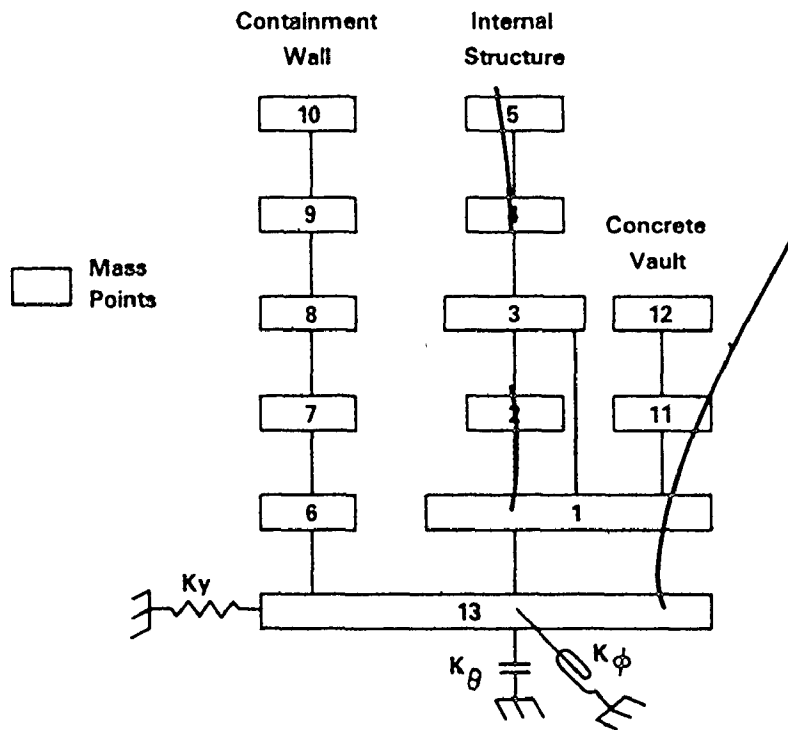


FIG. 2.6b VAULT MODE AT 10 Hz

Although this model was developed explicitly for the CANDU system it is quite similar in geometry and mass distribution to the mathematical models developed for other reactor systems (8,29). Therefore, results drawn from the use of this CANDU model, although perhaps unique in terms of their numerical values, are expected to be similar in character to results for other similar NPP systems.

2.4 Single-Degree-of-Freedom Models

Any structure of arbitrary form can be treated as a single-degree-of-freedom (SDOF) system if it is assumed that its displacements are restricted to a single shape (7). This generalized coordinate approach can be used to develop SDOF models representing the internal structure and reactor vault of the CANDU NPP.

A SDOF model shown in Fig. 2.7 has mass- m , stiffness- k , and viscous damping- c . Dynamic similitude between the SDOF model and the fundamental mode of the CANDU structure can be achieved by setting the SDOF frequency

$$f = \frac{1}{2\pi} \sqrt{\frac{k}{m}} \quad (2-1)$$

equivalent to the fundamental frequency of the appropriate CANDU structure (5.83 Hz for modelling the internal structure; 10 Hz for modelling the reactor vault) and by using the same structural damping (5%) in both cases. The resulting SDOF model is in generalized coordinates since the model k and m were incorporated into a single

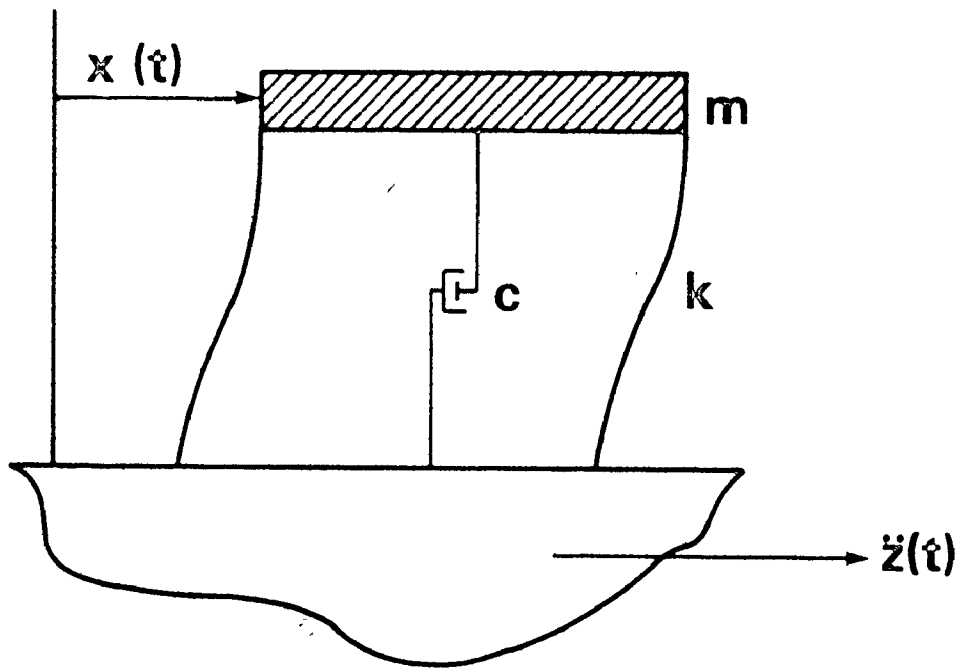


**FIG. 2.7 SINGLE - DEGREE - OF - FREEDOM
SYSTEM SUBJECTED TO GROUND
ACCELERATION $\ddot{z}(t)$**

parameter.

The third model parameter required is the product $\Gamma_j \phi_{ji}$ which is obtained from the CANDU dynamic analysis. Γ_j is the modal participation factor for mode j , and ϕ_{ji} is the CANDU mode shape at mass i for mode j . The product $\Gamma_j \phi_{ji}$ transforms SDOF generalized coordinate response into the same coordinate system as the CANDU response. Thus, numerical comparisons can be made directly between the model and CANDU. A summary of the requirements for SDOF modelling of dynamic responses at mass 4 and mass 12 is given in Table 2.5.

TABLE 2.5 SDOF MODELS OF CANDU STRUCTURES

MODEL	CANDU STRUCTURE	MODEL FREQUENCY	DAMPING	$\Gamma_j \phi_{ji}$
1	internal structure mass 4	5.83 Hz	5%	0.771
2	reactor vault mass 12	10.0 Hz	5%	1.178

Generalized coordinate time-history responses of each model can be evaluated using the Duhamel convolution integral

$$D_j(t) = \frac{1}{\omega_{d_j}} \int_0^t \ddot{x}_g(\tau) e^{-\zeta\omega_j(t-\tau)} \sin \omega_{d_j}(t-\tau) d\tau \quad (2-2)$$

where ω_j is the frequency for CANDU mode j (Table 2.5), $\ddot{x}_g(\tau)$ is the earthquake ground acceleration, and $\omega_{d_j} = \omega_j \sqrt{1-\zeta^2}$ is the damped modal frequency. The transformation of SDOF floor accelerations into the CANDU coordinate system is given by

$$\ddot{x}_i(t) = \Gamma_j \phi_{j1} \ddot{D}_j(t) \quad (2-3)$$

where $\ddot{D}_j(t)$ is the SDOF acceleration in generalized coordinates.

2.5 Summary

Dynamic analysis to evaluate the seismic floor response in a NPP structure requires that both the nature of the earthquake excitation and a mathematical model of the NPP system be defined. Criteria for the selection of earthquake records were discussed and 12 western USA records were selected to form an ensemble of possible earthquake ground motions. A mathematical model of a typical CANDU system was chosen and its physical and dynamic properties were presented. Using these properties, two SDOF models were designed having dynamic similitude with the fundamental modal responses of the CANDU internal structure and reactor vault.

Although the earthquake ground motions and NPP model deal with specific cases, it is felt that the ensemble of earthquake components should give a reasonably representative picture of the variations due to

different ground motions. The similarity of the model to those used by others should permit the outcome of the analysis to be applicable to the problem of evaluating seismic qualification test procedures for NPP's in a general sense, and not solely restricted to the CANDU system.

CHAPTER 3

PARAMETERS FOR SEISMIC MOTION CHARACTERIZATION

3.1 Introduction

The ground motions occurring during a real earthquake event can be extremely complex. An ensemble of records from several earthquakes will generally show wide variations in frequency content, amplitudes and duration and similar variations are often found in recordings taken at different sites during the same event. In the past, many qualitative and quantitative techniques have been introduced attempting to characterize these complex motions in simplified ways useful to seismic engineering applications. The major problem under consideration in this study however is not ground motion characterization but rather to examine seismically induced floor motions within a structure and to describe these motions through a set of characterization parameters which would be useful in seismic equipment qualification. In this context, seismic motion characterization implies that mathematical procedures (to be described in later sections of this chapter) are applied to an acceleration time-history to evaluate a characterization parameter.

After a careful review of the literature a set of parameters were selected on the basis that, having been successfully applied to seismic ground motion characterization by other researchers, they might also be expected to be promising candidates for characterizing floor motions.

These parameters are:

- (i) maximum acceleration
- (ii) floor response spectrum
- (iii) cumulative damage process
- (iv) root-mean-square acceleration
- (v) cumulative RMS function
- (vi) duration of strong motion.

The first two methods are standard techniques for describing floor motions, i.e. maximum acceleration and floor response spectrum and were included in the study to serve as familiar references against which the other techniques could be compared. In the following sections of this chapter each characterization parameter is described, the method of calculation is outlined, and its suitability for describing a seismic motion is discussed.

3.2 Maximum Acceleration

The maximum floor acceleration (maximum absolute peak) occurring during a seismic event is the simplest parameter which can be obtained from a time-history. However, an examination of even a few floor motion time-histories demonstrates some of the problems in using it as a meaningful parameter. Since a maximum value is only a description of the motion at a single instant in time, all other information about the record is lost. For example, site geological conditions are known to significantly influence the magnitude of the ground acceleration and, within a structure the maximum floor acceleration can be markedly

influenced by the effects of soil-structure interaction. The belief that a given peak value can be applied in different geographic areas or, for different types of structures in the same geographic area is erroneous. Local and regional geology and past seismological history must be considered when judging the maximum ground acceleration which is likely to occur in an area.

Structural mass, stiffness and damping are important factors influencing maximum in-structure elastic response while non-linear building behaviour will control response levels during very strong ground shaking. As later results will show, even if the maximum ground acceleration is constant the maximum floor acceleration can vary for different earthquakes.

Another factor which causes maximum acceleration to be a poor descriptor of response is that it provides no indication of the number of cycles of response occurring at or near the same amplitude. A series of several strong cycles at amplitudes below the maximum value, could create more severe seismic loads on floor-mounted equipment than a single large peak. A single high acceleration peak can be attributed to high frequency response and it will tend to act as an impulse. This means that the duration of the peak will generally be much less than the natural period of any floor-mounted equipment and, consequently, the single high acceleration pulse will have passed before there is time for the equipment to respond.

The use of maximum acceleration to describe seismic motions assumes that all relevant time-histories are similar in duration,

frequency content and envelope (15). This is far from being the case but nonetheless, maximum acceleration is a much used quantity, partly for historical reasons and partly in its use for bounding the high-frequency end of the response spectrum (13). It is the first "classical" technique referred to in section 3.1.

3.3 Response Spectrum

The second "classical" technique for describing earthquake motions is the response spectrum which provides a graphical display of the maximum responses of a family of single-degree-of-freedom systems when all are subjected to the same seismic motion. The family of SDOF systems are all assumed to have the same damping and their stiffness/mass ratios cover the range of significant frequencies in the seismic motion. When a spectral analysis is applied to in-structure floor motions the term floor response spectrum, abbreviated FRS, is commonly used. For nuclear power plant structures the FRS generally encompasses frequencies from 0.5 Hz to 33 Hz (23). The response spectrum technique is well-known, widely used and is described in detail in many references (7). A detailed explanation of its calculation and interpretation will not be given here, but Fig. 3.1 has been included to give a pictorial display of its construction and graphical form. Unless otherwise noted, all response spectra in this study are computed for SDOF systems having 1% damping.

The remaining techniques in this chapter present some newer approaches to characterizing seismic ground motion and are being

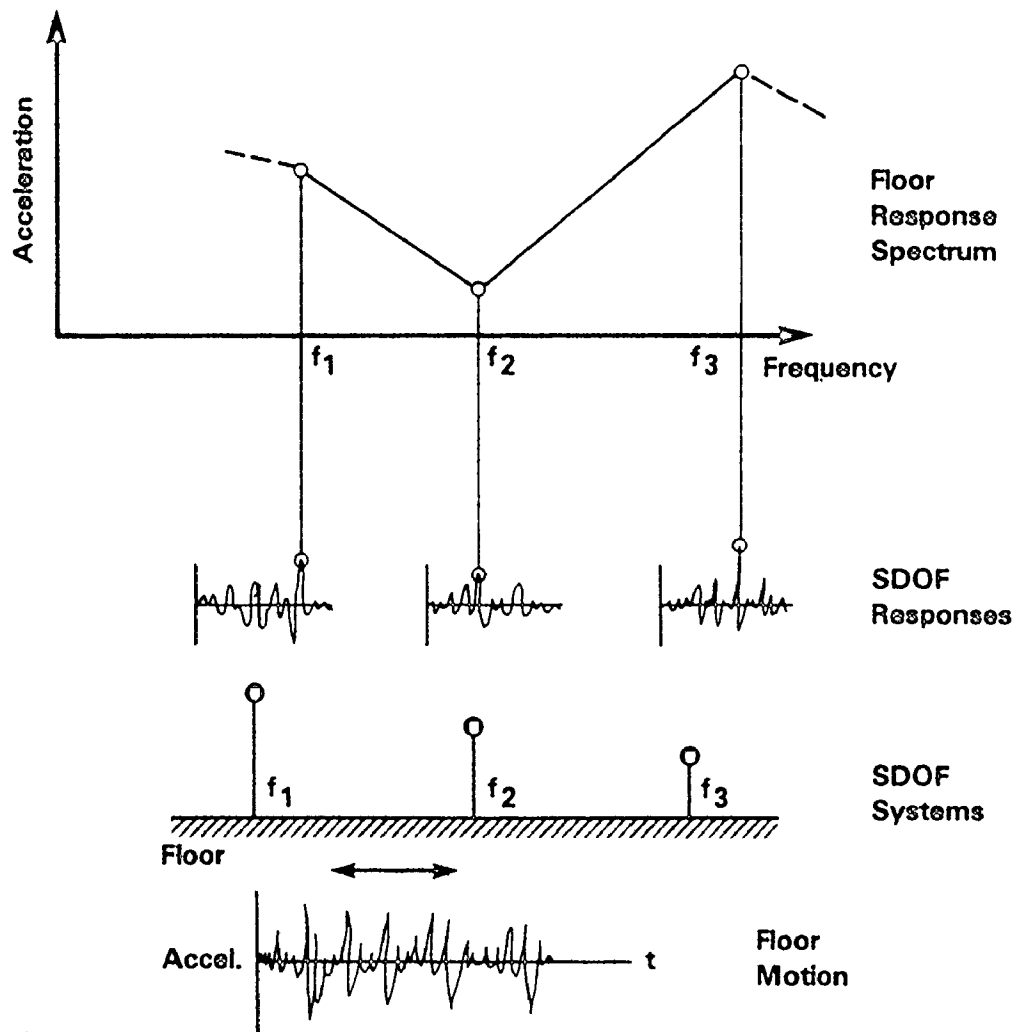


FIG. 3.1 DEVELOPMENT OF A FLOOR RESPONSE SPECTRUM

examined in this study as possible means of developing floor motion characterizations.

3.4 Cumulative Damage Process

Several of the drawbacks and limitations associated with the use of a single maximum acceleration value were discussed in Section 3.2. Instead of a single peak value, a more useful and meaningful approach would be to obtain a measurement which incorporates the amplitudes of all peaks in the floor motion time-history. Such a parameter could hopefully distinguish between a record containing many large amplitude peaks and another record (perhaps having the same maximum acceleration) which had a significantly fewer number of large amplitude cycles. The value of such a distinction could be helpful in comparing the severity of loading which different seismic floor motions might impose on a floor-mounted equipment component and in providing a basis for test equivalency.

The concept of cumulative damage is that every load cycle causes an incremental damage which is accumulated until a certain critical level is reached at which the specimen will fail (11). Seismic motion characterization based upon a cumulative damage process assumes that an equivalency exists when different vibration experiences would produce similar amounts of damage in a given specimen. The objective of using this type of theory as a characterization parameter is to provide a technique for measuring equivalency in terms of the equivalent number of cycles of a uniform amplitude motion required to accumulate the same

damage as the entire ensemble of random amplitude fluctuations in a seismic record (12).

The numerous theories which have been developed on cumulative damage processes may be classified as linear, nonlinear and phenomenological. Linear cumulative damage theories are based upon experimental S-N data (S = strain amplitude; N = number of cycles to failure) for various materials, geometries and other factors which may be desirable to include in a specialized theory. The fractions of useful life consumed by each load cycle are summed linearly, hence a linear theory, however the damage process itself may not necessarily be linear. Nonlinear theories assume there is an interaction between load history and damage, and phenomenological theories attempt to modify basic S-N curves on the basis of observed information from tests and theoretical models (11).

A linear cumulative damage theory proposed by Miner (22) has been selected in this study for characterizing seismic floor motions as a process which results in damage accumulation. Miner's theory, sometimes referred to as the Palmgren-Miner theory in recognition that Palmgren was the first to note the process of linear damage accumulation, is the most universally applied technique because of its simplicity and accuracy. Although it is convenient to retain the terminology associated with material fatigue and cumulative damage processes in the following developments, the mathematics remains the same whether the application is actually to material cyclic fatigue or to characterization of floor motion time histories.

Miner's cumulative damage theory can be introduced by first considering a set of reference values. If N_p cycles each having amplitude R_p (R is used here instead of S) cause a fatigue failure in a given material then the ratio $1/N_p$ is the fraction of damage done by one of the R_p -amplitude cycles. A summation of these damage ratios is straightforward when all strain amplitudes are the same, however when different strain cycles have different amplitudes their equivalence must be established using the S - N relationship. It is convenient and reasonable to consider the S - N relationship approximated by a straight line on a log-log plot, as shown in Fig. 3.2 (10). The equation for the linearized curve in Fig. 3.2 is given by

$$\log R = m \log N \quad (3-1)$$

where m is the slope of the linear segment. It is more convenient to work with a parameter β

$$\beta = -\frac{1}{m} \quad (3-2)$$

instead of m and so Eq. 3-1 becomes

$$\frac{1}{N} = R^\beta \quad (3-3)$$

The value of β is related to material properties and test conditions and has a value greater than unity. Physically, Eq. 3-3 describes the fact that smaller strain amplitudes R , will require a greater number of cycles N to cause a fatigue failure. Therefore, when a maximum strain amplitude of R_p has N_p cycles to failure and strain amplitude R requires N cycles, then the fraction of the total fatigue life at R_p used up by a

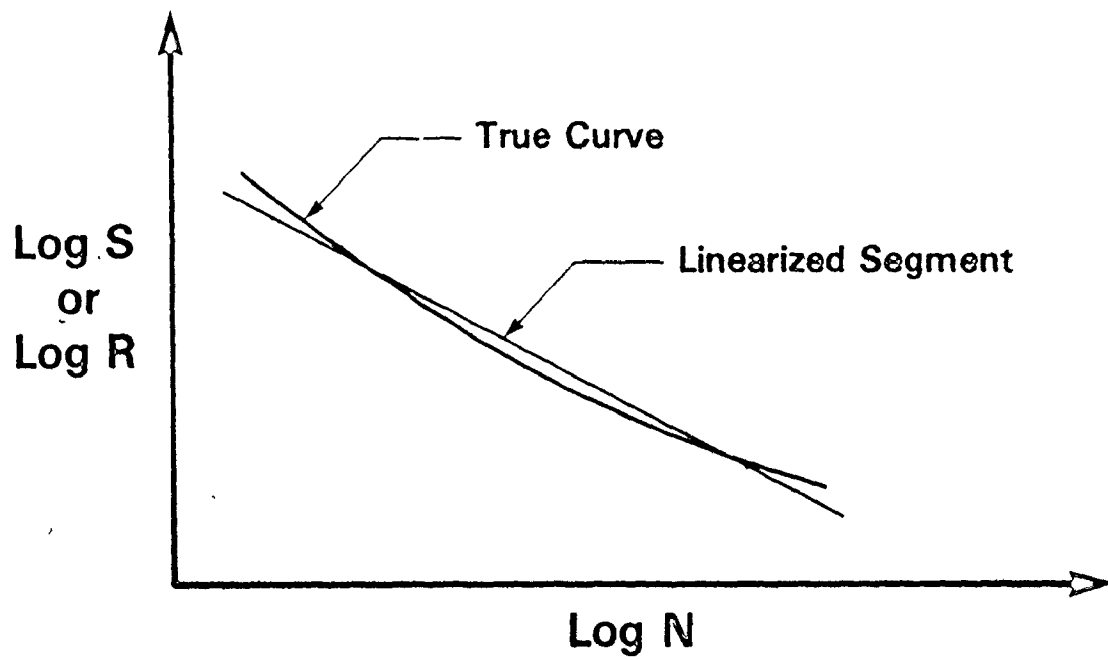


FIG. 3.2 LOGARITHMIC RELATIONSHIP FOR CUMULATIVE DAMAGE

single peak of amplitude R , is

$$\frac{N_p}{N} = \frac{(1/R_p)^\beta}{(1/R)^\beta} \quad (3-4)$$

$$\frac{N_p}{N} = \left(\frac{R}{R_p}\right)^\beta$$

Summing the ratios in Eq. 3-4 for all peaks R_i in the time-history gives the total number of equivalent fatigue cycles (31)

$$N_{eq} = \frac{1}{2} \sum_{i=1}^n \left(\frac{R_i}{R_p}\right)^\beta \quad (3-5)$$

The process described by this equation was adopted as the third characterization technique. The $1/2$ term is included because the S-N relationship considers strain amplitude as a peak-to-peak cycle whereas the summation has considered all positive and negative peaks. Fig. 3.3 illustrates the influence of β on the contribution each (R_i/R_p) ratio makes to the value of N_{eq} . In the heavily weighted case, $\beta=5$ for example, the contribution to N_{eq} by a peak ratio (R_i/R_p) less than about 0.5 is negligible.

The parameter introduced in Eq. (3-5) was based on the use of a reference value R_p which was rather arbitrarily selected as the maximum absolute peak in the time-history. This introduces a problem when several N_{eq} values are to be compared each having been based on a different R_p value. Normalizing N_{eq} values with respect to a single reference value can solve this problem.

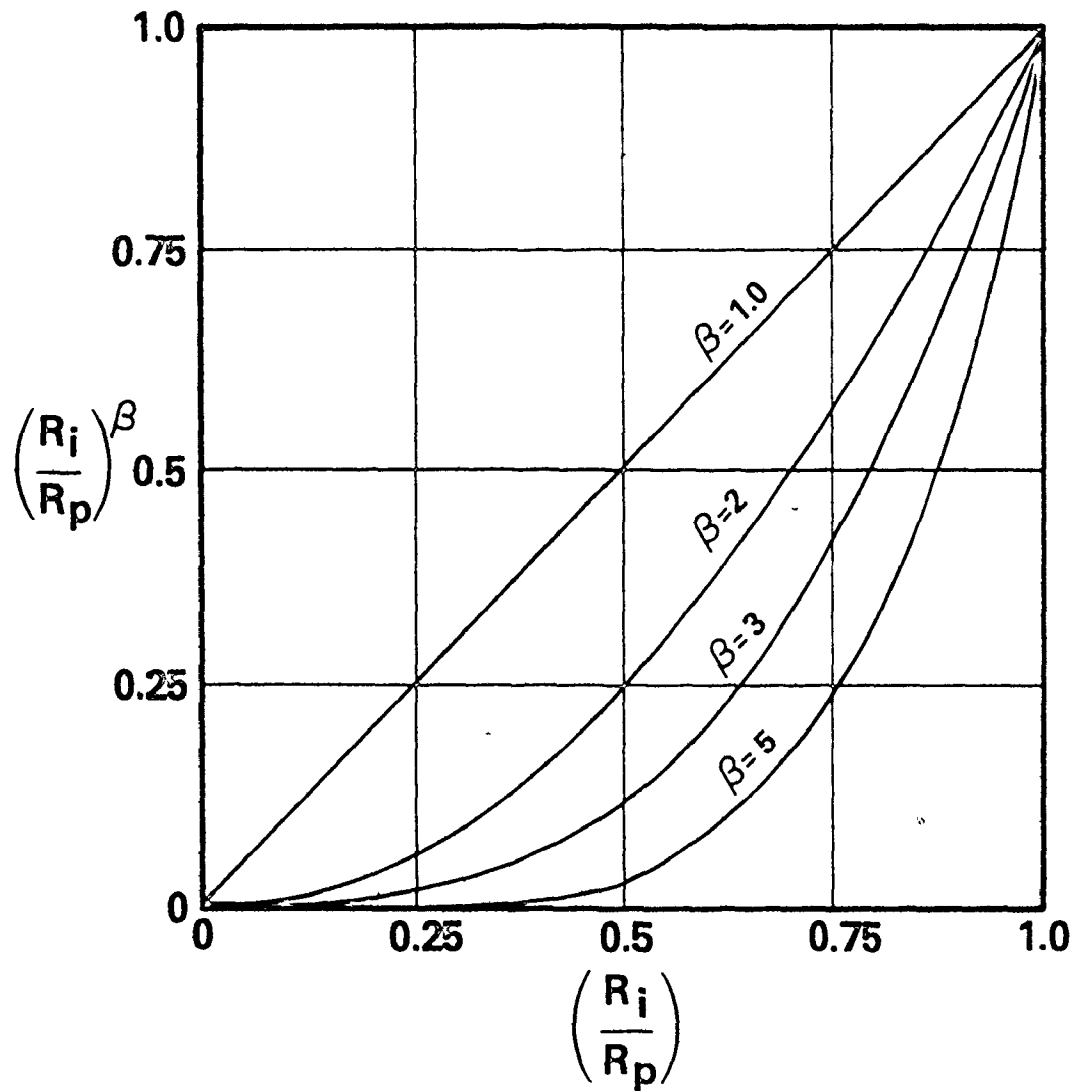


FIG. 3.3 INFLUENCE OF THE EXPONENT β

Eq. 3-5 can be written in a slightly different manner as,

$$N_{eq} = \frac{1}{2} \left(\frac{1}{R_p}\right)^\beta \sum_{i=1}^n (R_i)^\beta \quad (3-6)$$

Incorporating a reference value R_f for normalization Eq. 3-6 becomes,

$$\begin{aligned} N_{eq} \left(\frac{R_p}{R_f}\right)^\beta &= \frac{1}{2} \left(\frac{R_p}{R_f}\right)^\beta \left(\frac{1}{R_p}\right)^\beta \sum_{i=1}^n (R_i)^\beta \\ &= \frac{1}{2} \left(\frac{1}{R_f}\right)^\beta \sum_{i=1}^n (R_i)^\beta \\ &= \frac{1}{2} \sum_{i=1}^n \left(\frac{R_i}{R_f}\right)^\beta \end{aligned} \quad (3-7)$$

Since N_{eq} has already been calculated in Eq. 3-5, the normalized value \bar{N}_{eq} can easily be obtained using the left-hand side of Eq. 3-7,

$$\bar{N}_{eq} = \left(\frac{R_p}{R_f}\right)^\beta N_{eq} \quad (3-8)$$

For convenience, if R_f is taken as 1.0 the normalization reduces to,

$$\bar{N}_{eq} = R_p^\beta N_{eq} \quad (3-9)$$

A simple physical example providing some insight into this procedure first considers the characterization of a single hypothetical time-history record shown in Fig. 3.4, then sub-divides it into smaller records and characterizes each of these shorter segments.

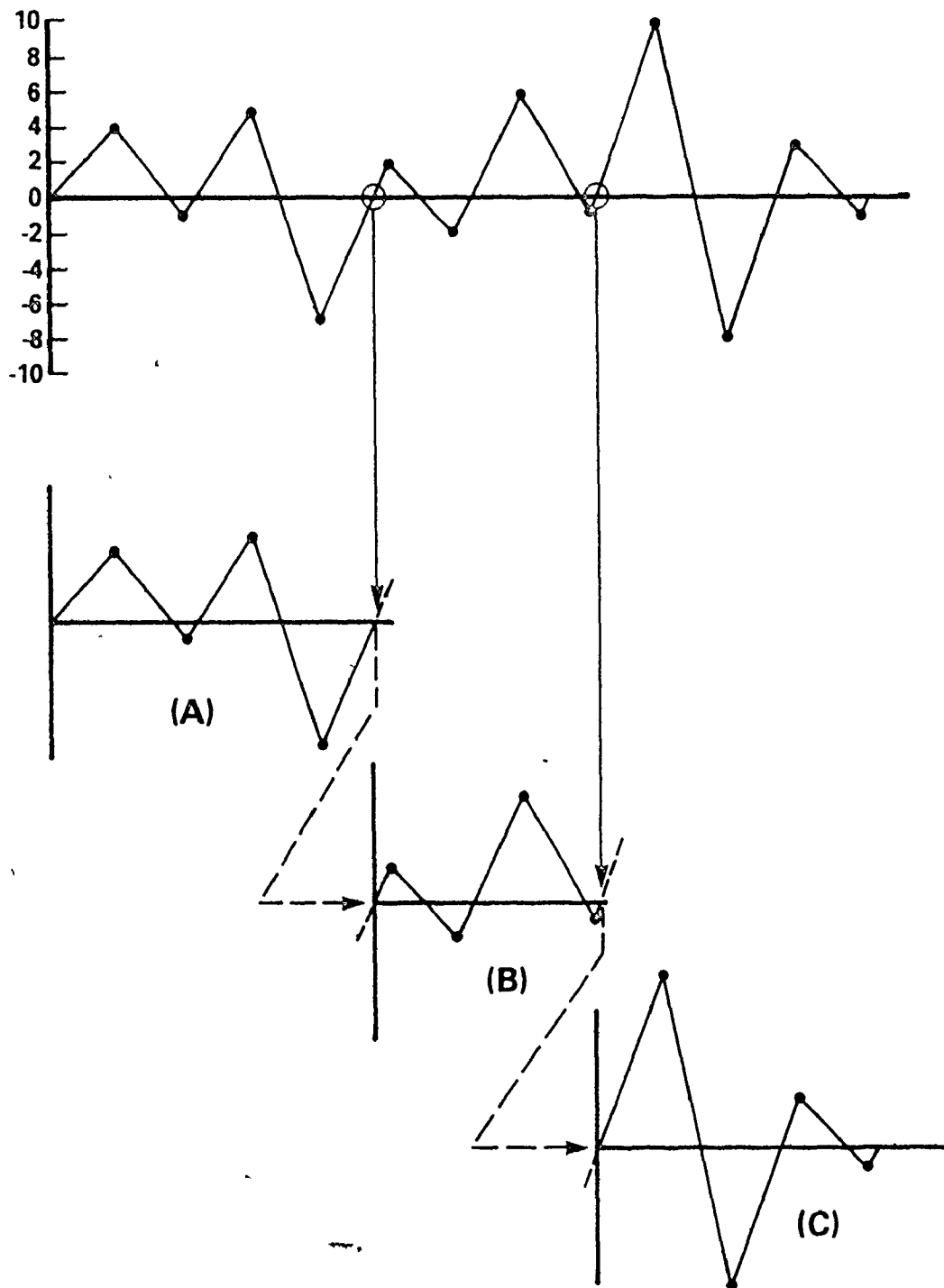


FIG. 3.4 TWO VERSIONS OF A HYPOTHETICAL TIME HISTORY

The peak value in the record is $R_p = 10$. Applying Eq. 3-5 with $\beta = 2$ gives

$$\begin{aligned} N_{eq1} &= \frac{1}{2} \sum_{i=1}^{12} \left(\frac{R_i}{10}\right)^2 \\ &= \frac{1}{2} \left(\frac{1}{10}\right)^2 \{4^2 + 1^2 + 5^2 + \dots + 1^2\} \\ &= 1.550 \end{aligned}$$

Now, consider the record to be sub-divided into three shorter segments A, B, C which occur sequentially as shown in Fig. 3.4. For each of these segments N_{eq} can be evaluated, referencing Eq. 3-5 to the peak occurring within each segment; thus

$$\begin{aligned} N_{eqA} &= \frac{1}{2} \sum_{i=1}^4 \left(\frac{R_i}{7}\right)^2 \\ &= 0.929 \end{aligned}$$

and similarly $N_{eqB} = .625$, $N_{eqC} = .870$. By normalizing each of N_{eqA} , N_{eqB} , N_{eqC} and N_{eq1} to a common R_f , the sum of the normalized values for the three segments should equal the normalized value for the whole record. Mathematically this is

$$\left(\frac{1}{R_{p1}}\right)^B (R_{pA}^B N_{eqA} + R_{pB}^B N_{eqB} + R_{pC}^B N_{eqC}) = N_1$$

or

$$\bar{N}_{eqA} + \bar{N}_{eqB} + \bar{N}_{eqC} = \bar{N}_1 \quad (3-11)$$

where R_f has been taken equal to 10 (see Eq. 3-9). Substituting the numerical values gives

$$\begin{aligned} \bar{N}_{eqA} + \bar{N}_{eqB} + \bar{N}_{eqC} &= .455 + .225 + .870 \\ &= 1.550 \end{aligned}$$

and $\bar{N}_1 = 1.550$

The equality of these two results was to be expected since N_1 is a linear summation across the whole record. This simple numerical case provides a rather appealing look at the summation and normalization procedures especially from the point of view of an accumulative process. The cumulative effect of several short records should be the same whether they are considered as separate and distinct earthquakes or whether they are considered as consecutive phases of one event.

To summarize this section, a theory of cumulative damage has been adopted to provide a parameter for seismic motion characterization. In later sections this technique will be applied to an ensemble of floor motion time-histories to evaluate an equivalence parameter (N_{eq}) for each record. Comparisons of N_{eq} values from different records can be made by normalizing each with respect to a common reference value.

3.5 Root-Mean-Square Acceleration

The root-mean-square (RMS) acceleration in strong ground motion records has been studied by McCann and Shah (21). Their developments have suggested that a two-parameter description using RMS acceleration and duration of strong motion provides a more meaningful characterization of seismic motions than previous single parameter quantities. Characterizing ground motions in this manner follows a similar idea suggested by Housner (15). The next three sections of this chapter are devoted to describing the dual parameters of RMS acceleration and duration. The first section is concerned with the concept of RMS acceleration, the next section describes the extension of RMS acceleration to formulate the cumulative RMS function, and the third section introduces a method of calculating duration of strong motion.

In the time domain the RMS of a continuous function $a(\tau)$ over a specified time interval $(0,t)$ is defined as

$$\text{CRF}(t) = \left\{ \frac{1}{t} \int_0^t a^2(\tau) d\tau \right\}^{1/2} \quad (3-12)$$

The integral property causes the RMS to be less susceptible to large fluctuations due to high peak values in $a(\tau)$. This is very desirable for a seismic characterization parameter because a short duration, high amplitude peak does not significantly affect levels of response and therefore it should not have a major influence on the value of the parameter. Since earthquake acceleration time-histories are used in digitized format, Eq. 3-12 must be applied in its discrete form

$$\text{CRF}(t) = \left\{ \frac{1}{t} \sum_{i=1}^n a^2(\tau_i) \Delta\tau \right\}^{1/2} \quad (3-13)$$

where $a(\tau_i)$ is the acceleration at time τ_i , and $\Delta\tau$ is the interval of digitization. Arias (2) proposed an intensity function which uses the area under the squared acceleration time-history as a measure of the total energy per unit mass E , dissipated by all SDOF oscillators during the entire record. Expressing the Arias intensity as

$$E = \int_0^t a^2(\tau) d\tau \quad (3-14)$$

enables the RMS function to be written as

$$\text{CRF}(t) = \sqrt{\frac{E}{t}} \quad (3-15)$$

which is an average value of power (the square root of the average input rate of energy) for the time t .

A very convenient property of the RMS function is that it can be equally well defined in the frequency domain as

$$\text{CRF}(t) = \left\{ \frac{1}{t} \int_0^{2\pi f_m} G(\omega) d\omega \right\}^{1/2} \quad (3-16)$$

where f_m is the maximum frequency occurring in the time-history between 0 and t , and $G(\omega)$ is the power spectral density of $a(\tau)$

$$G(\omega) = \frac{1}{t} |F(\omega)|^2 \quad (3-17)$$

In Eq. 3-17 $F(\omega)$, the Fourier transform of $a(\tau)$ is

$$F(\omega) = \int_0^{\infty} a(\tau) e^{-i\omega\tau} d\tau \quad (3-18)$$

and $|F(\omega)|$ is the Fourier amplitude spectrum. The function $a(\tau)$ takes on non-zero values only in the interval $(0, t)$ hence the limits of integration in Eq. 3-18 can be adjusted to reflect this finite duration. For a numerical evaluation of RMS acceleration in the frequency domain Eq. 3-16 can be rewritten as

$$\text{CRF}(t) = \left\{ \frac{1}{t} \int_0^{2\pi f_m} [G_1^2(\omega) + G_2^2(\omega)] d\omega \right\}^{1/2} \quad (3-19)$$

where

$$G_1(\omega) = \int_0^t a(\tau) \cos \omega\tau d\tau \quad (3-20)$$

$$G_2(\omega) = \int_0^t a(\tau) \sin \omega\tau d\tau \quad (3-21)$$

Root-mean-square acceleration is a statistical summary about all the acceleration peaks $a(\tau_i)$ occurring within a given interval of time $(0, t)$, and therefore contains a significantly greater amount of information than does a single maximum value. Although the RMS value is also a single number, information on various acceleration levels is not "lost". If the amplitudes in the original process (the earthquake time-history) are assumed to have a Gaussian distribution with zero mean

then the RMS acceleration can be related to any specified acceleration level in a probabilistic manner (25).

3.6 Cumulative RMS Function

Alternatively the RMS acceleration can be expressed as the cumulative RMS function

$$CRF(t) = \left\{ \frac{1}{t} \int_0^t a^2(\tau) d\tau \right\}^{1/2} \quad (3-22)$$

At any time t_k the discrete form of Eq. 3-22 is

$$CRF(t_k) = \left\{ \frac{\sum_{i=1}^k a^2(t_i)}{(n-1)} \right\}^{1/2} \quad k = 2, 3, \dots, N \quad (3-23)$$

where N is the total number of points in the digitized time-history. The typical appearance of the CRF for earthquake ground motions is shown in Fig. 3.5 for the 1954 Eureka N79E component.

Study of the CRF from a number of earthquake records reveals several characteristics: (1) the CRF builds up rather quickly (within the first few seconds) to a maximum value then decays, at a much slower rate, to the final RMS value for the entire record, (2) the CRF provides an indication of the times at which pulses of energy arrive by the location of the peaks on the curve, (3) since the RMS acceleration is related to the seismic energy input via Eq. 3-15 it can be used to

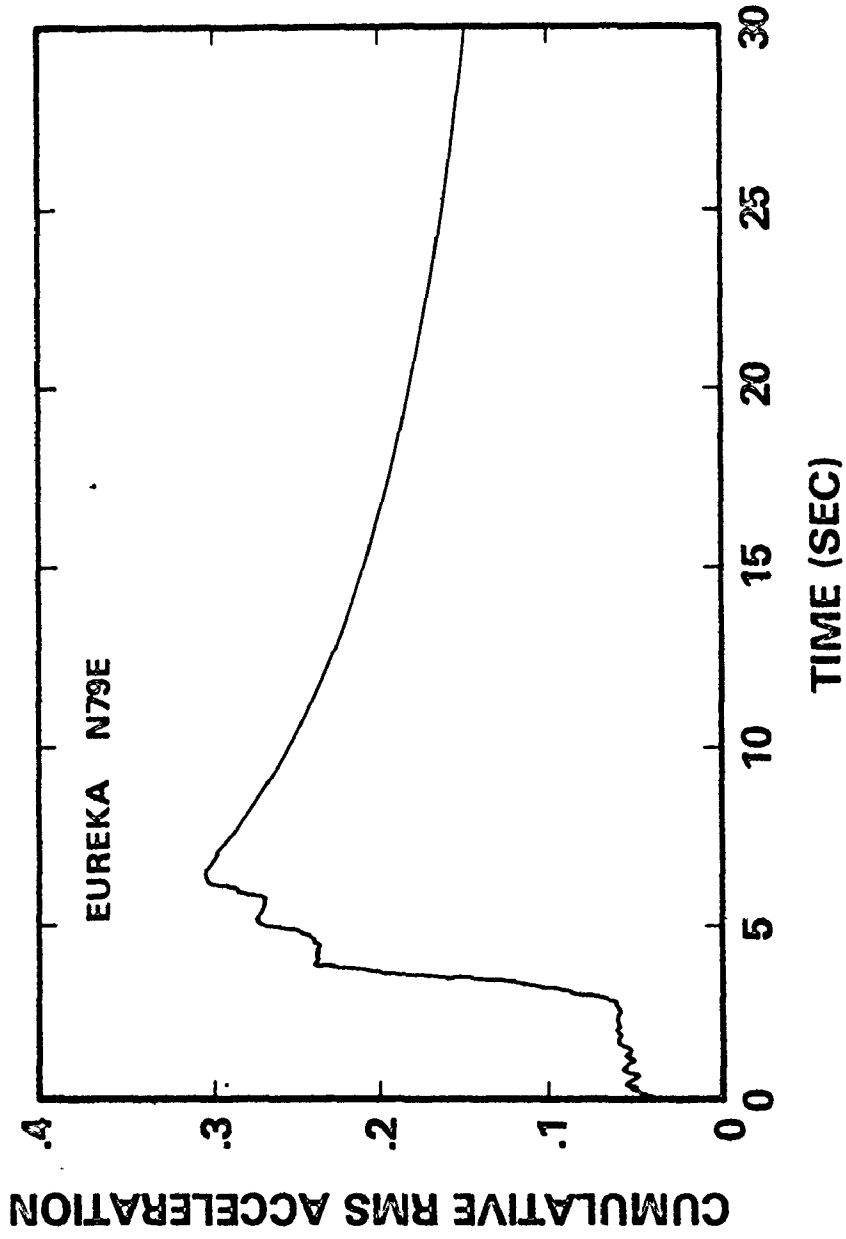


FIG. 3.5 CUMULATIVE RMS FUNCTION

evaluate the cumulative energy of the seismic motion.

The principles behind RMS and CRF can be combined to define a duration of strong motion, the second parameter in the two-parameter characterization.

3.7 Duration of Strong Seismic Motion

The duration of strong motion T_d , can be defined as the duration of time in which the incoming seismic energy is always increasing (21). Increased rates of arrival of seismic energy result in a positive slope of the CRF and conversely, when the rate of energy arrival is decreasing the CRF has negative slope. In this context $D(\text{CRF})$, the derivative of the CRF, is a useful quantity for determining regions of positive and negative slopes of the CRF and to define the strong motion phase.

Differentiating Eq. 3-22 gives

$$\begin{aligned} \frac{d(\text{CRF}(t))}{dt} &= \frac{1}{2} \left\{ \frac{1}{t} \int_0^t a^2(\tau) d\tau \right\}^{-1/2} \left\{ \frac{1}{t} a^2(\tau) - \frac{1}{t^2} \int_0^t a^2(\tau) d\tau \right\} \\ &= \frac{a^2(\tau) - \frac{1}{t} \int_0^t a^2(\tau) d\tau}{2t \left\{ \frac{1}{t} \int_0^t a^2(\tau) d\tau \right\}^{1/2}} \end{aligned} \quad (3-24)$$

If $a(\tau)$ is a continuous integrable function then the derivative can be expressed analytically, otherwise a numerical solution will be necessary. In more symbolic notation Eq. 3-24 is

$$D(\text{CRF}(t)) = \frac{[a(t)]^2 - [\text{CRF}(t)]^2}{2t \text{CRF}(t)} \quad (3-25)$$

This formulation permits a straightforward interpretation of the significance of the CRF derivative. At a given point in time $[a(t)]^2$ is a measure of the instantaneous power of the input signal and $[\text{CRF}(t)]^2$ is a measure of the average power of the signal up to that time. Since the CRF is always positive, the derivative can only be negative when $[a(t)]^2 < [\text{CRF}(t)]^2$. When this condition becomes permanent at time T_e , $D(\text{CRF}(t))$ will go and remain negative, signalling that the strong motion has ended. Similarly, the beginning of strong motion (when the average rate of energy arrival becomes significant) can be determined by reversing the time-history, calculating the CRF and $D(\text{CRF})$ for this reversed record, and taking the beginning of the duration of strong motion as the time (T_b) when $D(\text{CRF})$ goes and remains negative. This forward and reverse procedure is illustrated by Fig. 3.6 as it applies to the 1954 Eureka N79E ground motion. Figure 3.6a shows the Eureka time-history (scaled to 1g peak) and Figs. 3.6b and 3.6c show its CRF and $D(\text{CRF})$, respectively. The final cutoff time of $T_e = 6.36$ sec is shown by the arrow in Fig. 3.6c indicating the last positive value of the derivative and in Fig. 3.6b the permanent change from positive to negative slope of the CRF is also indicated. Figures 3.6d, 3.6e and 3.6f show a similar operation for the reversed time-history to establish T_b . Since Fig. 3.6f is a reversed record, the beginning of strong motion is determined by measuring backwards from the end of the reversed time-history giving $T_b = 30 - 26.90 = 3.10$ sec. In this example the

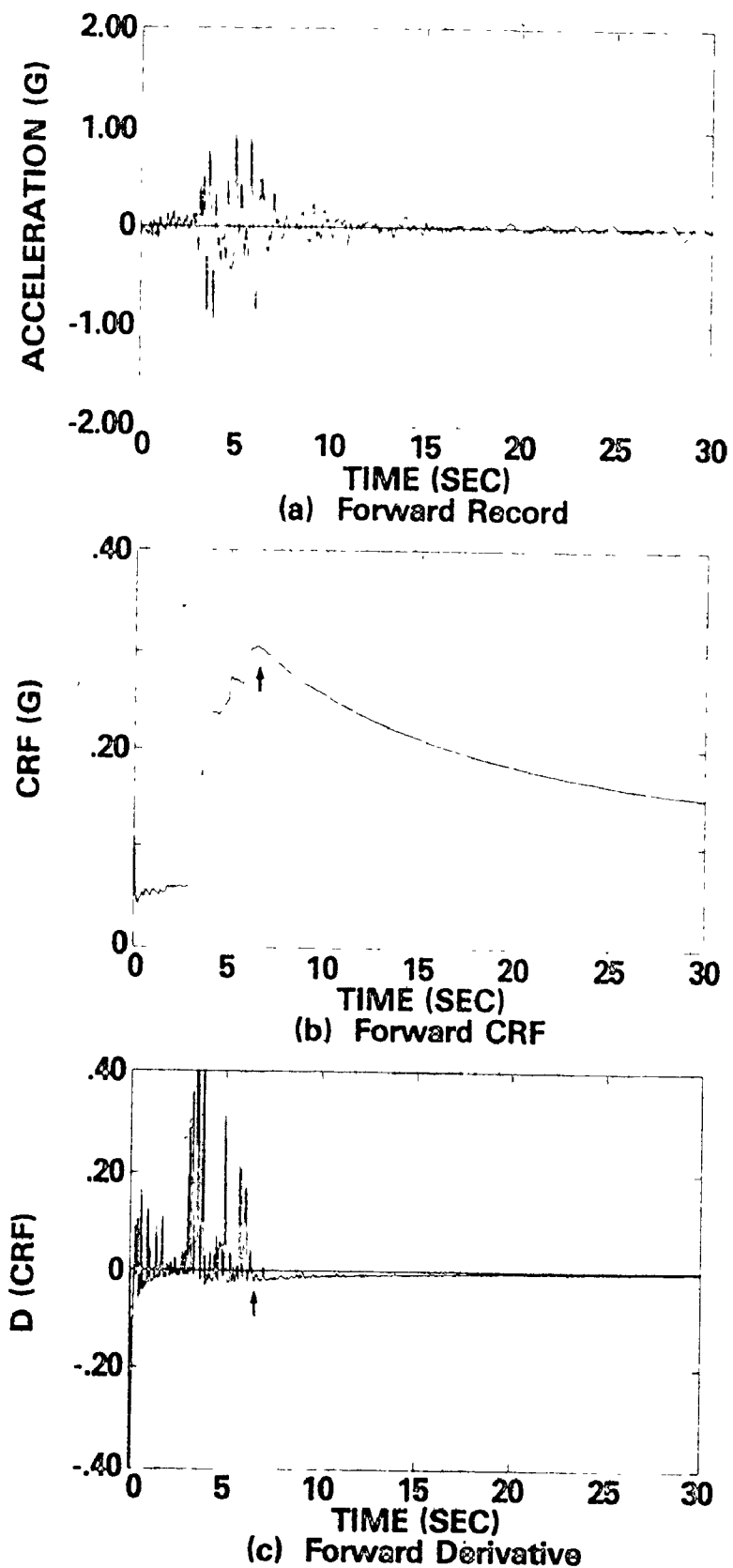


FIG. 3.6 DETERMINING DURATION OF STRONG MOTION FOR EUREKA N79E GROUND MOTION.

proposed duration is $6.36 - 3.10 = 3.26$ seconds.

At this stage the RMS acceleration for the duration T_d can be calculated to complete the two-parameter, RMS-duration characterization. Mathematically, the two parameters can be summarized as

(i) RMS acceleration for duration of strong motion:

$$A_{\text{rms}} = \left(\frac{1}{T_d} \int_{T_b}^{T_e} a^2(t) dt \right)^{1/2}$$

(ii) duration of strong motion:

$$T_d = T_e - T_b$$

This definition of duration of strong-motion has been applied to a large number of earthquake ground motion records by McCann and Shah and they compared the results of their method to three other techniques for duration calculations. A method developed by Bolt based duration on an acceleration cutoff point of 0.05 g while Trifunac and Brady used a bracketing of the cumulative seismic energy in the 5 to 95 percent range. Vanmarcke and Lai used random vibration theory and assumed the strong motion part to be a stationary process with constant frequency content.

The RMS-duration method outlined above produces durations which generally lie somewhere between the Trifunac-Brady results and the Vanmarcke-Lai results. The Trifunac-Brady method tends to produce longer durations than the RMS method, and the Vanmarcke-Lai technique somewhat shorter durations. The Bolt durations show a considerable

scatter of data points without any discernable trend, probably as a result of the somewhat arbitrary 0.05 g cutoff level.

The Bolt and Trifunac-Brady methods both impose rather arbitrary constraints, Bolt's method on acceleration, and Trifunac and Brady's on the bounds of the cumulative energy. The advantage offered by McCann and Shah's method is that duration evolves from an application of basic mathematical techniques to the earthquake record without imposing artificial or arbitrary constraints which could affect the results in an unpredictable manner.

3.8 Summary

Traditional parameters for describing seismic floor motions are generally limited to maximum floor acceleration and a floor response spectra. Maximum acceleration looks at only one instant of time and ignores all other information. A response spectrum contains significantly more information but its original development for structural strength evaluation was based on considerations very different from those required for equipment seismic qualification. For these applications, characterization parameters must provide more information than is afforded by these two methods.

Newer parameters such as using cumulative damage theory, RMS acceleration, cumulative RMS function and duration of strong-motion each emphasize and describe particular characteristics of an acceleration time-history. Cumulative damage processes attempt to emphasize the presence of large amplitude peaks and suppress the importance of the

frequently occurring, small amplitude cycles. The dual-parameters of RMS acceleration and duration use a consistent theoretical approach based on energy in the seismically induced motions. A definition of duration of strong motion describes the important time segment of a seismic excitation (from the point of view of incoming energy) and the RMS acceleration for this duration measures the average value of power, or input rate of seismic energy. The cumulative RMS function graphically shows the arrival time(s) of the pulse(s) of energy and is an important step in the calculation of duration of strong motion.

In later chapters these parameters will be applied; (1) to characterize the 12 seismic ground motions in order to understand the source of excitation, (2) to single-degree-of-freedom systems to gain an understanding of response characteristics of simple structures, and finally, (3) to calculate floor motions within a CANDU nuclear reactor building to describe the seismic environment in which reactor equipment must operate.

CHAPTER 4

CHARACTERIZATION OF HARMONIC MOTIONS

4.1 Introduction

By virtue of the complexity of real earthquake ground motions and structural responses, characterizations of their time-series must be implemented using numerical computer solutions. Before proceeding to this stage, a major advantage is afforded by considering harmonic motions which can be characterized analytically rather than through numerical methods. The closed-form analytical solutions which are possible for these types of motions tend to be more useful in providing a basic understanding of each characterization technique. From this type of analysis a basic frame of reference can be established to judge the characterizations of real earthquake events and to review the realism afforded by test simulation using single frequency motions. This chapter is devoted to the analytical characterization of three single frequency motions, (i) a limited-duration sine, (ii) a sine beat, (iii) a decaying sinusoid, with the assumption that these motions represent either a floor motion response or the motion of a shake table during a seismic test. Reference to these two situations will be made interchangeably.

4.2 Constant Amplitude Sinusoidal Motion

A constant amplitude sinusoidal acceleration $\ddot{z}(t)$ with frequency

Ω may be expressed as

$$\ddot{z}(t) = A \sin \Omega t \quad (4-1)$$

The following sections develop characteristics of this motion by applying each of the techniques from Chapter 3.

4.2.1 Maximum Acceleration

The maximum floor (or shake table) acceleration A_m occurring during the sinusoidal motion $\ddot{z}(t)$ is simply $A_m = A$.

4.2.2 Response Spectrum and Quasi-Resonant Response

As discussed in Section 3.3, a response spectrum graphically portrays the maximum responses of a family of SDOF systems subjected to the same base motion. The differential equation describing SDOF responses in terms of relative displacements is

$$\ddot{x} + 2\zeta\omega\dot{x} + \omega^2 x = A \sin \Omega t \quad (4-2)$$

which has a general solution composed of a transient and a steady-state component:

$$x(t) = e^{-\zeta\omega t} (B \sin \omega_d t + C \cos \omega_d t) + \frac{A}{\omega^2} \frac{1}{[1 - u^2]^2 + [2\zeta u]^2} [1 - u^2] \sin \Omega t - 2\zeta u \cos \Omega t \quad (4-3)$$

where $u = \frac{\Omega}{\omega}$ is the ratio of input frequency to SDOF natural frequency.

Since damping will be small the approximation that damped frequency equals undamped natural frequency ($\omega_d = \omega\sqrt{1 - \zeta^2} \approx \omega$) is justifiable. Constants B and C depend upon initial conditions, $x(0)$ and $\dot{x}(0)$.

Some simplifications can be made in Eq. 4-3 to obtain an expression for response amplification for a limited number of cycles of sinusoidal input. The steady-state component of the displacement can be written as

$$x_{ss}(t) = \rho \sin(\omega t - \theta) \quad (4-4)$$

where

$$\rho = \frac{A}{\omega} [(1 - u^2)^2 + (2\zeta u)^2]^{-1/2} \quad (4-5)$$

and θ , the phase angle by which the response lags behind the applied loading is given by

$$\theta = \tan^{-1} \left(\frac{2\zeta u}{1 - u^2} \right) \quad (4-6)$$

This leads to a more compact form of the general solution:

$$x(t) = e^{-\zeta\omega t} (B \sin \omega t + C \cos \omega t) + \rho \sin(\omega t - \theta) \quad (4-7)$$

In many vibration problems steady-state conditions are of primary interest and the transient terms are usually neglected. Seismic engineering problems are of a different nature however, as the strong phase of earthquake shaking usually lasts only a few seconds and transients can be quite influential in determining the overall response. Choosing initial conditions, $x(0) = \dot{x}(0) = 0$ and including the transient

term in Eq. 4-7, B and C become

$$B = \rho (\zeta \sin \theta - u \cos \theta) \quad (4-8)$$

$$C = \rho \sin \theta \quad (4-9)$$

Although response has been expressed in terms of displacements, the right-hand side of the differential equation (Eq. 4-2) is an acceleration function. The second derivative of Eq. 4-7 gives the relative acceleration of the SDOF system which is more convenient for comparing inputs and responses; thus

$$\begin{aligned} \ddot{x}(t) = & \omega^2 e^{-\zeta\omega t} [(B\zeta^2 + 2C\zeta - B) \sin \omega t \\ & + (C\zeta^2 - 2B\zeta - C) \cos \omega t] - \rho\Omega^2 \sin(\Omega t - \theta) \end{aligned} \quad (4-10)$$

For a limited-duration of N cycles of sine motion, t in Eq. 4-10 has a final value of $t = N/\Omega$. Using this and computed values of ρ , θ , B , and C from Eqs. 4-5, 4-6, 4-8, 4-9, respectively, amplification factors can be calculated for a SDOF system at any frequency ratio u and any (low) level of damping ζ . Frequency response curves giving the amplifications for 1% damping are shown in Fig. 4.1 with the number of full cycles of sinusoidal base motion indicated next to each curve.

At resonance ($u = 1.0$) considerable simplification is possible by replacing Ω with ω ; thus, previous expressions become

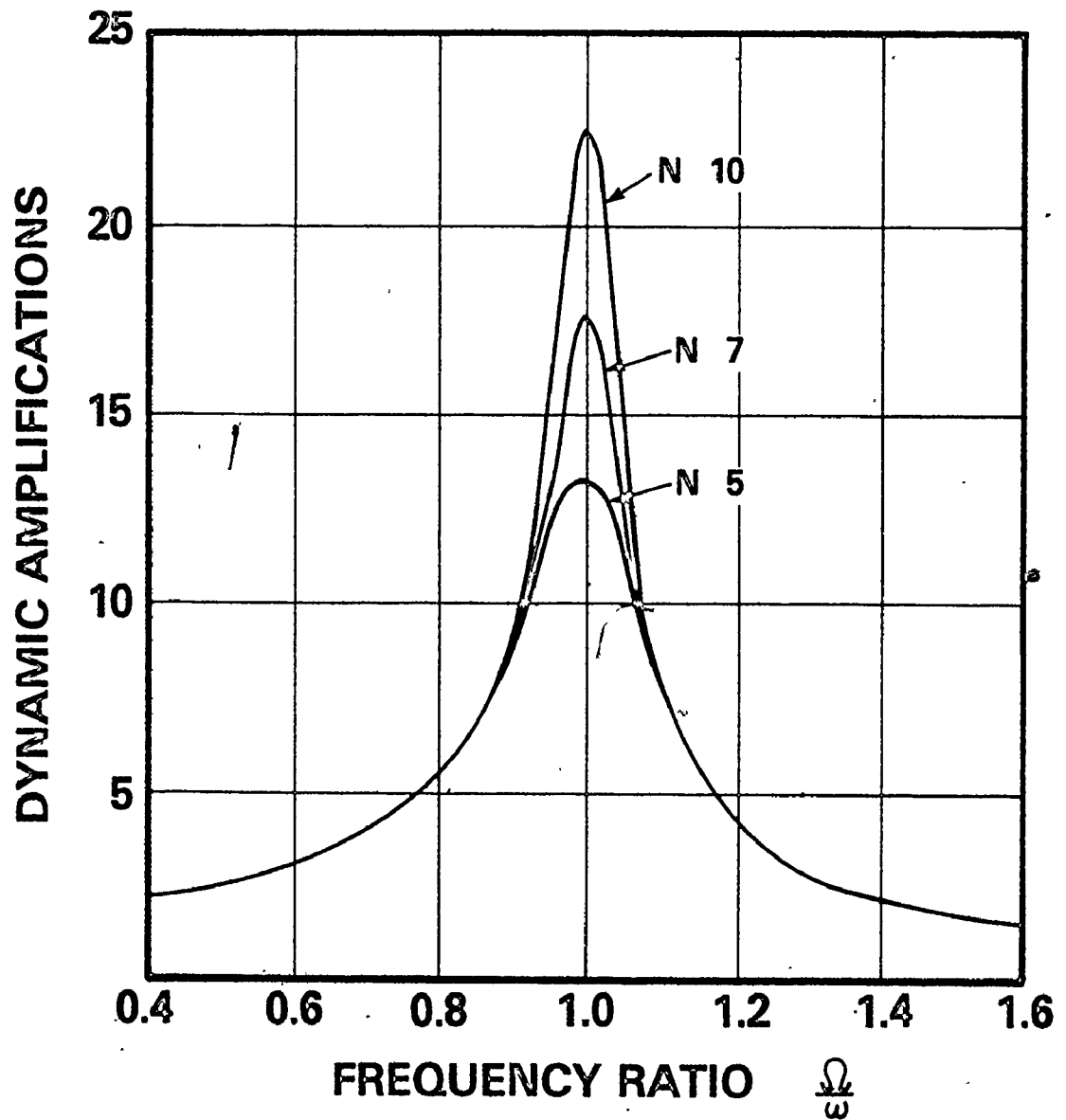


FIG. 4.1 SDOF RESPONSE TO A CONSTANT AMPLITUDE SINUSOIDAL MOTION

$$\rho = \frac{1}{2\zeta\omega} \quad \theta = \frac{\pi}{2} \quad (4-11)$$

$$B = \frac{1}{2\omega} \quad C = \rho$$

The general solution for quasi-resonant acceleration response $\ddot{x}_r(t)$ is then obtained from Eqs. 4-10 and 4-11 as follows:

$$\ddot{x}_r(t) = \frac{1}{2\zeta} e^{-\zeta\omega t} [(\zeta^3 + \zeta)\sin \omega t + (-\zeta^2 - 1)\cos \omega t] + \cos \omega t \quad (4-12)$$

The trigonometric terms involving ζ and higher orders of ζ , are very small compared to the other terms, hence these can be neglected to arrive at an approximate expression:

$$\ddot{x}_r(t) \approx \frac{1}{2\zeta} (1 - e^{-\zeta\omega t}) \cos \omega t \quad (4-13)$$

Under steady-state conditions it is clear that Eq. 4-13 gives a maximum value of $1/2\zeta$. When the input sine motion is a limited duration of N cycles, quasi-resonant amplification factors Q are given by

$$Q = \frac{1}{2\zeta} (1 - e^{-2\pi\zeta N}) \quad (4-14)$$

The influence of damping and duration of input on the quasi-resonant response is illustrated in Fig. 4.2 by a plot of the response ratio $2\zeta Q$ vs N for 1, 2, 5, and 10 percents damping. This clearly shows the rapid rise to near steady-state response at increased levels of damping.

As a final point of investigation, the case of zero damping gives an upper bound on the maximum possible SDOF response. Eq. 4-12 becomes

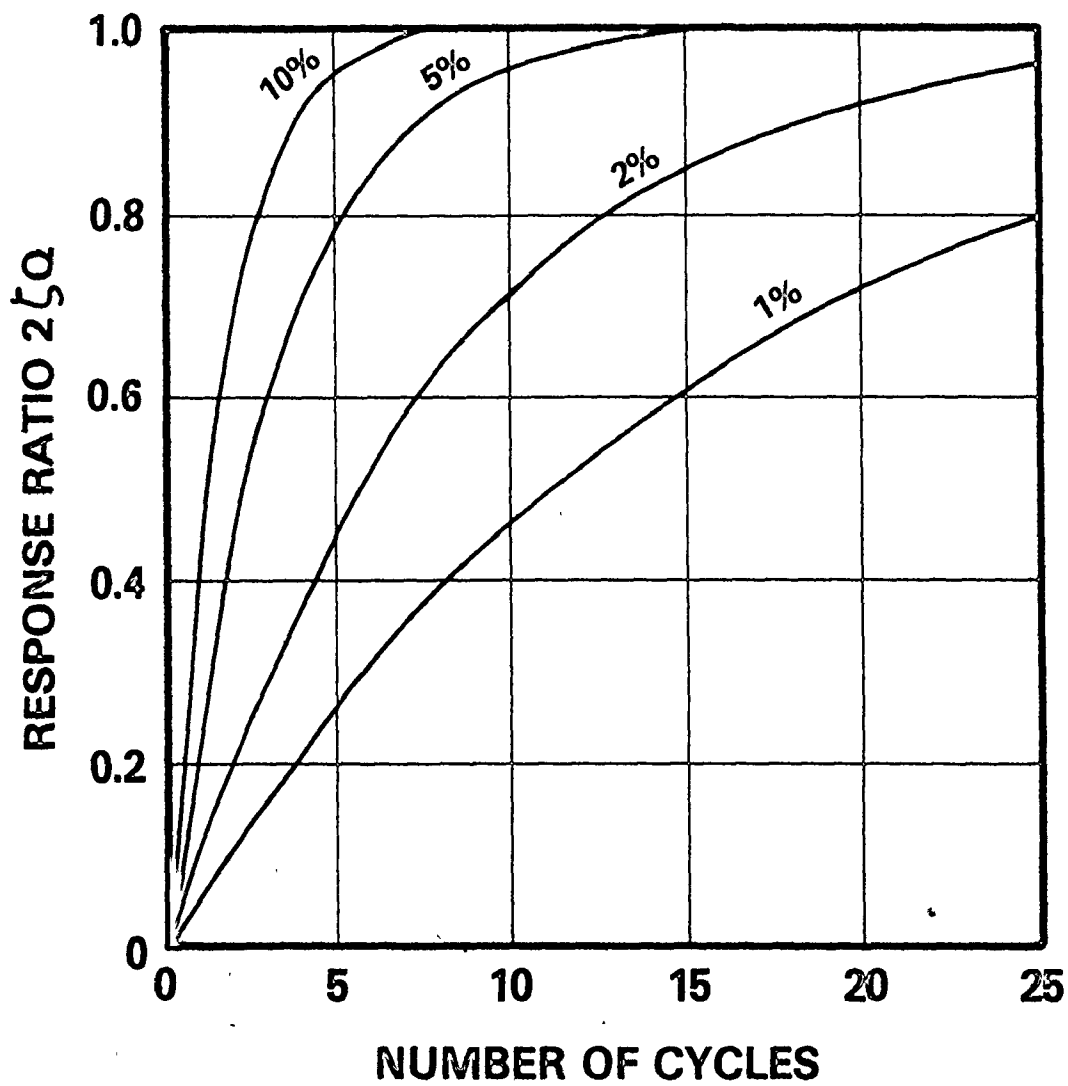


FIG. 4.2 QUASI - RESONANT RESPONSE FOR LIMITED DURATION SINE MOTIONS

indeterminate for $\zeta = 0$, but when L'Hospital's rule is applied, the resonant response of an undamped system is

$$\ddot{x}_{r0}(t) = \frac{1}{2}(\sin \omega t - \omega t \cos \omega t) \quad (4-15)$$

which becomes

$$\ddot{x}_{r0}(t) = \frac{1}{2}(\sin 2\pi N - 2\pi N \cos 2\pi N) \quad (4-16)$$

for N cycles. Q -factors obtained from the enveloping nature of the response are

$$Q = \pi N \quad (4-17)$$

indicating that response continues to grow by an amount π at each cycle.

4.2.3 Cumulative Damage Process

The motivation behind using a cumulative damage concept is to attempt to equate the effects of a number of cycles of various amplitudes to an equivalent number of constant amplitude cycles. Applied to a sine motion, this type of analysis does not yield any new information as each sine cycle has the same amplitude and therefore, contributes equally to the cumulative total. The number of equivalent cycles N_{eq} (Eq. 3-5), is equal to the number of sine cycles in the limited-duration motion therefore, compared to an equal number of cycles N of any other type of motion a pure sine accumulates the highest N_{eq} value.

Relative to a fatigue environment, it can be said that a constant amplitude sinusoidal floor motion would be expected to result in a

greater accumulation of damage in a floor-mounted equipment component than any other type of floor motion having the same peak amplitude, duration and frequency.

4.2.4 Root-Mean-Square Acceleration and Duration

The time variation of the RMS acceleration for a sine motion is given by

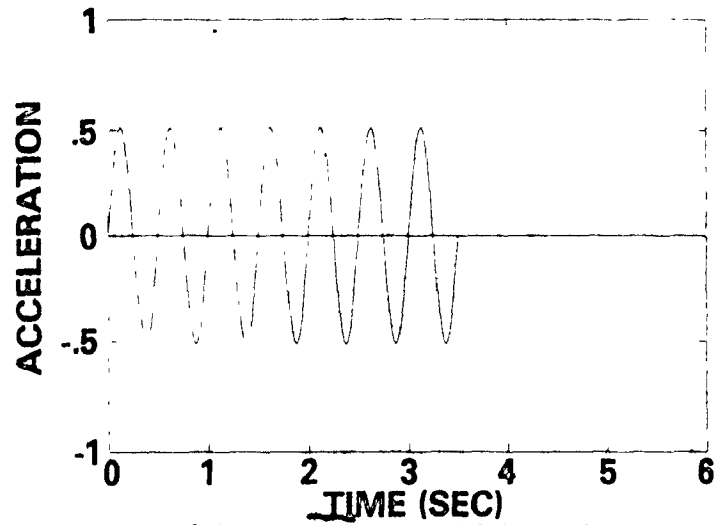
$$\text{CRF}(t) = \left[\frac{1}{t} \int_0^t A^2 \sin^2 \Omega \tau \, d\tau \right]^{1/2} \quad (4-18)$$

This integral can be evaluated using trigonometric identities to yield

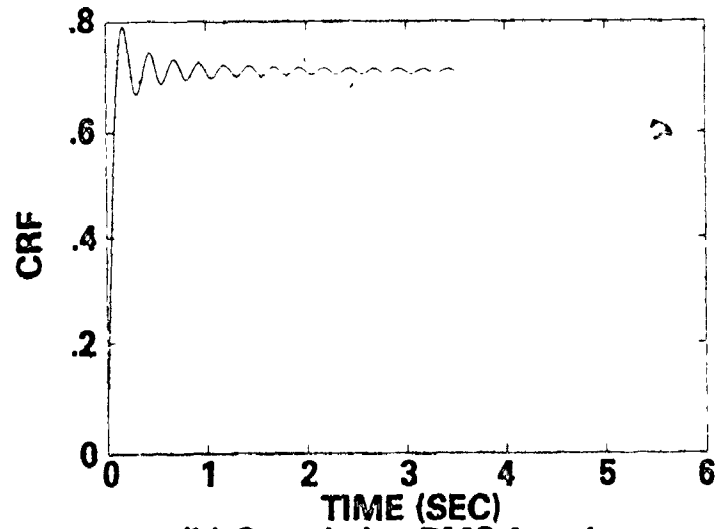
$$\text{CRF}(t) = \left\{ \frac{A^2}{2t} \left[t - \frac{1}{2\Omega} \sin(2\Omega t) \right] \right\}^{1/2} \quad (4-19)$$

The expression in Eq. 4-19 clearly shows a constant term and an oscillatory term which causes the CRF to fluctuate about the constant value. For long duration sine motions, t becomes large and the oscillatory component will die out. This can be shown by taking the limit of the CRF (the limiting value of the RMS) as t approaches infinity:

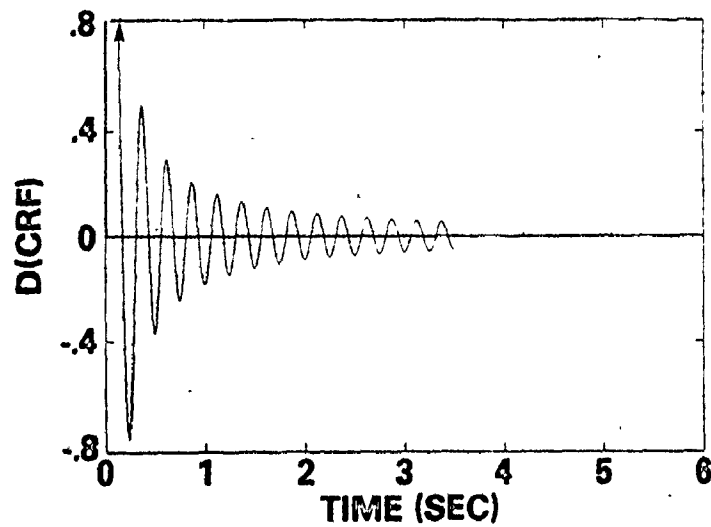
$$\begin{aligned} \lim_{t \rightarrow \infty} \{\text{CRF}(t)\} &= \lim_{t \rightarrow \infty} \left\{ \frac{A^2}{2} \left[1 - \frac{1}{2\Omega t} \sin(2\Omega t) \right] \right\}^{1/2} \\ &= \frac{A}{\sqrt{2}} \end{aligned} \quad (4-20)$$



(a) 7-cycle sinusoidal motion



(b) Cumulative RMS function



(c) Derivative of CRF

FIG. 4.3 CRF AND D(CRF) FOR A SINE MOTION

Thus, for a continuous sinusoidal motion the RMS value is simply $A/\sqrt{2}$. A 7-cycle sine motion and its CRF are shown in Fig. 4.3a and 4.3b, clearly illustrating the dying out of the oscillatory component and the limiting value of the CRF at large values of t .

It is easy to show that the CRF will exactly equal $A/\sqrt{2}$ each time a quarter-cycle of input motion has been completed (ie., whenever $\ddot{z}(t)$ is a maximum, minimum, or zero). Using Eq. 4-20, the sine term can be written as

$$\sin 2\Omega t = \sin 4\pi \frac{t}{T} \quad (4-21)$$

where $T = 2\pi/\Omega$, the period of the sine motion. This term equals zero whenever

$$t = \frac{nT}{4} \quad n = 1, 2, \dots \quad (4-22)$$

or in other words, at every quarter-cycle of input motion CRF(t) is equal to the steady-state RMS value.

A method of measuring the duration of strong shaking consistent with the concept of RMS was outlined in section 3.7. The derivative of Eq. 4-18 can be written directly using the result of Eq. 3-25:

$$\frac{d}{dt}(\text{CRF}(t)) = \frac{d}{dt} \left[\left\{ \frac{A^2}{2t} \int_0^t \sin^2 \Omega \tau \, d\tau \right\}^{1/2} \right] \quad (4-23)$$

$$= \frac{A^2 \left[\sin^2 \Omega t - \frac{1}{2t} \left(t - \frac{1}{2\Omega} \sin 2\Omega t \right) \right]}{2t \left[\frac{A^2}{2t} \left(t - \frac{1}{2\Omega} \sin 2\Omega t \right) \right]^{1/2}} \quad (4-24)$$

This function is illustrated in Fig. 4.3c for the 7-cycle sine motion.

When a complete number of cycles N of base input motion has occurred

$$\omega t = 2\pi N \quad (4-25)$$

and consequently the trigonometric terms are zero; then

$$\frac{d}{dt} \text{CRF}(t) = - \frac{A}{2\sqrt{2t}} \quad (4-26)$$

which means that $D(\text{CRF})$ will be negative after a complete number of cycles has elapsed. In the limit, as t approaches infinity, Eq. 4-24 goes to zero but in an oscillating manner. Therefore, there is never a time after which $D(\text{CRF})$ remains negative. This means that the end of the duration of strong-motion occurs at the end of the sinusoidal input. The fact that $D(\text{CRF})$ is negative at this point (Eq. 4-26) does not affect the result as the derivative would again oscillate through a positive region if another cycle of motion were to occur.

The beginning of strong motion is calculated in a similar manner by using the input record in reversed order. Equivalent to reversing a sine record is to use the negative of the forward record, that is

$$\begin{aligned} \ddot{z}(t)_{\text{rev}} &= - \ddot{z}(t)_{\text{fwd}} \\ &= - A \sin \omega t \end{aligned} \quad (4-27)$$

The functions CRF and $D(\text{CRF})$ are unchanged by this procedure, consequently the beginning of strong motion occurs at the start of the

sine signal.

To summarize, for a complete number of cycles of sinusoidal motion having amplitude A , the entire duration of the sinusoid is considered as the strong motion phase ($T_d = NT$) and the RMS acceleration is $A/\sqrt{2}$, regardless of the number of cycles.

4.3 Sine-Beat Motion

Perhaps one of the most straightforward ways to visualize the graphical form of a sine beat is to consider a pulse of sinusoidal cycles enveloped by a half-sine wave, as illustrated in Fig. 4.4. The half-sine envelope is drawn as a dashed line and the sine beat waveshape is shown as a solid line. In Fig. 4.4, let the period of the enveloping wave be represented by T_b (the beat period), the period of each sine wave in the pulse by T_t (the test or table motion period), and let N be the number of cycles per beat pulse. Since the envelope of each beat pulse is a half-sine, T_b can be expressed in terms of N and T_t ;

$$T_b = 2NT_t \quad (4-28)$$

and consequently, the test and beat frequencies are given by

$$\Omega_t = \frac{2\pi}{T_t} \quad (4-29)$$

$$\Omega_b = \frac{2\pi}{T_b}$$

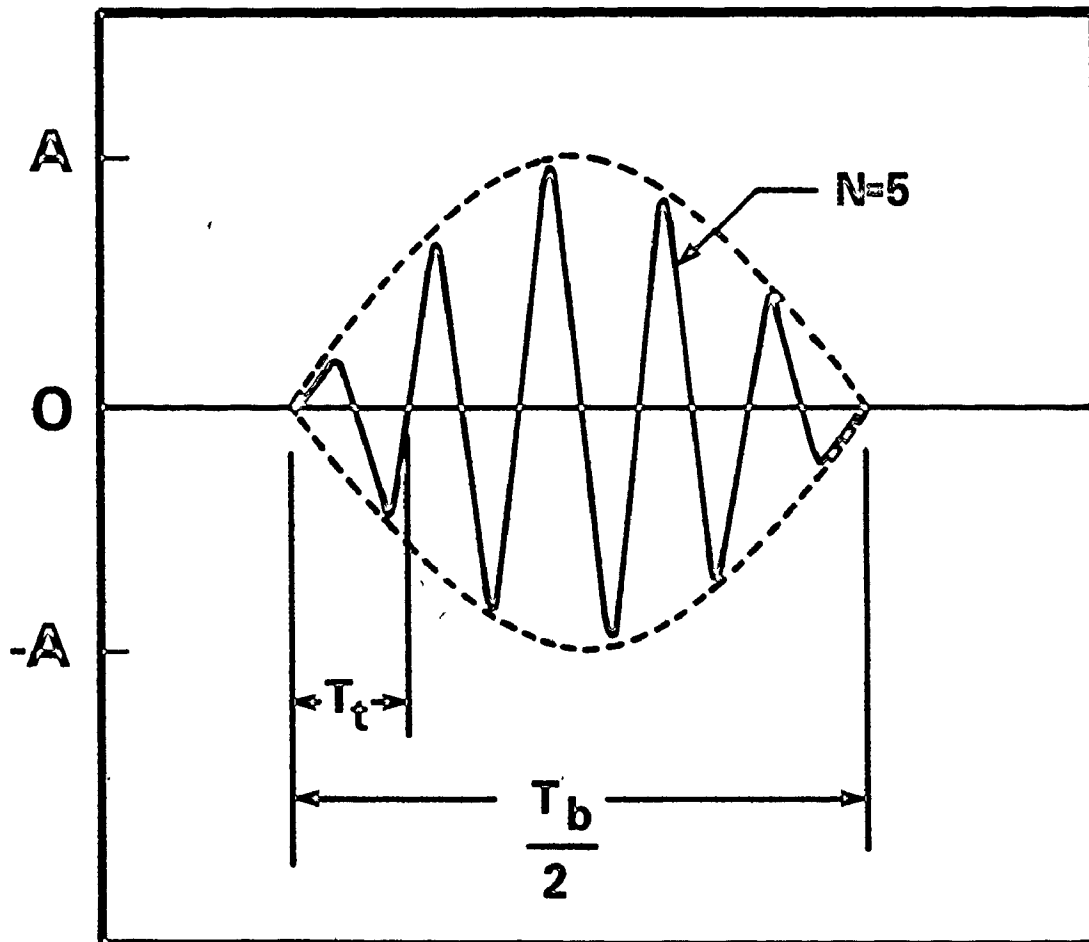


FIG. 4.4 SINE BEAT PULSE

$$= \frac{\pi}{NT_t} \quad (4-30)$$

Thus, in terms of an enveloping function a sine beat acceleration can be expressed in the form

$$\ddot{z}(t) = -A \sin \Omega_b t \cdot \sin \Omega_t t \quad (4-31)$$

The negative sign facilitates some of the later mathematical developments and is not significant in a physical sense.

A second interpretation of a sine beat vibration can be made by writing Eq. 4-31 in a different but equivalent form using the following trigonometric identity:

$$-2 \sin \left(\frac{\Omega_1 - \Omega_2}{2} \right) \sin \left(\frac{\Omega_1 + \Omega_2}{2} \right) = \cos \Omega_1 - \cos \Omega_2 \quad (4-32)$$

The Ω_1 and Ω_2 terms are related to the frequencies in Eq. 4-31:

$$\frac{\Omega_1 + \Omega_2}{2} = \Omega_t \quad (4-33)$$

$$\frac{\Omega_1 - \Omega_2}{2} = \Omega_b$$

Solving for Ω_1 and Ω_2 and introducing N from Eq. 4-30 gives

$$\Omega_1 = \Omega_t + \Omega_b \quad (4-34)$$

$$\Omega_2 = \Omega_t - \Omega_b$$

Therefore, the second equivalent formulation of a sine beat acceleration is

$$\ddot{z}(t) = \frac{A}{2} (\cos \Omega_1 t - \cos \Omega_2 t) \quad (4-35)$$

This expression demonstrates the well known fact that addition of two sinusoidal components having slightly different frequencies produces a sine beat.

In a mathematical sense, the cosine terms are representative of two vectors rotating at slightly different frequencies with a resultant (the amplitude envelope of $\ddot{z}(t)$) varying in absolute value between zero and A. In a physical sense, Eq. 4-35 provides an explanation for the appearance of beats in a structural response. If it is assumed that a structure has a fundamental frequency of say Ω_2 , and an earthquake occurring at the site has a large spectral content at a frequency of Ω_1 , then if Ω_1 and Ω_2 are close together (say 1 Hz separation) this slight off-resonance excitation can set up beat pulses in the structure's response.

Another instance where beating is sometimes noticeable is during a sweep test in seismic qualification. Sweep testing is often used as an exploratory test to find resonant frequencies and equipment responses at low levels of excitation by subjecting a test specimen to a sinusoidal shake table motion having a continuously increasing frequency component. A sweep rate of 2 octaves per minute is fairly typical. If the equipment component has a well defined natural frequency then a beating response may be observed just after the table motion passes through the equipment's resonant frequency. In this situation the equipment will

still be responding at its resonant frequency but the table input motion will have now moved on to a slightly higher frequency. These closely spaced frequencies create the situation described by Eq. 4-35 and, depending on equipment damping can result in a noticeable sine beat response of the equipment. However, since the table frequency is continuously increasing the beating will last only momentarily until the frequencies move farther apart.

In the following sections the descriptions provided by both Eq. 4-31 and Eq. 4-35 will be used to develop the characterizations of a sine beat motion.

4.3.1 Maximum Acceleration

The maximum acceleration A_m , of the envelope of a sine beat is $A_m = A$. This is clear in Eq. 4-31; in Eq. 4-35 the cosine terms can sum to a maximum value of 2 which is then multiplied by the $A/2$ coefficient. When there are only a few cycles per beat, the maximum of the actual beat motion will fall somewhat below the maximum value of the envelope as peaks in the beat motion will not fall exactly on the point where the envelope reaches its maximum. Table 4.1 shows the actual peak as a decimal percentage of the envelope peak for various sine beat motions.

TABLE 4.1 MAXIMUM VALUES OF SINE BEATS

N	Ratio: A_m beat/ A_m envelope
3	0.967
5	0.987
7	0.992

Even for a small number of cycles per beat, the ratio is very nearly equal to 1.0 and in the following sections no distinction is made of this small difference.

4.3.2 Response Spectrum and Quasi-Resonant Response

The equation of motion for a SDOF system subjected to a sine beat acceleration is

$$\ddot{x} + 2\zeta\omega\dot{x} + \omega^2x = \frac{A}{2} (\cos \Omega_1 t - \cos \Omega_2 t) \quad (4-36)$$

The general solution for displacement response (assuming small damping) is

$$x(t) = e^{-\zeta\omega t} (B \sin \omega t + C \cos \omega t) \\ + M_1 \cos \omega_1 t + N_1 \sin \omega_1 t + M_2 \cos \Omega_2 t + N_2 \sin \Omega_2 t \quad (4-37)$$

where

$$M_i = (-1)^{i+1} \frac{A}{2} \frac{(\omega^2 - \Omega_i^2)}{(\omega^2 - \Omega_i^2)^2 + (2\zeta\omega\Omega_i)^2} \quad i = 1, 2$$

(4-38)

$$N_i = (-1)^{i+1} \frac{A}{2} \frac{2\zeta\omega\Omega_i}{(\omega^2 - \Omega_i^2)^2 + (2\zeta\omega\Omega_i)^2} \quad i = 1, 2$$

Using initial conditions $x(0) = \dot{x}(0) = 0$, B and C can be evaluated:

$$B = -\frac{1}{\omega} \{ \zeta\omega(M_1 + M_2) + \Omega_1 N_1 + \Omega_2 N_2 \}$$

(4-39)

$$C = -(M_1 + M_2)$$

Differentiating Eq. 4-37 twice produces the acceleration response of the SDOF system:

$$\ddot{x}(t) = \omega^2 e^{-\zeta\omega t} \{ [(\zeta^2 - 1)B + 2\zeta C] \sin \omega t + [(\zeta^2 - 1)C - 2\zeta B] \cos \omega t \}$$

$$-\Omega_1^2 (M_1 \cos \Omega_1 t + N_1 \sin \Omega_1 t) - \Omega_2^2 (M_2 \cos \Omega_2 t + N_2 \sin \Omega_2 t) \quad (4-40)$$

The steady state component $\ddot{x}_{ss}(t)$, can be expressed in a more concise form using trigonometric identities:

$$\ddot{x}_{ss}(t) = -\Omega_1^2 \sqrt{M_1^2 + N_1^2} \sin(\Omega_1 t - \theta_1) - \Omega_2^2 \sqrt{M_2^2 + N_2^2} \sin(\Omega_2 t - \theta_2) \quad (4-41)$$

where

$$\theta_i = \tan^{-1} \left(-\frac{M_i}{N_i} \right) \quad i = 1, 2 \quad (4-42)$$

At this point it becomes convenient to define two parameters, ϕ and ψ , as follows:

$$\phi = 1 + \frac{1}{2N} \quad (4-43)$$

$$\psi = 1 - \frac{1}{2N}$$

and substitute these into Eq. 4-34 (using $\Omega_t = 2N\Omega_b$ from Eq. 4-28) to express Ω_1 and Ω_2 in terms of Ω_t ; thus:

$$\Omega_1 = \Omega_t \phi \quad (4-44)$$

$$\Omega_2 = \Omega_t \psi$$

This gives a clearer physical interpretation of the problem as only the SDOF natural frequency ω and the test (or floor motion) frequency Ω_t are needed in the formulation. The 't' subscript on Ω_t can now be dropped and future reference to Ω will implicitly mean Ω_t .

Utilizing the two new parameters, other terms in the equations of motion can be simplified to involve ϕ , ψ and Ω , instead of 1 and 2 subscripts. After some algebraic manipulation with Eqs. 4-38 and 4-44, M_1, N_1, M_2, N_2 can be reduced to $M_\phi, N_\phi, M_\psi, N_\psi$ as follows:

$$M_{\phi} = \frac{A}{2} \frac{(1-(u_{\phi})^2)^2}{(1-(u_{\phi})^2)^2 + (2\zeta u_{\phi})^2}$$

$$N_{\phi} = \frac{A}{2} \frac{2\zeta u_{\phi}}{(1-(u_{\phi})^2)^2 + (2\zeta u_{\phi})^2}$$

(4-45)

$$M_{\psi} = -\frac{A}{2} \frac{(1-(u_{\psi})^2)^2}{(1-(u_{\psi})^2)^2 + (2\zeta u_{\psi})^2}$$

$$N_{\psi} = -\frac{A}{2} \frac{2\zeta u_{\psi}}{(1-(u_{\psi})^2)^2 + (2\zeta u_{\psi})^2}$$

Parameters B and C from Eq. 4-39 can be rewritten as

$$B = -\{\zeta(M_{\phi} + M_{\psi}) + u(\phi N_{\phi} + \psi N_{\psi})\}$$

$$C = -(M_{\phi} + M_{\psi})$$

(4-46)

Finally, as the end result the acceleration response can be rewritten in the following manner:

$$\ddot{x}(t) = \omega^2 e^{-\zeta\omega t} \{[(\zeta^2 - 1)B + 2\zeta C] \sin \omega t + [(\zeta^2 - 1)C - 2\zeta B] \cos \omega t\}$$

$$- \frac{A}{2} (u_{\phi})^2 \rho_{\phi} \sin(\Omega_{\phi} t - \theta_{\phi})$$

$$- \frac{A}{2} (u_{\psi})^2 \rho_{\psi} \sin(\Omega_{\psi} t - \theta_{\psi})$$

(4-47)

where

$$\rho_{\phi} = [(1-(u\phi)^2)^2 + (2\zeta u\phi)^2]^{-1/2} \quad (4-48)$$

$$\rho_{\psi} = [(1-(u\psi)^2)^2 + (2\zeta u\psi)^2]^{-1/2}$$

and

$$\theta_{\phi} = \tan^{-1} \left(-\frac{M_{\phi}}{N_{\phi}} \right) \quad (4-49)$$

$$\theta_{\psi} = \tan^{-1} \left(-\frac{M_{\psi}}{N_{\psi}} \right)$$

SDOF amplifications (assumes $A = 1.0$) as described by Eq. 4-47 are plotted in Fig. 4.5 as a function of frequency ratio u for various numbers of cycles per beat N and 1% damping. The values of N are shown beside their respective curves.

It is interesting to compare the sine beat response with the response due to a limited duration sine motion (Eq. 4-10). For a very large number of cycles per beat, both ϕ and ψ approach limiting values of 1. Hence, in the limit as $N \rightarrow \infty$

$$\begin{aligned} \rho_{\phi} &= \rho_{\psi} \\ M_{\phi} &= -M_{\psi} \\ N_{\phi} &= -N_{\psi} \end{aligned} \quad (4-50)$$

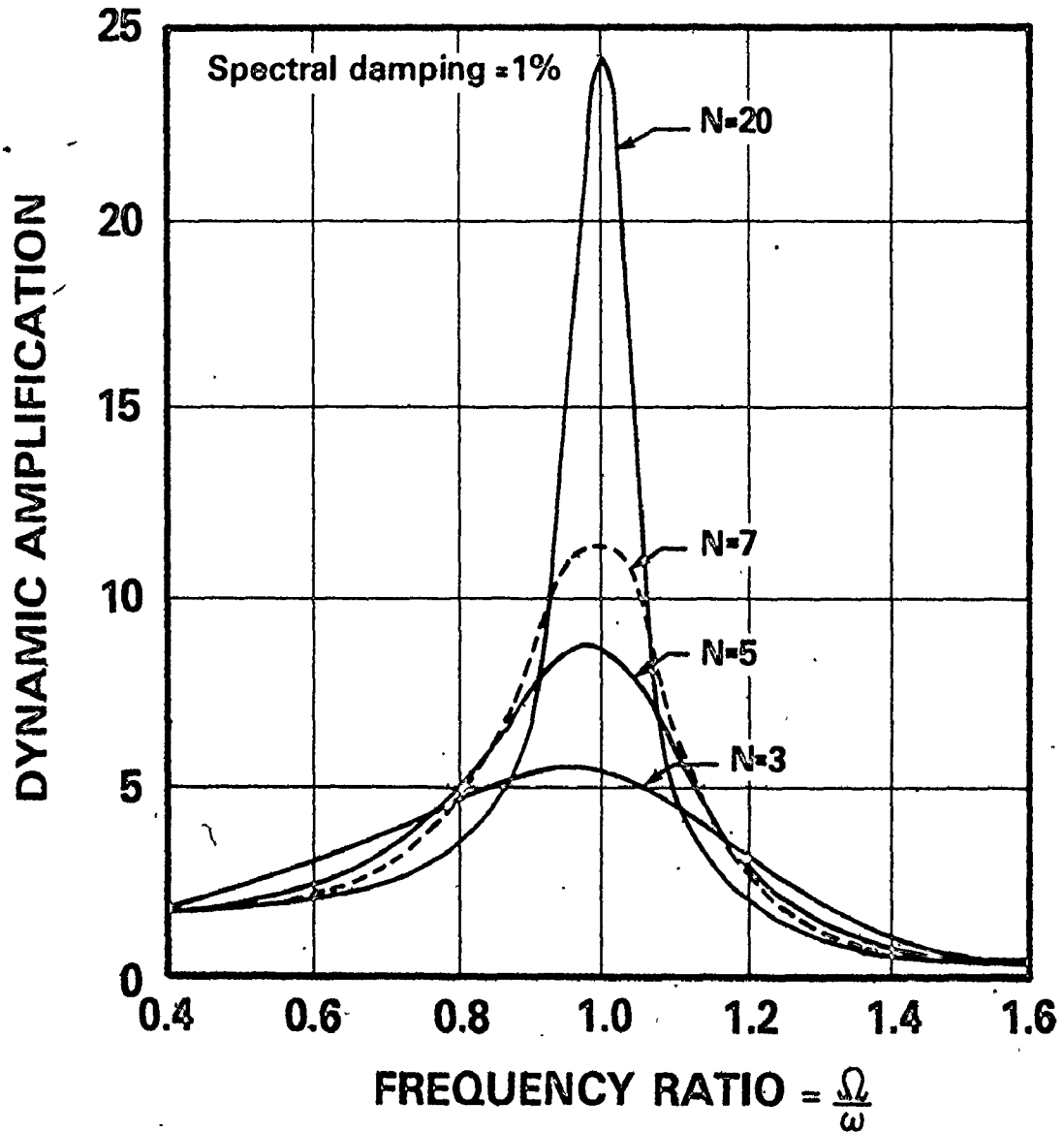


FIG. 4.5 SDOF RESPONSE TO A SINE BEAT

consequently, $B = C = 0$

$$\theta_{\phi} = \theta_{\psi} \quad (4-51)$$

Only steady-state terms remain and these can be reduced to

$$\ddot{x}_{ss}(t) = -A u^2 \rho \sin(\Omega t - \theta) \quad (4-52)$$

At resonance the maximum value is

$$|\ddot{x}_{ss}(t)|_{\max} = \frac{A}{2\zeta} \quad (4-53)$$

Eqs. 4-52 and 4-53 are the same as those obtained for sinusoidal motion. Intuitively this behaviour is to be expected since a sine beat having a large number of cycles per beat will have many cycles occurring in the region near the peak of the beat envelope. A SDOF system will see these cycles as being essentially a constant amplitude sine wave which results in the SDOF response approaching the levels of response due to a steady-state sinusoidal excitation.

The next step in examining SDOF response considers the specialized case of resonant amplification at zero damping when N is small. Under these conditions the terms in the general response (Eq. 4-47) reduce as follows:

$$\begin{aligned}
 M_{\phi} &= \frac{A}{2\omega^2(1-\phi^2)} \\
 M_{\psi} &= -\frac{A}{2\omega^2(1-\psi^2)} \\
 N_{\phi} &= N_{\psi} = 0 \\
 B &= 0 \\
 C &= \frac{A}{2\omega^2} \left[\frac{1}{1-\psi^2} - \frac{1}{1-\phi^2} \right] \\
 \theta_{\phi} &= \theta_{\psi} = \frac{\pi}{2}
 \end{aligned} \tag{4-54}$$

Hence, resonant response at zero damping $\ddot{x}_{ro}(t)$, can be written directly in terms of ϕ and ψ :

$$\ddot{x}_{ro}(t) = \omega^2(-C) \cos \omega t + (\Omega\phi)^2 M_{\phi} \cos \Omega\phi t + (\Omega\psi)^2 M_{\psi} \cos \Omega\psi t \tag{4-55}$$

Replacing the terms in M , C and Ω with Eqs. 4-54 yields

$$\ddot{x}_{ro}(t) = \frac{A}{2} \left\{ \left[\frac{1}{1-\phi^2} - \frac{1}{1-\psi^2} \right] \cos \omega t - \frac{\phi^2}{1-\phi^2} \cos \omega\phi t + \frac{\psi^2}{1-\psi^2} \cos \omega\psi t \right\} \tag{4-56}$$

The time required for N complete cycles is

$$t = \frac{2\pi N}{\omega} \tag{4-57}$$

and at this time the cosine terms in Eq. 4-56 are

$$\begin{aligned}\cos \omega t &= \cos 2N\pi = +1 \\ \cos \omega \phi t &= \cos(2N+1)\pi = -1 \\ \cos \omega \psi t &= \cos(2N-1)\pi = -1\end{aligned}\tag{4-58}$$

Applying these conditions to $\ddot{x}_{ro}(t)$ provides the quasi-resonant response amplification Q at the end of N cycles of sine beat motion:

$$Q = \frac{1}{2} \left\{ \frac{1}{1-\phi^2} - \frac{1}{1-\psi^2} + \frac{\phi^2}{1-\phi^2} - \frac{\psi^2}{1-\psi^2} \right\}\tag{4-59}$$

Substituting for ϕ and ψ in terms of N , and after a considerable algebraic reduction;

$$Q = \frac{1}{2} \left| \frac{64N^3}{(-4N-1)(4N-1)} \right|\tag{4-60}$$

Neglecting the -1 terms in the denominator provides an approximate expression for undamped Q :

$$Q \approx 2N\tag{4-61}$$

For $N=3$ the error in Q using the approximation of Eq. 4-61 is less than 1% and this error decreases for larger values of N . The benefit of this simple expression is that it establishes, very accurately, the upper bound on response for any SDOF system subjected to a single sine beat pulse.

To summarize the resonant response, Fig. 4.6 shows quasi-resonant amplifications Q as functions of damping for several values of N . The Q values are the maximum values of $\ddot{x}(t)$ defined by Eq. 4-47 with $u = 1$. The resonant amplification curve for steady-state sinusoidal motion ($Q = 1/2\zeta$) is also shown on the plot for comparison purposes. The upper bound on Q of twice the number of cycles per beat is the point at which each curve intersects the vertical axis.

4.3.3 Cumulative Damage Process

For a sine beat motion the first peak occurs when $\Omega_t t = \pi/2$, the second peak at $3\pi/2$, and so on, until the sine beat ends by which time $2N$ peaks will have occurred. Mathematically, the times at which these peaks occur are given by

$$t_i = \frac{1}{4f_t} (2i-1) \quad i = 1, 2, \dots, 2N \quad (4-62)$$

where $f_t = \Omega_t/2\pi$. To evaluate the number of equivalent cycles N_{eq} , the enveloping function

$$R_i = A \sin \Omega_b t_i \quad (4-63)$$

must be evaluated at each of the times t_i given above. (R_i is the same parameter as in Eq. 3-2.) Substituting Eq. 4-62 into Eq. 4-63 and using the fact that $f_t = 2Nf_b$, results in

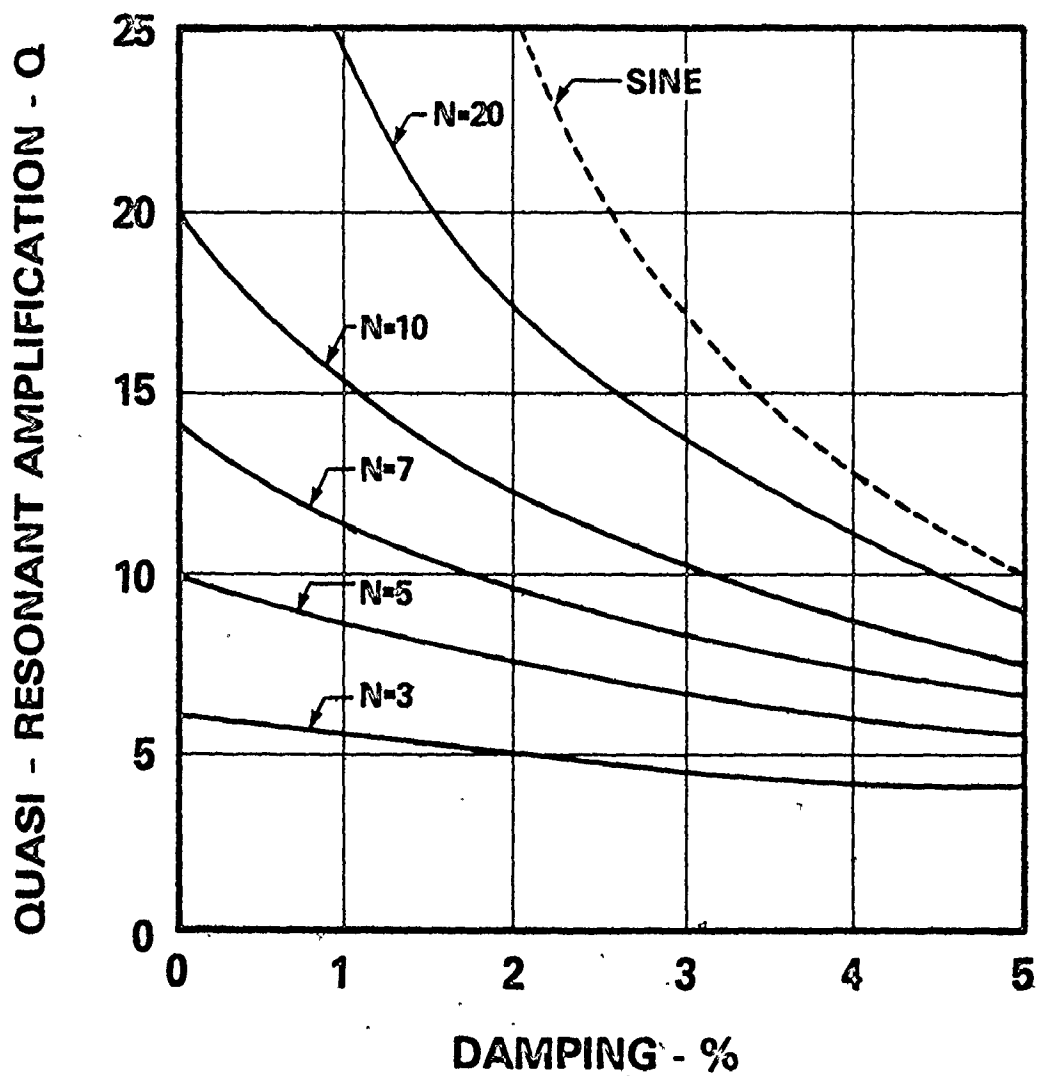


FIG. 4.6 QUASI - RESONANT AMPLIFICATIONS FOR SINE BEAT MOTIONS

$$R_i = A \sin \frac{\pi}{4N} (2i-1) \quad i = 1, 2, \dots, 2N \quad (4-64)$$

Owing to the symmetry in the sine beat, the number of equivalent cycles N_{eq} can be evaluated by using one-half the beat pulse: thus,

$$\begin{aligned} N_{eq} &= \frac{1}{2} \sum_{i=1}^{2N} \left| \sin \frac{\pi}{4N} (2i-1) \right|^\beta \\ &= \sum_{i=1}^N \left| \sin \frac{\pi}{4N} (2i-1) \right|^\beta \end{aligned} \quad (4-65)$$

where it has been assumed that the reference peak is $R_p = A$ (see Eq. 3-2). Figure 4.7 is a plot of the number of equivalent cycles N_{eq} for various durations of beat pulse and for comparison the upper bound case of a sinusoidal motion is also plotted.

The number of applied cycles shown on the x-axis of Fig. 4.7 covers the range which might be generally useful in seismic qualification testing. It is readily apparent from this plot that a sine beat test is much less severe, in terms of a cumulative damage process, than is a sinusoidal motion of the same number of cycles. Values of β , of 1, 3 and 5 result in sine beat N_{eq} values which are approximately 63%, 42% and 33%, respectively, below those achieved for the sinusoidal case.

4.3.4 Root-Mean-Square Acceleration and Duration

The variation of RMS acceleration as a function of time for a sine beat motion is:

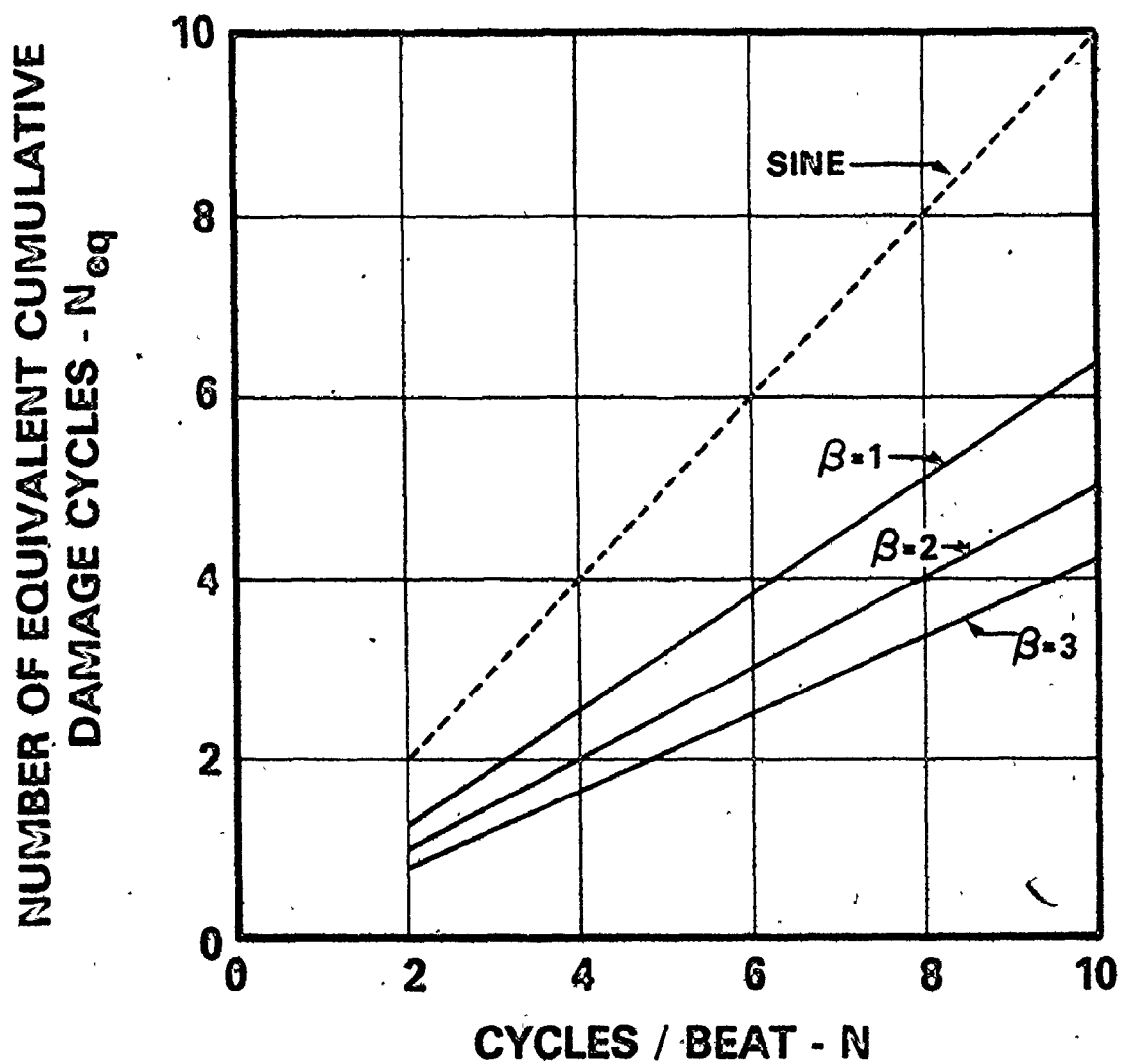


FIG. 4.7 CYCLES OF CUMULATIVE DAMAGE
FOR A SINE BEAT

$$\text{CRF}(t) = \left\{ \frac{A^2}{4t} \int_0^t (\cos \Omega_1 \tau - \cos \Omega_2 \tau)^2 d\tau \right\}^{1/2}. \quad (4-66)$$

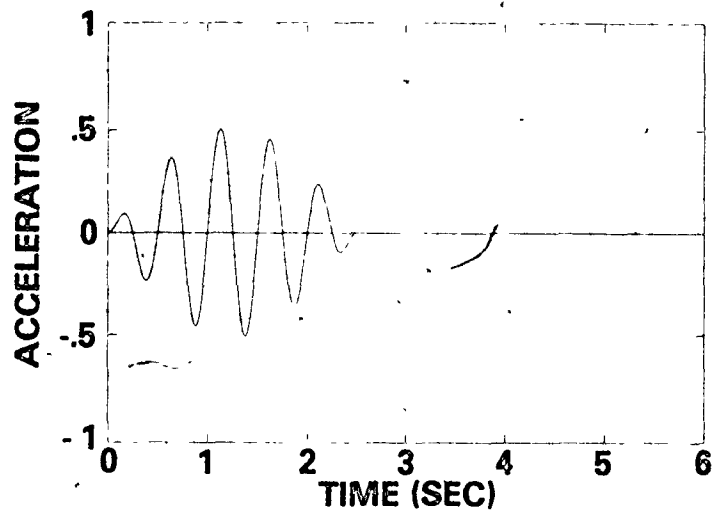
Expanding the integrand, integrating and substituting for Ω_1 and Ω_2 in terms of Ω , ϕ and ψ finally gives

$$\begin{aligned} \text{CRF}(t) = \left\{ \frac{A^2}{4t} \left[t + \frac{1}{4\Omega\phi} \sin 2\Omega\phi t + \frac{1}{4\Omega\psi} \sin 2\Omega\psi t - \frac{1}{\Omega(\phi+\psi)} \sin \Omega(\phi+\psi)t \right. \right. \\ \left. \left. - \frac{1}{\Omega(\phi-\psi)} \sin \Omega(\phi-\psi)t \right] \right\}^{1/2} \quad (4-67) \end{aligned}$$

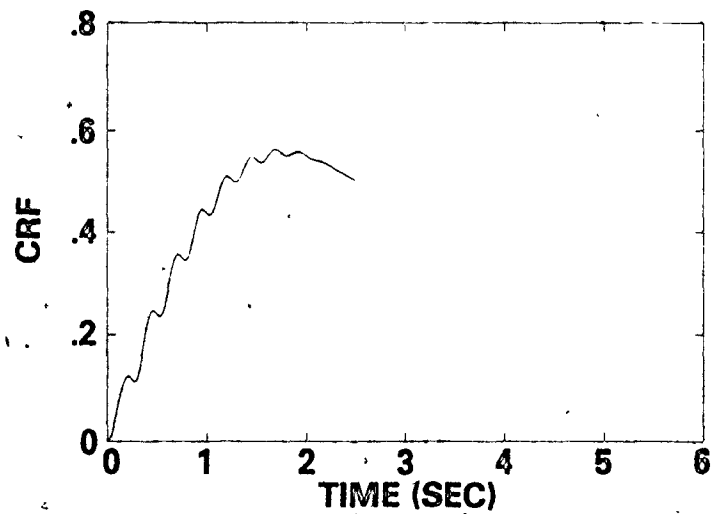
The time at the end of a N cycle beat pulse is $t = NT$, hence all sine terms in Eq. 4-67 become zero and $\text{CRF}(t)$ reduces to the RMS acceleration for the entire pulse:

$$\begin{aligned} \text{CRF} &= \left\{ \frac{A^2}{4t} [t] \right\}^{1/2} \\ \text{RMS} &= \frac{A}{2} \quad (4-68) \end{aligned}$$

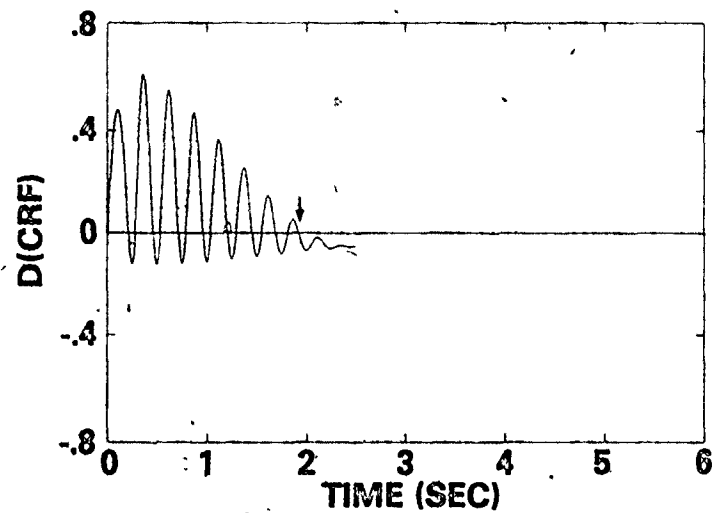
Therefore, in a sine beat pulse having any number of cycles the RMS acceleration for the whole pulse is simply one-half the peak value of the beat envelope. A 5-cycle sine beat motion and its CRF are shown in Figs. 4.8a and 4.8b. The peaking and subsequent decline of the CRF to a final value of $A/2$ indicates that the slope of the CRF permanently becomes negative before the end of the pulse and hence the duration of strong motion will end before the beat pulse is over. The mark in Fig. 4.8c points to the time when the derivative permanently goes negative.



(a) 5-cycle sine beat pulse



(b) Cumulative RMS Function



(c) Derivative of CRF

FIG. 4.8 CRF AND D(CRF) FOR A SINE BEAT

It is useful to note the contribution made by each of the terms in the CRF. Rewriting Eq. 4-67 and substituting $\Omega = 2\pi/T$; $\phi + \psi = 2$; and $\phi - \psi = 1/N$, gives

$$\text{CRF}(t) = \left\{ \frac{A^2}{4t} \left[t + \frac{N}{4\pi(2N+1)} \sin 2\pi \frac{(2N+1)}{N} \frac{t}{T} + \frac{N}{4\pi(2N-1)} \sin 2\pi \frac{(2N-1)}{N} \frac{t}{T} - \frac{NT}{2\pi} \sin \frac{2\pi}{N} \frac{t}{T} - \frac{T}{4\pi} \sin 4\pi \frac{t}{T} \right] \right\}^{1/2} \quad (4-69)$$

After each half-cycle of sine motion the ratio t/T will be an integer multiple of $1/2$ and therefore the last trigonometric term will always be zero. In the case of the first and second trigonometric terms, their coefficients will be much less than unity even for small N values (i.e., for $N=3$, the coefficients of the first and second terms are 0.034 and 0.048, respectively). These terms can be neglected. The final result is an approximate expression for the cumulative RMS function which is very similar to the CRF equation for a sine motion (Eq. 4-19):

$$\text{CRF}(t) \approx \left\{ \frac{A^2}{4t} \left[t - \frac{NT}{2\pi} \sin \frac{2\pi}{N} \frac{t}{T} \right] \right\}^{1/2} \quad (4-70)$$

Reiterating a previous comment, owing to the assumptions on the values of t/T this equation is only valid at times when a number of complete half-cycles have occurred.

The general expression for peak amplitudes of a beat motion has been given in Eq. 4-64. Using this formulation it is possible to find the first and last half-sines which have power levels above the average pulse power $(A/2)^2$. Mathematically, these peaks occur when

$$|R_i|^2 \geq \left(\frac{A}{2}\right)^2 \quad (4-71)$$

The first and last peaks to satisfy this condition mark the beginning and end, respectively, of the strong motion phase. Taking the square root of both sides of Eq. 4-71 and substituting into Eq. 4-64 gives the condition which must exist for the strong motion phase:

$$\sin \left[\frac{\pi}{4N} (2i-1) \right] \geq \frac{1}{2} \quad i = 1, 2, \dots, 2N \quad (4-72)$$

The smallest index value i , to satisfy this relationship, say i_1 , is the first peak of strong motion. This occurs in the first half of the beat pulse (when $i \leq N$). Similarly, the smallest value of i , say i_2 , in the interval $N+1 \leq i \leq 2N$ which satisfies Eq. 4-72 is the last strong motion peak. The number of cycles of strong motion N_{sm} , is given by

$$N_{sm} = \frac{1}{2} (i_2 - i_1 + 1) \quad (4-73)$$

and the duration of strong motion T_d is

$$T_d = N_{sm} T \quad (4-74)$$

where T is the period of the sine beat motion. This procedure is illustrated by Fig. 4.9 where peaks have been numbered $i=1$ to $i=10$, and the RMS level is indicated. Peaks numbered $i=3$ to $i=8$ inclusive lie above the RMS level and are in the strong motion phase.

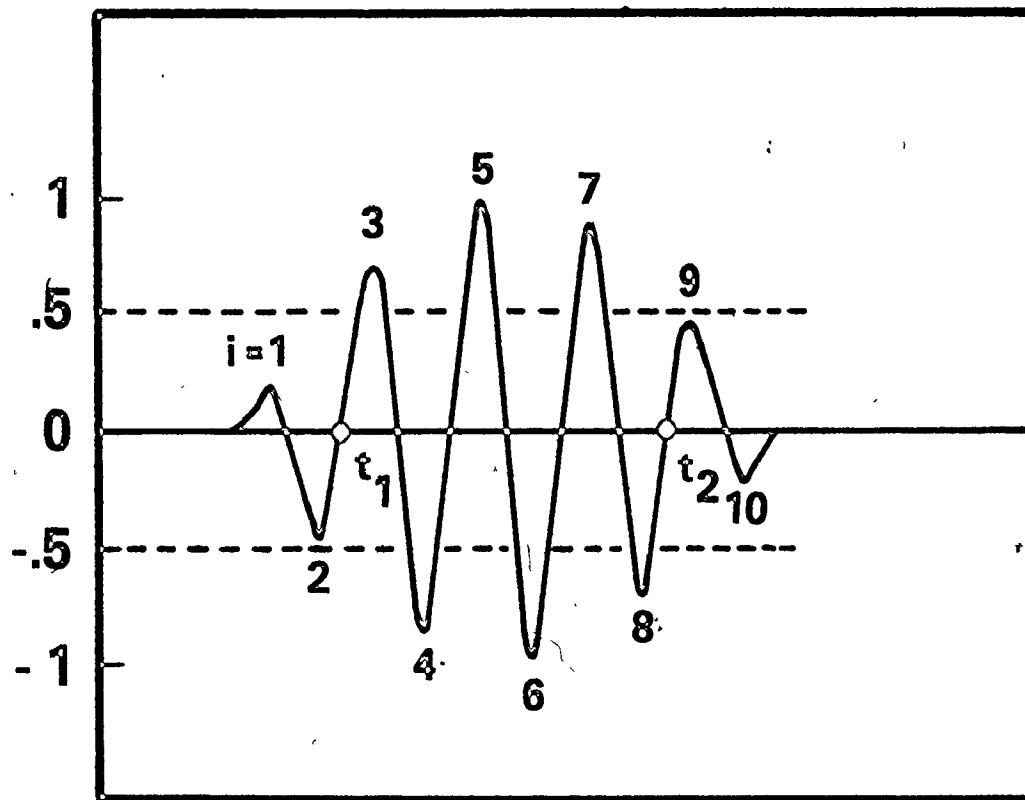


FIG. 4.9 DETERMINING THE PHASE OF STRONG BEAT MOTION

Equation 4-72 can be solved for i in terms of N giving

$$i \geq \frac{1}{2} \left\{ \frac{4N}{\pi} \sin^{-1} \left(\frac{1}{2} \right) + 1 \right\} \quad (4-75)$$

therefore
$$i \geq \frac{N}{3} + \frac{1}{2}$$

This will give non-integer values for i , consequently the appropriate index number for the first peak of strong motion is the first integer (i_1) greater than the i calculated in Eq. 4-75. For example, in the case cited above for 5 cycles/beat, Eq. 4-75 gives $i_1 = 2.166$ and therefore the correct value for i_1 is the next largest integer, namely $i_1 = 3$.

Table 4.2 and Fig. 4.10 show some results of Eq. 4-75 applied to sine beats of various lengths. Table 4.2 gives a few sets of duration data in terms of "strong" peaks and "strong" cycles (N_{sm}) while Fig. 4.10 compares the N_{sm} with the total number of beat cycles. Since values of N_{sm} have been expressed in terms of complete cycles the line in Fig. 4.10 increases in a step fashion from one integer value of N_{sm} to the next. The importance of this plot is to show that essentially a constant relationship exists between N_{sm} and N for a sine beat of any length; that is

$$N_{sm} = \frac{2}{3} N \quad (4-76)$$

where N_{sm} should be rounded off to the nearest integer. Eq. 4-76 is the solid line through the steps in Fig. 4.10. For comparison purposes, the line for a pure sinusoid is also shown on the plot, reiterating the

TABLE 4.2 DURATIONS OF STRONG MOTION FOR SINE BEATS

CYCLES/BEAT (N)	PEAKS* $\geq \frac{A}{2}$ (first; last) ($i_1; i_2$)	DURATION† N_{sm} (cycles)
3	2 ; 5	2
5	3 ; 8	3
6	3 ; 10	4
7	3 ; 12	5
9	4 ; 15	6
10	4 ; 17	7

* referring to i values (i.e. Eq. 4-72)

† using Eq. 4-70

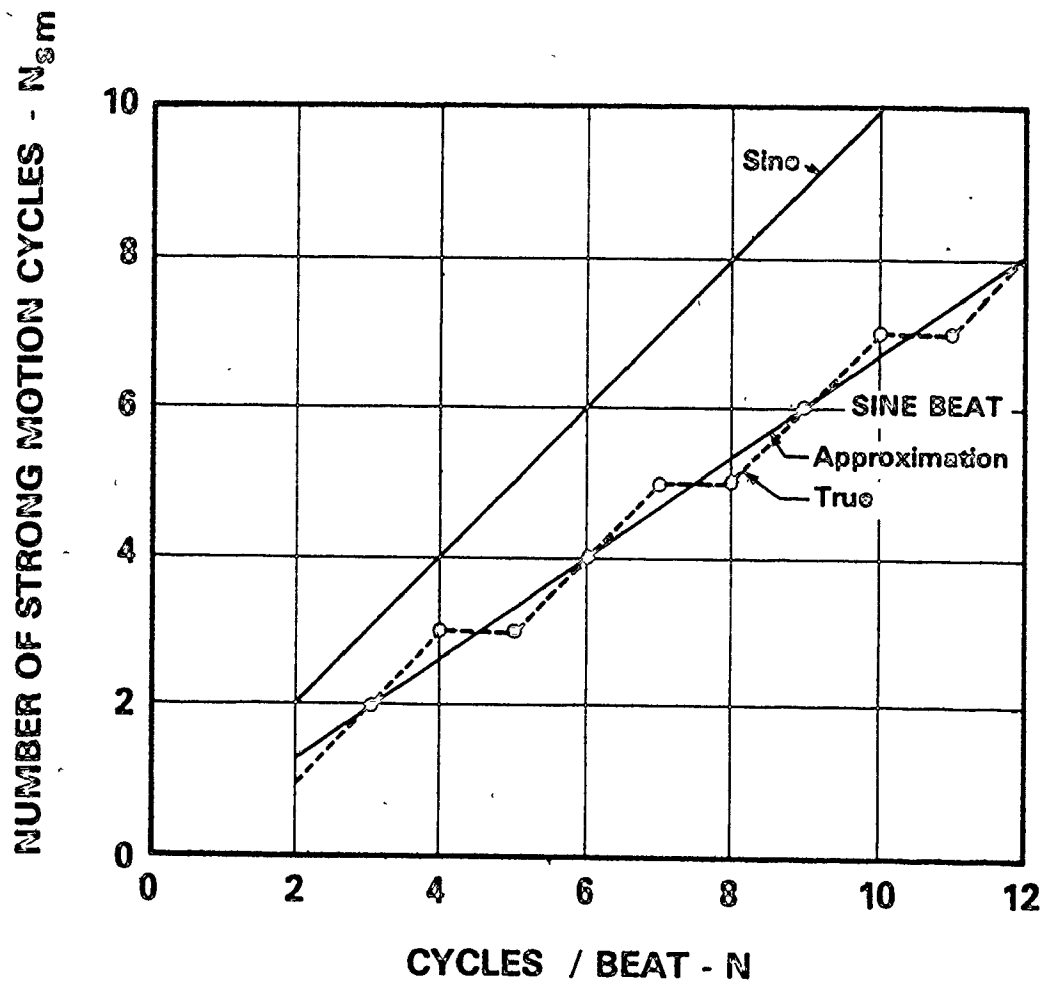


FIG. 4.10 CYCLES OF STRONG MOTION FOR A SINE BEAT

observation of section 4.3.4 that for sinusoidal motion, all cycles are "strong" cycles.

Now that a method for finding the duration of strong motion has been developed the strong phase RMS acceleration can be calculated. The terms within the square brackets of Eq. 4-70 must be evaluated over the interval of strong motion T_d , as these are the product of an integration. Letting t_1 be the time at which the i_1 half-cycle begins and t_2 be the time at which the i_2 half-cycle ends (see Fig. 4-9) then $T_d = t_2 - t_1$ is the duration of strong motion. Evaluating the CRF over this interval gives

$$\text{CRF} \int_{t_1}^{t_2} = \left\{ \frac{A^2}{4T_d} \left[t_2 - \frac{NT}{2\pi} \sin \frac{2\pi t_2}{NT} - t_1 + \frac{NT}{2\pi} \sin \frac{2\pi t_1}{NT} \right] \right\}^{1/2} \quad (4-77)$$

Although T appears in Eq. 4-77 the CRF is actually independent of period because the ratios t_1/T , t_2/T and T/T_d are constant once the number of cycles per beat have been defined. This can lead to further simplification as T can conveniently be given a value of 1 second and it can be stipulated that the CRF is considered only for half-cycle increments of the sine beat. Hence, t_1 and t_2 must have either whole or half-integer values. As an example, if $i_1 = 2$ (the second peak of sine beat motion is the first peak in the strong phase) then $t_1 = 0.5$ sec since the half-cycle containing the second peak begins at 0.5 seconds. Similarly, if $i_2 = 8$ then $t_2 = 4$ sec. On this basis simple relationships can be set up to equate the times t_1 and t_2 to the strong motion peaks i_1 and i_2 as follows

$$t_1 = \frac{1}{2} (i_1 - 1) \quad (4-78)$$

$$t_2 = \frac{i_2}{2}$$

Values for i_1 and i_2 are available from Table 4.2 or Eq. 4-75.

The t_1 and t_2 values above cause the two sine terms in Eq 4-77 to be of equal value but opposite in sign because of the anti-symmetrical occurrence of the peaks i_1 and i_2 about the zero line. Eq. 4-77 therefore can be reduced to

$$[\text{CRF}]_{T_d} \approx \left\{ \frac{A^2}{4T_d} \left[T_d - \frac{N}{\pi} \sin \frac{2\pi}{N} t_1 \right] \right\}^{1/2} \quad (4-79)$$

This is the RMS acceleration for the strong motion phase of an N cycle sine beat.

Numerically evaluating Eq. 4-79 for several N values reveals that strong phase RMS accelerations closely cluster around a value of approximately 0.6A. The slight scatter around this value is due to the approximations made in the derivation of Eq. 4-79.

4.4 Decaying Sinusoidal Motion

The use of a decaying sinusoid to describe an earthquake has been applied on a theoretical basis by several researchers. Evidence from seismographic records indicates that such motions do occur during some earthquakes, as for example, at increasing distance from the source where ground motion tends to a harmonic oscillation. The accelerogram recorded at Golden Gate Park, San Francisco, March 22, 1957 shows a distinctive decaying sinusoid at a constant rate of damping. Decaying sinusoidal motion can also produce structure and equipment responses very similar to those resulting from random or artificially generated earthquake motions (9).

A segment of a decaying sinusoidal acceleration

$$\ddot{z}(t) = Ae^{-\alpha t} \sin \Omega t \quad (4-80)$$

is illustrated in Fig. 4.11. The exponent α , can be written as a product of a decay parameter μ and the sinusoidal frequency Ω , therefore the decaying sinusoid may be expressed as

$$\ddot{z}(t) = Ae^{-\mu\Omega t} \sin \Omega t \quad (4-81)$$

The following sections outline the characterizations of a decaying sinusoidal motion.

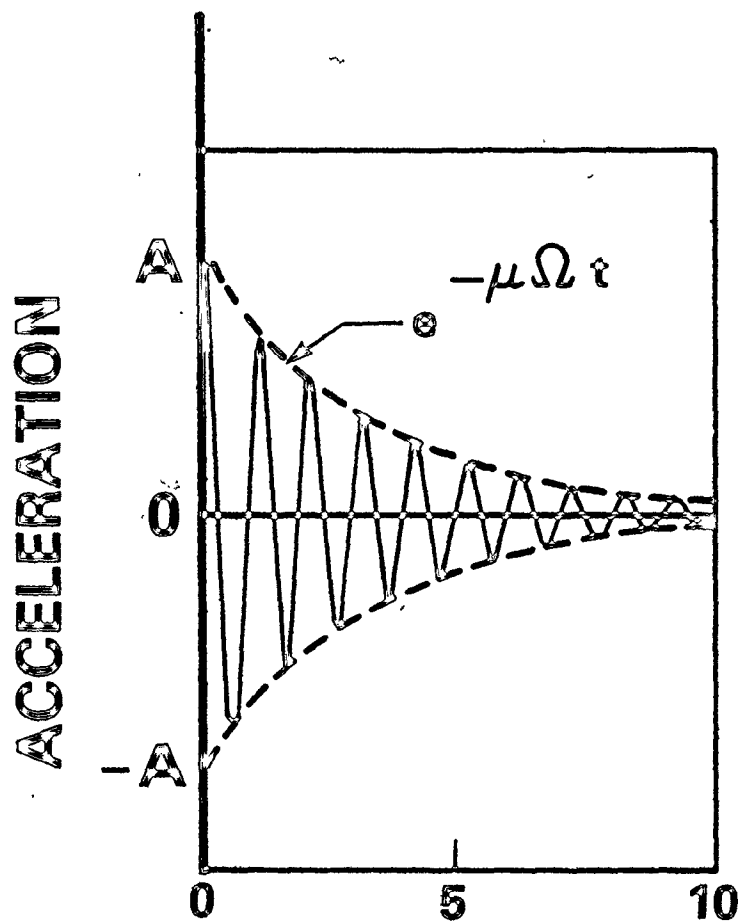


FIG. 4.11 DECAYING SINUSOID

4.4.1 Maximum Acceleration

The decaying sinusoid described by Eq. 4-81 will always have a maximum peak value A_m which is less than the value of the coefficient A . When μ is small this difference will be small and for the limiting case of $\mu=0$ the equation reduces to a sinusoid with constant amplitude A . At increasingly large levels of μ the ratio A_m/A can become significantly less than 1.0. Knowing that the first peak of the sinusoid will occur when $\omega t = \pi/2$, then A_m/A can be evaluated as

$$\frac{A_m}{A} = e^{-\mu \frac{\pi}{2}} \quad (4-82)$$

The decaying sinusoid described by Eq. 4-81 is in a convenient form for mathematical analysis since the coefficient A is general. This form will be used in subsequent sections. In some testing applications however, it may be necessary to create a decaying sinusoidal shake table motion having a specified maximum acceleration. This can easily be achieved by modifying the amplitude coefficient in Eq. 4-81 by a scale factor $A^* = A/A_m$, such that

$$\ddot{z}(t) = A^* e^{-\mu \omega t} \sin \omega t \quad (4-83)$$

Unless $\mu=0$, A^* will be greater than the desired maximum table motion A , but the rate of decay will give the first peak of the motion at the required A amplitude. Eq. 4-83 is in a convenient form for programming into a computer controlled test facility to create a decaying sinusoidal table motion having any desired combination of parameters.

4.4.2 Response Spectrum and Quasi-Resonant Response

The relative response of a SDOF system to a decaying sinusoidal base motion is described by the following differential equation

$$\ddot{x} + 2\zeta\omega\dot{x} + \omega^2 x = A e^{-\mu\Omega t} \sin \Omega t \quad (4-84)$$

Complex algebra is a convenient method for solving this type of equation since the right-hand side may be written as

$$e^{-\mu\Omega t} \sin \Omega t = \text{Im}[e^{(i-\mu)\Omega t}] \quad (4-85)$$

where Im denotes the imaginary part, and $i = \sqrt{-1}$, hence the complementary solution is of the form

$$x_p = G e^{(i-\mu)\Omega t} \quad (4-86)$$

where G is a constant.

The general solution for displacement response is

$$x(t) = e^{-\zeta\omega t} (C \cos \omega t + B \sin \omega t) + \frac{A}{\omega^2} \frac{e^{-\mu\Omega t}}{V_1^2 + V_2^2} (V_1 \sin \Omega t - V_2 \cos \Omega t) \quad (4-87)$$

where

$$V_1 = 1 - u^2 + (\mu u)^2 - 2\zeta\mu u$$

$$V_2 = 2u(\zeta - \mu)$$

$$B = \frac{A}{\omega^2} \frac{1}{V_1^2 + V_2^2} ((\zeta - \mu u) V_2 - u V_1) \quad (4-88)$$

$$C = \frac{A}{\omega^2} \frac{V_2}{V_1^2 + V_2^2}$$

and B and C were evaluated using initial conditions of $x(0) = \dot{x}(0) = 0$.

The acceleration response of the SDOF system is given by

$$\begin{aligned} \ddot{x}(t) = & \omega^2 e^{-\zeta \omega t} \{ [(\zeta^2 - 1) C - 2\zeta B] \cos \omega t + [(\zeta^2 - 1) B + 2\zeta C] \sin \omega t \} \\ & + \frac{A u^2 e^{-\mu \Omega t}}{V_1^2 + V_2^2} \{ [(1 - \mu)^2 V_2 - 2\mu V_1] \cos \Omega t + [(\mu^2 - 1) V_1 - 2\mu V_2] \sin \Omega t \} \end{aligned} \quad (4-89)$$

The dynamic response of a 1% damped SDOF system due to a decaying sinusoid, as described by Eq. 4-89 above, is plotted in Fig. 4.12 as a function of frequency ratio and decay parameter μ . The coefficient A has been set equal to one.

The SDOF response can be readily compared to the response due to a sine motion by considering the value of μ . When μ is zero, there is no envelope decay and all cycles are full amplitude. Eqs. 4-88 and 4-89 reduce to the more simplified versions presented in section 4.2 for sinusoidal response and the exponential involving μ is unity hence, the equation for acceleration response becomes equivalent to Eq. 4-7, the response due to a constant amplitude sine motion.

The resonant response of a SDOF system can be examined by reducing Eqs. 4-88 to the following forms:

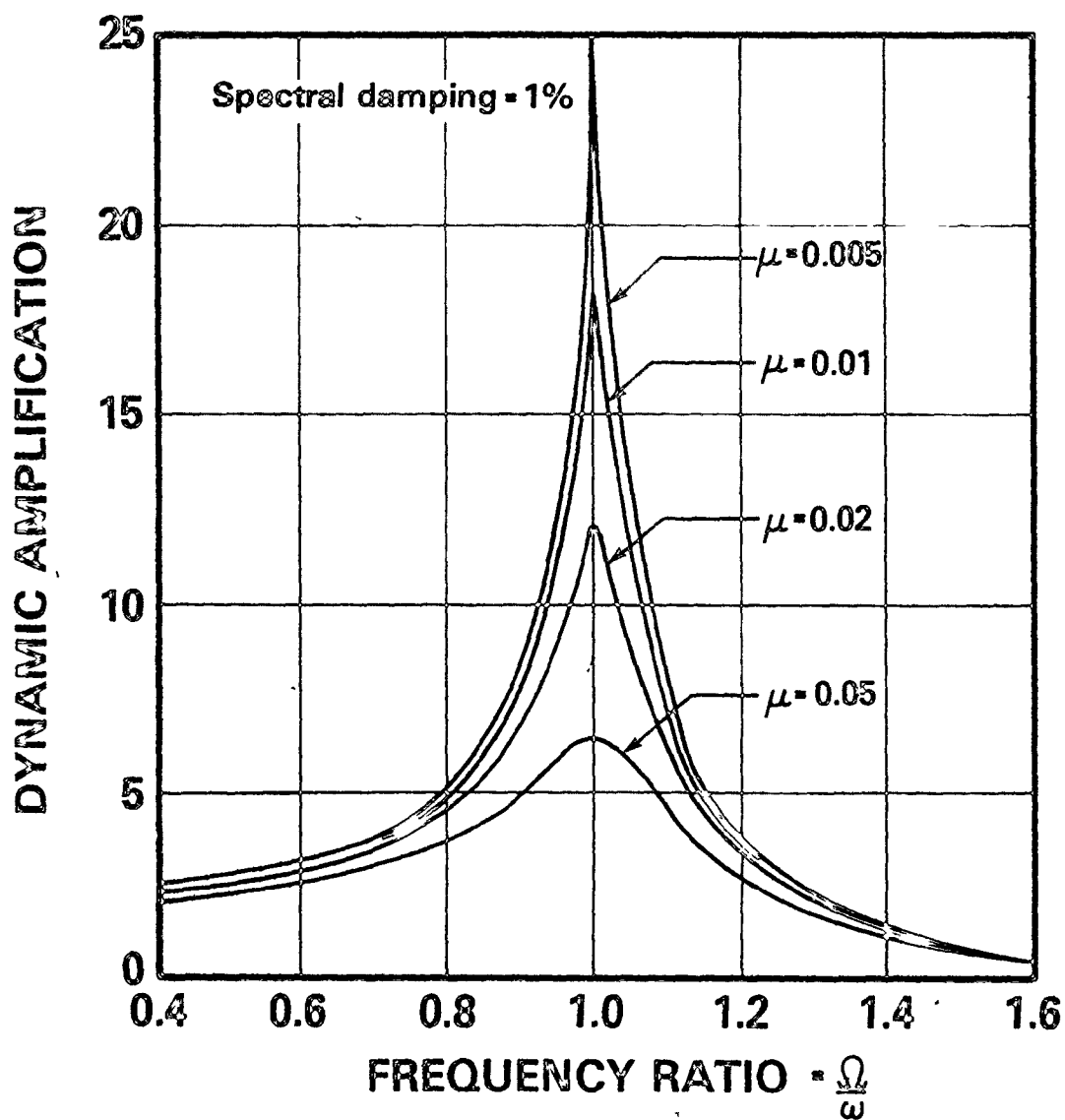


FIG. 4.12 SDOF RESPONSE TO A DECAYING SINUSOID


$$V_1 = \mu^2 - 2\zeta\mu$$

$$V_2 = 2(\zeta - \mu)$$

$$B = \frac{A}{\omega^2} \frac{1}{V_1^2 + V_2^2} ((\zeta - \mu) V_2 - V_1) \quad (4-90)$$

$$C = \frac{A}{\omega^2} \frac{V_2}{V_1^2 + V_2^2}$$

After considerable algebraic reduction, and by neglecting all terms higher than first order in the numerator, the SDOF acceleration at resonance may be approximated by



$$\ddot{x}_r(t) = [e^{-\mu\Omega t} - e^{-\zeta\Omega t}] \frac{V_2 \cos\Omega t}{V_1^2 + V_2^2} \quad (4-91)$$

This equation is convenient for evaluating the resonant amplification factors for a pair of ζ and μ values. The exponential functions control the overall response amplitude decay and a reasonable approximation of the time of maximum response can be made by assuming that the peak of the oscillating component described by the cosine term will occur near the peak of the exponential envelope. For the low dampings assumed in the approximations i.e., $\leq 15\%$ damping, this will be true because the envelope of the response will stay close to its maximum value long enough for the cosine term to oscillate through a peak. Thus, to find the maximum value of $\ddot{x}_r(t)$:

$$\frac{d}{dt} (e^{-\mu\Omega t} - e^{-\zeta\Omega t}) = 0 \quad (4-92)$$

hence

$$\Omega t = \frac{1}{\zeta - \mu} \ln \left(\frac{\zeta}{\mu} \right) \quad (4-93)$$

By back-substituting into Eq. 4-91 and considering that $\cos \Omega t$ attains a value close to unity, then the resonant amplifications are

$$|\ddot{x}_r(t)|_{\max} \approx |(e^{-\mu\Omega t} - e^{-\zeta\Omega t}) \frac{2(\zeta - \mu)}{(\mu^2 - 2\zeta\mu)^2 + (2(\zeta - \mu))^2}| \quad (4-94)$$

Figure 4.13 is a plot of resonant amplification factors for SDOF systems having various damping ratios ζ , as a function of the decay parameter μ of the input motion. These curves have been obtained using a full solution without the successive stages of approximation used in deriving Eq. 4-94. Approximations using Eq. 4-94 are generally in very good agreement with the values shown in Fig. 4.13 except for some slight discrepancies at larger damping levels because higher order terms were dropped in the approximation process. Amplifications for the specialized case of $\mu=0$ are illustrated at their steady-state values of $1/2\zeta$.

4.4.3 Cumulative Damage Process

A convenient interpretation of a decaying sinusoid is to consider a SDOF system undergoing a damped free vibration decay. The level of response at the i^{th} peak (at time t_i) is given by

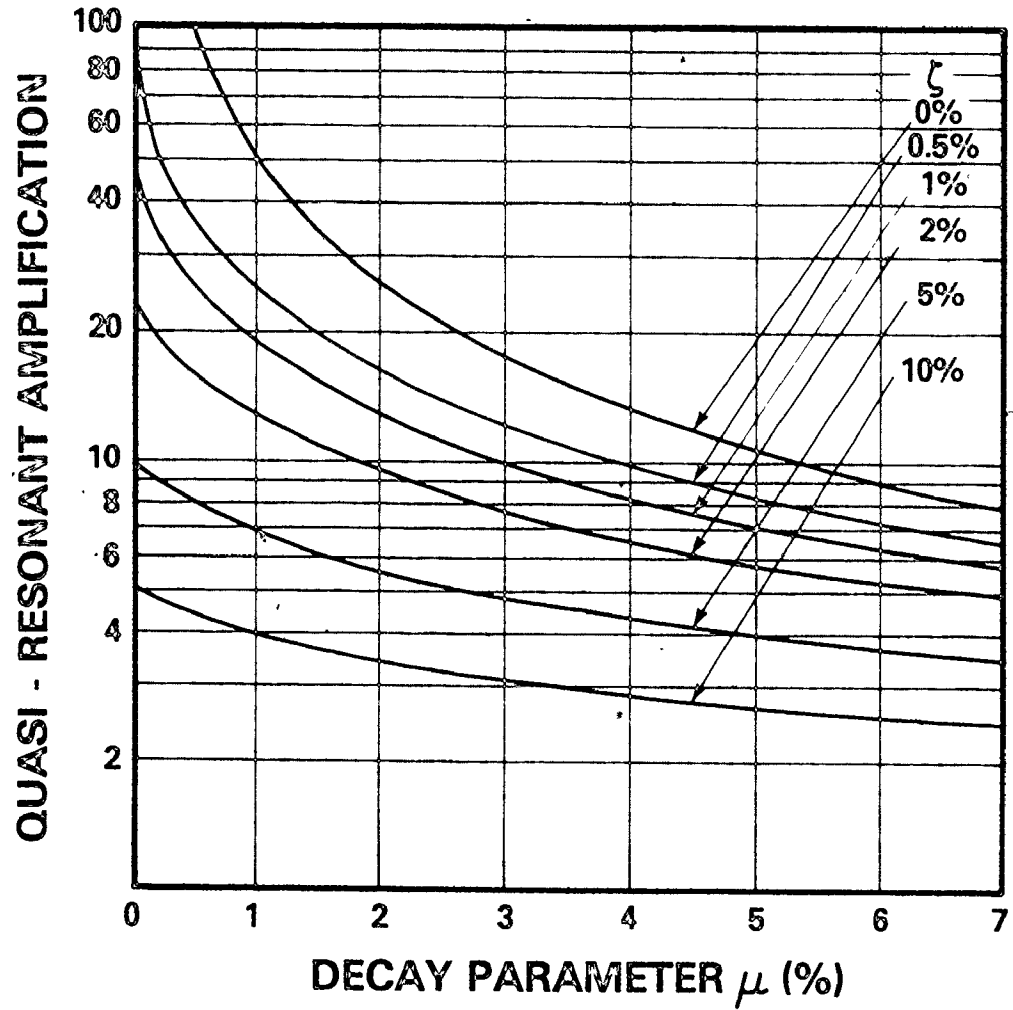


FIG. 4.13 QUASI - RESONANT AMPLIFICATIONS FOR DECAYING SINUSOIDAL MOTIONS

$$\begin{aligned}
 R_i &= A^* \exp[-\alpha t] \\
 &= A^* \exp\left[-\frac{\pi}{2} \mu(2i-1)\right] \quad i = 1, 2, \dots, 2N \quad (4-95)
 \end{aligned}$$

The R_i values can be summed to determine the number of cycles of constant amplitude sine motion which would be equivalent to the decaying sinusoid; thus

$$N_{eq} = \frac{1}{2} \sum_{i=1}^{2N} (A^* \exp\left[-\frac{\pi}{2} \mu(2i-1)\right])^\beta \quad (4-96)$$

$$= \frac{1}{2} \sum_{i=1}^{2N} A^{*\beta} \exp\left[-\frac{\pi}{2} \mu\beta(2i-1)\right] \quad (4-97)$$

Equation 4-96 shows the summation quite clearly in terms of peaks in the decaying sinusoid while Eq. 4-97 is more useful for generalizing about N_{eq} values. Incorporating the β exponent into the envelope term allows general curves to be plotted for values of the joint parameter $\mu\beta$ as shown in Fig. 4.14. From these curves the number of equivalent cycles of constant amplitude can be determined for a pair of μ and β values. For normalization purposes, the A^* term in Eq. 4-97 was calculated by the method of Eq. 4-83 so that the first and largest peak value of the decaying sinusoid would be equal to 1.0.

Figure 4.14 also shows the curves for the sine beat and upperbound sinusoidal cases. It is apparent that certain equivalence relationships could be established between the limited-duration sine, sine beat and decaying sine on the basis of similarity of N_{eq} values.

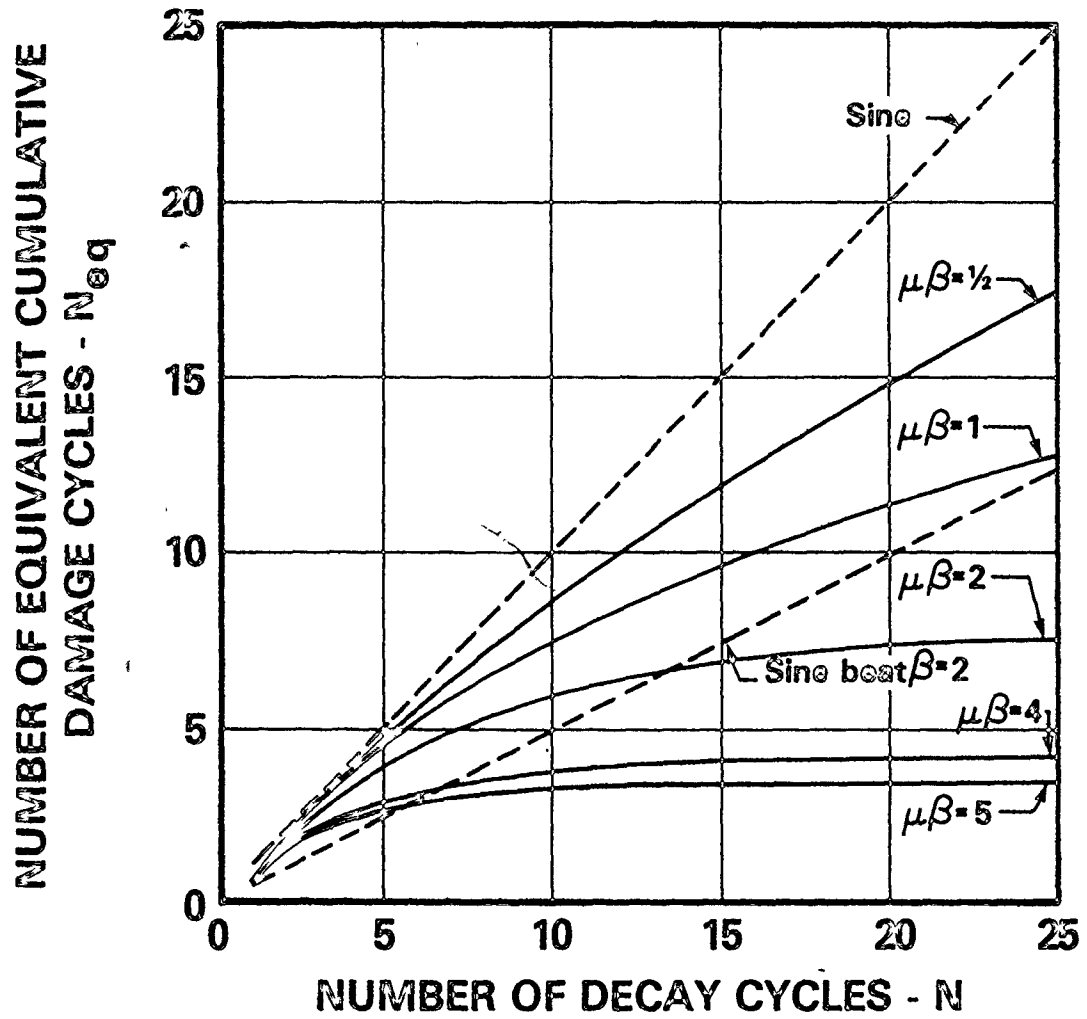


FIG. 4.14 COMPARISONS OF CUMULATIVE DAMAGE PROCESS FOR HARMONIC MOTIONS

Development and discussion of such relationships will comprise part of Chapter 6.

4.4.4 Root-Mean-Square Acceleration and Duration

Analytic expressions of RMS acceleration for a constant amplitude sine and a sine beat have been derived in previous sections. The RMS accelerations for these waveforms are independent of time when the motion consists of a complete number of cycles. The case for a decaying sinusoid is not as straightforward because amplitudes of successive cycles are different and there is not a natural end to the motion as there is for a sine beat pulse.

The cumulative RMS function for a decaying sinusoid is given by

$$\text{CRF}(t) = \left\{ \frac{A^*2}{t} \int_0^t e^{-2\mu\Omega\tau} \sin^2 \Omega\tau \right\}^{1/2} \quad (4-98)$$

This can be rewritten using trigonometric identities as

$$\text{CRF}(t) = \left\{ \frac{A^*2}{2t} \int_0^t e^{-2\mu\Omega\tau} (1 - \cos 2\Omega\tau) d\tau \right\}^{1/2} \quad (4-99)$$

When the integration is performed (the second integral can be evaluated from a table of integrals) the CRF becomes

$$\text{CRF}(t) = \frac{A^*}{2} \left\{ \frac{1}{\mu\Omega t} (1 - e^{-2\mu\Omega t}) - \frac{1}{\Omega t (1 + \mu^2)} [e^{-2\mu\Omega t} (\sin 2\Omega t - \mu \cos 2\Omega t) + \mu] \right\}^{1/2} \quad (4-100)$$

Fig. 4.15 illustrates the CRF and D(CRF) for a typical decaying sinusoid.

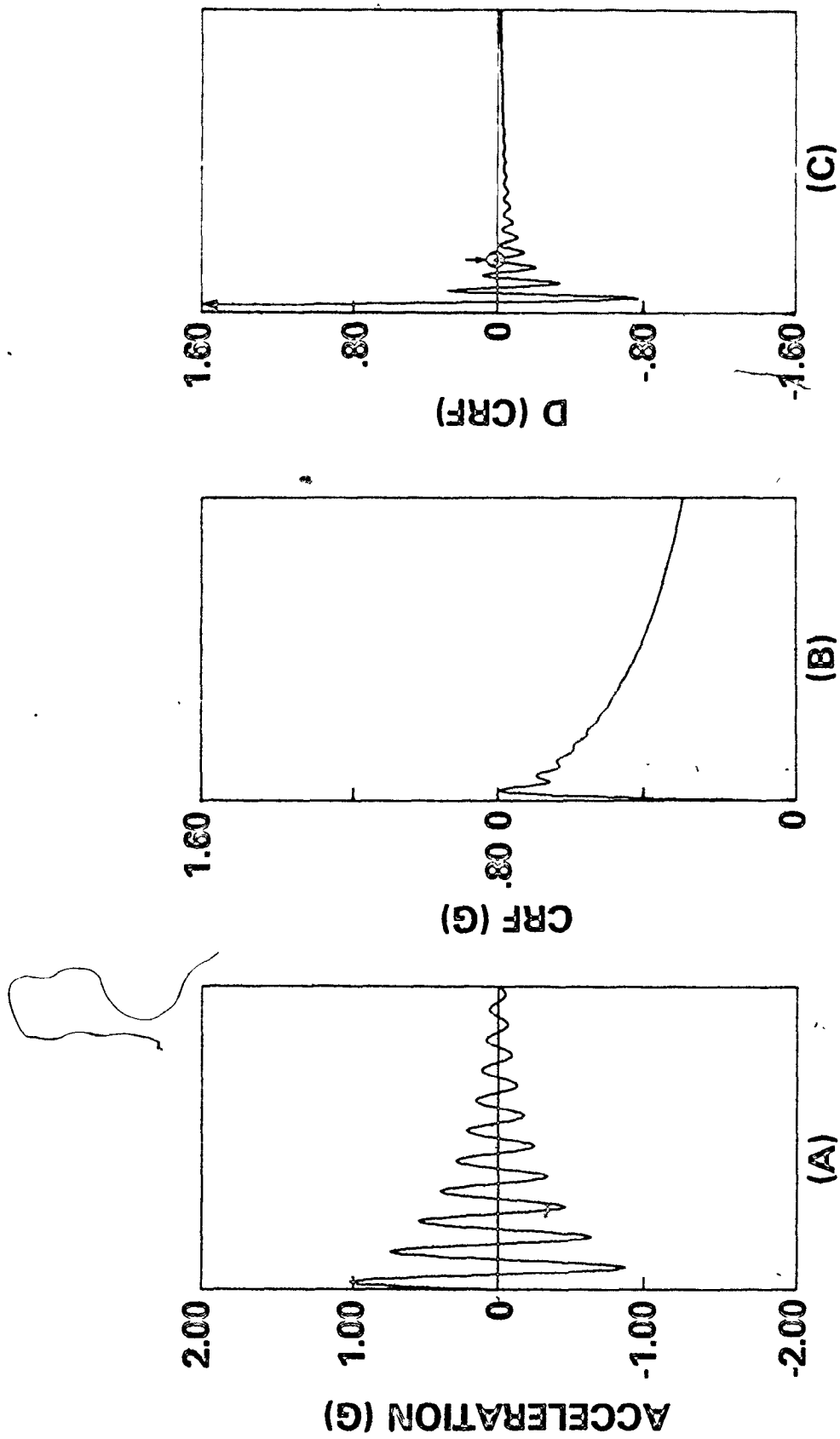


FIG. 4.15 RMS FUNCTIONS OF A DECAYING SINUSOID

Eq. 4-100 can be checked by allowing μ to approach zero. Taking $\lim_{\mu \rightarrow 0} \text{CRF}(t)$ shows that the CRF reduces to the CRF equation for sinusoidal excitation as described in section 4.3.4.

The exponential decay indicates that a phase of strong motion will only exist for a limited time since the power content of the continuously decreasing amplitudes will eventually drop below the average power level. A complete number of half-sine cycles (cycle length = π) will occur whenever

$$\omega t = \pi i \quad i = 1, 2, \dots, 2N \quad (4-101)$$

where N is the number of full cycles. Under this condition the sine and cosine terms in Eq. 4-100 become

$$\sin 2\omega t = \sin 2\pi i = 0 \quad (4-102)$$

and

$$\cos 2\omega t = \cos 2\pi i = +1$$

Thus, the CRF for i half-cycles can be written as

$$\begin{aligned} \text{CRF}(t) &= \frac{A^*}{2} \left\{ \frac{1 - e^{-2\mu\pi i}}{\mu\pi i} - \frac{\mu(1 - e^{-2\mu\pi i})}{\pi i(1 + \mu^2)} \right\}^{1/2} \\ &= \frac{A^*}{2} \left\{ \frac{1 - e^{-2\mu\pi i}}{\mu i \mu (1 + \mu^2)} \right\}^{1/2} \quad i = 1, 2, \dots, 2N \end{aligned} \quad (4-103)$$

The final version of Eq. 4-103 is significantly easier to handle than Eq. 4-100 and provides as much insight into the behaviour of the

CRF as does the complete function.

The duration of strong motion can now be computed by applying Eq. 4-103 to the basic concepts of instantaneous and average power. The beginning of strong motion in a decaying sinusoid is at time $t=0$ when the motion commences since the first cycle has the maximum amplitude and gives the maximum power contribution of any of the successive cycles.

The last half-cycle of strong motion requires

$$[\text{CRF}(t)]^2 \geq [\ddot{z}(t)]^2$$

or

$$\frac{A^2}{4} \left\{ \frac{1 - e^{-2\mu\pi i}}{\mu\pi i(1 + \mu^2)} \right\} \geq A^2 e^{-2\mu\pi i} \quad (4-104)$$

where Eq. 4-103 has been used for $\text{CRF}(t)$, and $[\ddot{z}(t)]^2$ is evaluated by Eq. 4-101. The cross-over point from positive to negative CRF occurs when the value of i creates an equality. Neglecting the μ^2 term since μ will generally be quite small, and rewriting in the form of an equality gives

$$e^{-2\mu\pi i} (1 + 4\mu\pi i) = 1$$

therefore

$$\ln(1 + 4\mu\pi i) = 2\mu\pi i \quad (4-105)$$

For non-zero μ , Eq. 4-105 is satisfied when $i\mu = 1/5$, therefore the number of cycles N_{sm} in the strong motion phase is

$$N_{sm} = \frac{1}{10\mu} \quad (4-106)$$

On the plot of $D(\text{CRF})$ in Fig. 4.15c, for the 5% damped sinusoid, the circle shows the point where the $D(\text{CRF})$ permanently becomes negative thus ending the strong motion phase.

The simple expression from Eq. 4-106, plotted in Fig. 4.16, permits a very easy evaluation of the duration of strong motion for a decaying sinusoidal motion having any specified decay parameter μ . Unlike the sine and sine beat motions, N_{sm} for a decaying sine is independent of the number of cycles of input, provided that $N \geq 1/10\mu$.

The RMS acceleration for the strong motion phase A_{rms} is obtained by substituting $\mu = 1/5$ back into Eq. 4-103:

$$A_{rms} = \frac{A^*}{2} \left\{ \frac{1 - e^{-2\pi/5}}{\frac{\pi}{5} (1 + \mu^2)} \right\}^{1/2} \quad (4-107)$$

The term $1 + \mu^2$ will always be close to 1.0 for small rates of decay, hence the strong phase RMS acceleration can be approximated as

$$\begin{aligned} A_{rms} &= \frac{A^*}{2} (1.067) \\ &= .53A \end{aligned} \quad (4-108)$$

showing that it is independent of any attributes of the input motion such as frequency, rate of decay, or total length of signal. This is not too surprising because the CRF from Eq. 4-103 is (neglecting the μ^2 term) a function only of the product μi which is a constant. Therefore, the strong phase RMS acceleration must also be a constant.

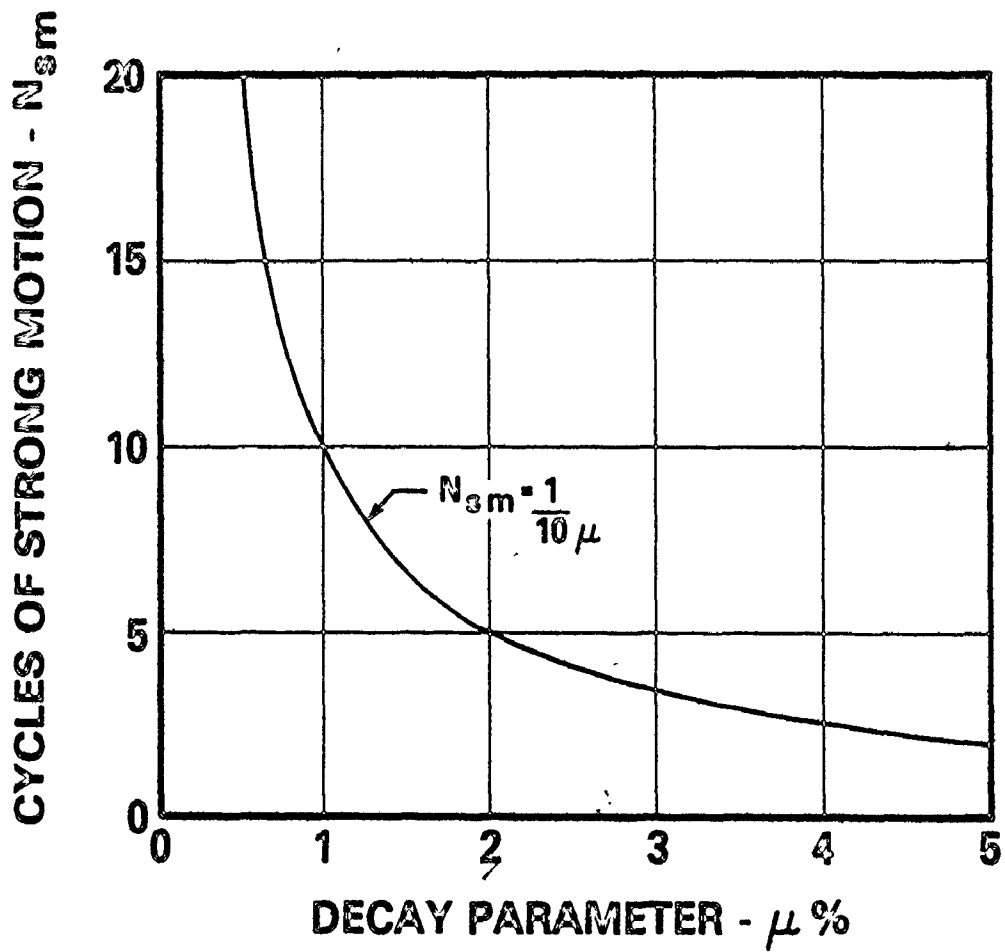


FIG. 4.16 DURATION OF STRONG MOTION FOR A DECAYING SINUSOID

4.5 Summary

This chapter has developed motion characterizations for three basic types of harmonic waveforms from a purely theoretical approach. Some brief comments have been made on aspects of the characterizations but a full utilization of the information contained in this chapter awaits the subsequent analysis and discussions on characteristics of real seismic motions.

Table 4.3 should provide a useful summary of the motion characteristics discussed in this chapter.

TABLE 4.3 CHARACTERISTICS OF HARMONIC MOTIONS

CHARACTERISTIC	SINE	SINE BEAT	DECAYING SINUSOID
(1) Basic Equation	$\sin \Omega t$	$(\sin \Omega_b t)(\sin \Omega_t t)$	$e^{-\mu \Omega t} \sin \Omega t$
(2) Total Duration	N cycles	N cycles/beat	$N \geq 1/10\mu$
(3) SDOF Response:			
general	Eq. 4-10	Eq. 4-47	Eq. 4-89
max.; zero damping	$Q = \pi N$	$Q = 2N$	if $\begin{cases} \mu=0 \\ \zeta \neq 0 \end{cases} Q = 1/2\zeta$
max.; damped system	$1/2\zeta$	Fig. 4.5	Fig. 4.13
(4) Cumulative Damage, N_{eq}	N	Fig. 4.7	Fig. 4.14
(5) Cycles of Strong Motion	N	$\approx 2/3 N$	$1/10\mu$
(6) RMS Acceleration for Strong Motion	$1/\sqrt{2}$.60	.53
(7) Shape of CRF	sharp rise then flat	sharp rise then slow decline	very sharp rise then exponential decline

1

CHAPTER 5
RESULTS AND DISCUSSIONS

5.1 Introduction

In the preliminary stages of examining the parametric data, the recognized effect of site soil conditions on site response spectra (28) made it seem plausible to also examine other parameters on a site dependent basis. Therefore, each parameter was statistically summarized into means and standard deviations by grouping records together on the basis of site soil conditions. As the final results will show, this was a useful classification for some but not all parameters. The site soil classification for earthquake ground motions (see section 2.2.1) was as follows: rock sites - Lankershim and Caltech Seismological Lab; stiff soil sites - El Centro and Hollywood; deep cohesionless sites - Eureka and Orion.

In this chapter, ground and floor motion characterization data are presented and discussed at some length and where possible, numerical values are suggested as parameter estimates.

5.2 Floor Motion Time-Histories

Some general observations can be made about CANDU seismic floor responses in the time domain without regard to location within the reactor structure. In the first 10 seconds or so the floor motions have typically demonstrated sustained high levels of response with evidence

of some multi-frequency components. Beyond about 15 seconds the amplitudes die down and in some instances pulses of sine beats, (Fig. 5.1a) or segments of decaying sinusoids were observed. Structural responses on deep cohesionless sites (Fig. 5.1b) showed a distinct attenuation of some of the high frequency component after 15 seconds but it was much more difficult to detect any such evidence in responses on rock or stiff soil sites.

Two SDOF systems were proposed in Section 2.4 as possible models for studying the seismic response behaviour of the CANDU internal structure and reactor vault. Comparisons of SDOF model time-histories with the corresponding CANDU responses indicates that mass 4 time domain responses were closely simulated by the 5.83 Hz model but the 10 Hz model did not provide nearly as good a representation of the vault's mass 12 response. To provide an illustrative example, the structural responses due to the Lankershim N-S ground motion in Fig. 5.2 can be considered. The floor responses of mass 4 within the internal structure of the multi-degree-of-freedom CANDU model and of the representative 5.83 Hz SDOF model are shown in Fig. 5.3a and 5.3b. The remarkable similarities in both time dependent amplitudes and apparent frequency (number of zero-up-crossings per unit time) are consistent with the responses calculated for almost all SDOF models representing mass 4. The only deviation from this trend occurred during the last 15 seconds on deep cohesionless sites where the attenuation of high frequency components in the ground motions also showed up in the CANDU response but naturally, these lower frequency responses could not occur in the

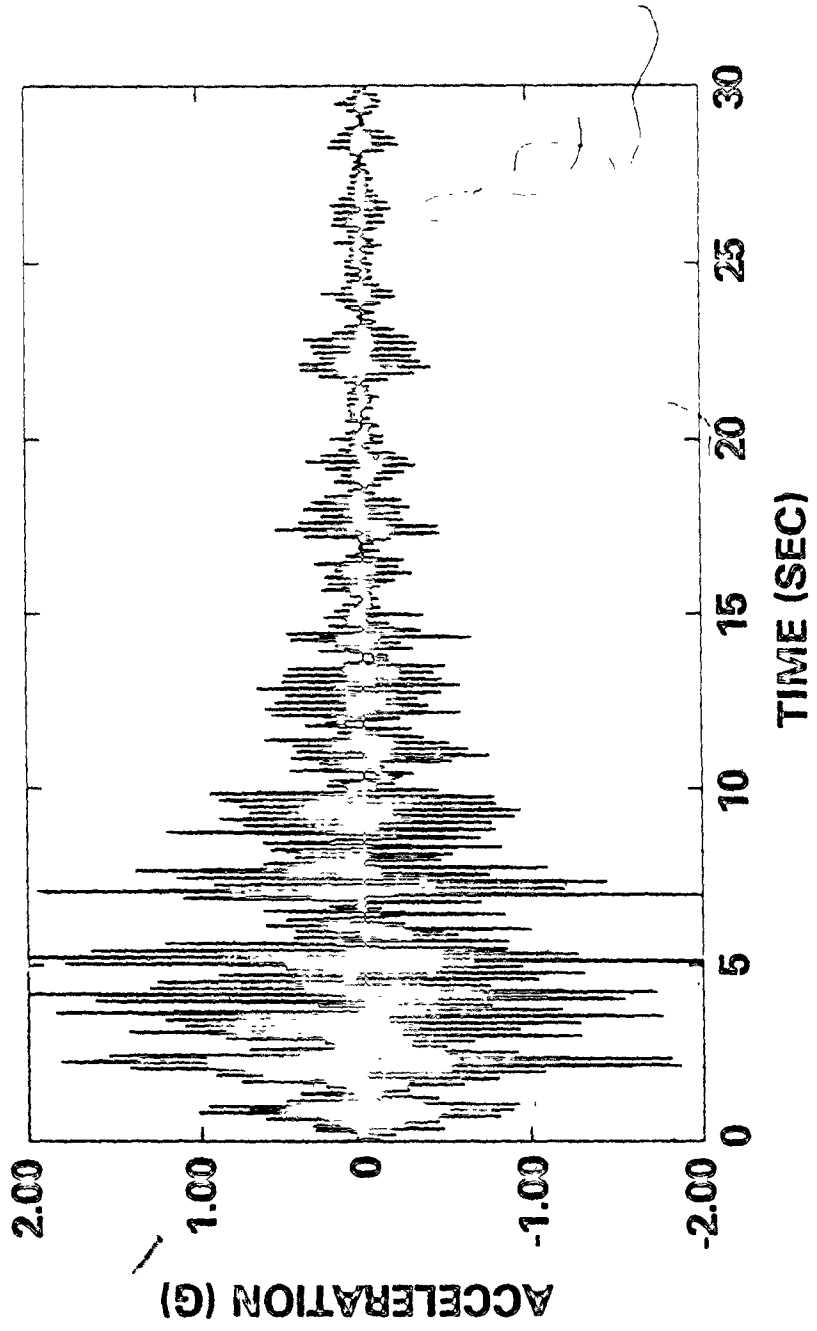


**FIG. 5.1a CANDU MASS 4 FLOOR RESPONSE
TO CALTECH SEISMOLOGICAL LAB
RECORD, N-S COMPONENT**

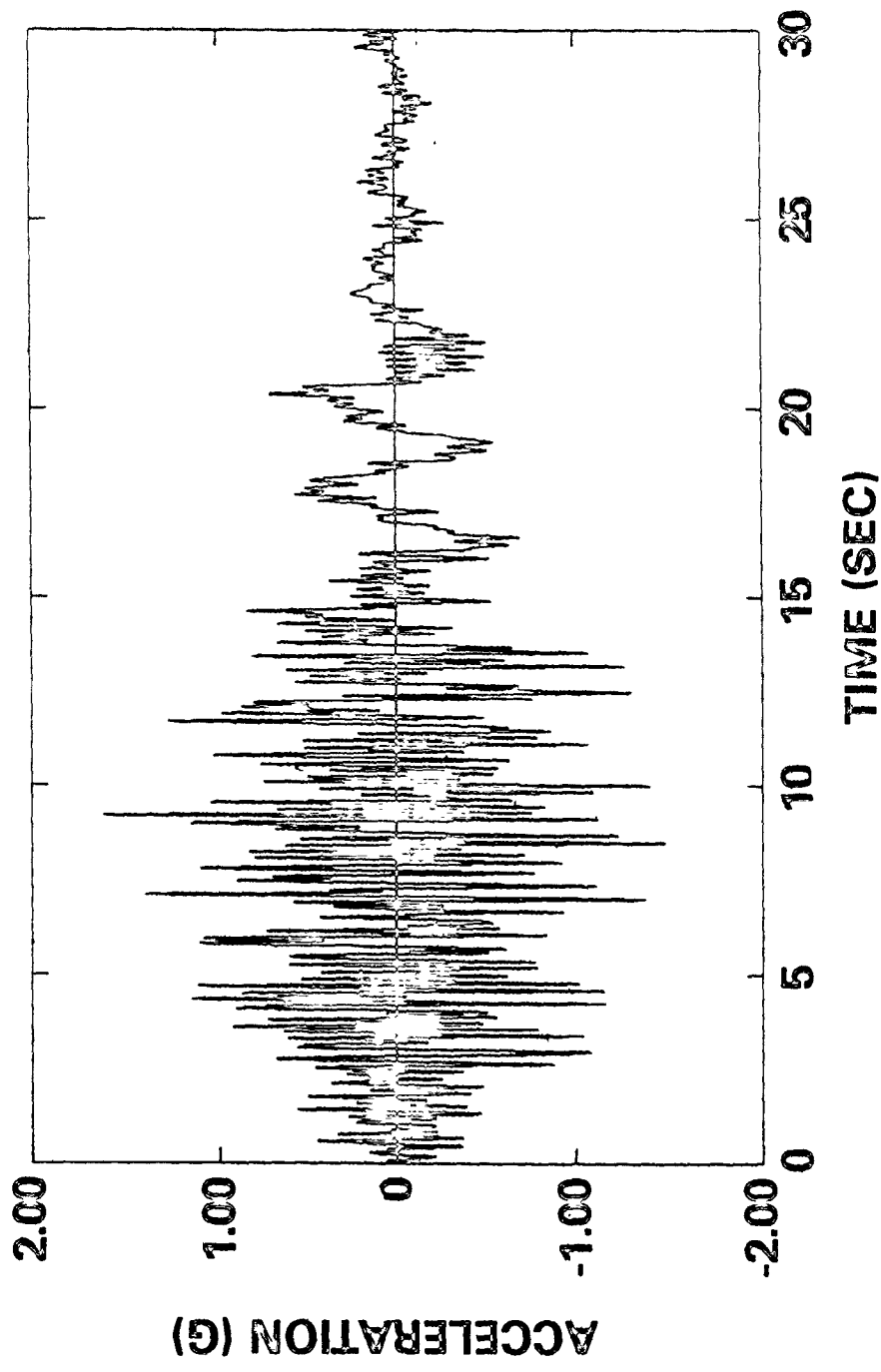
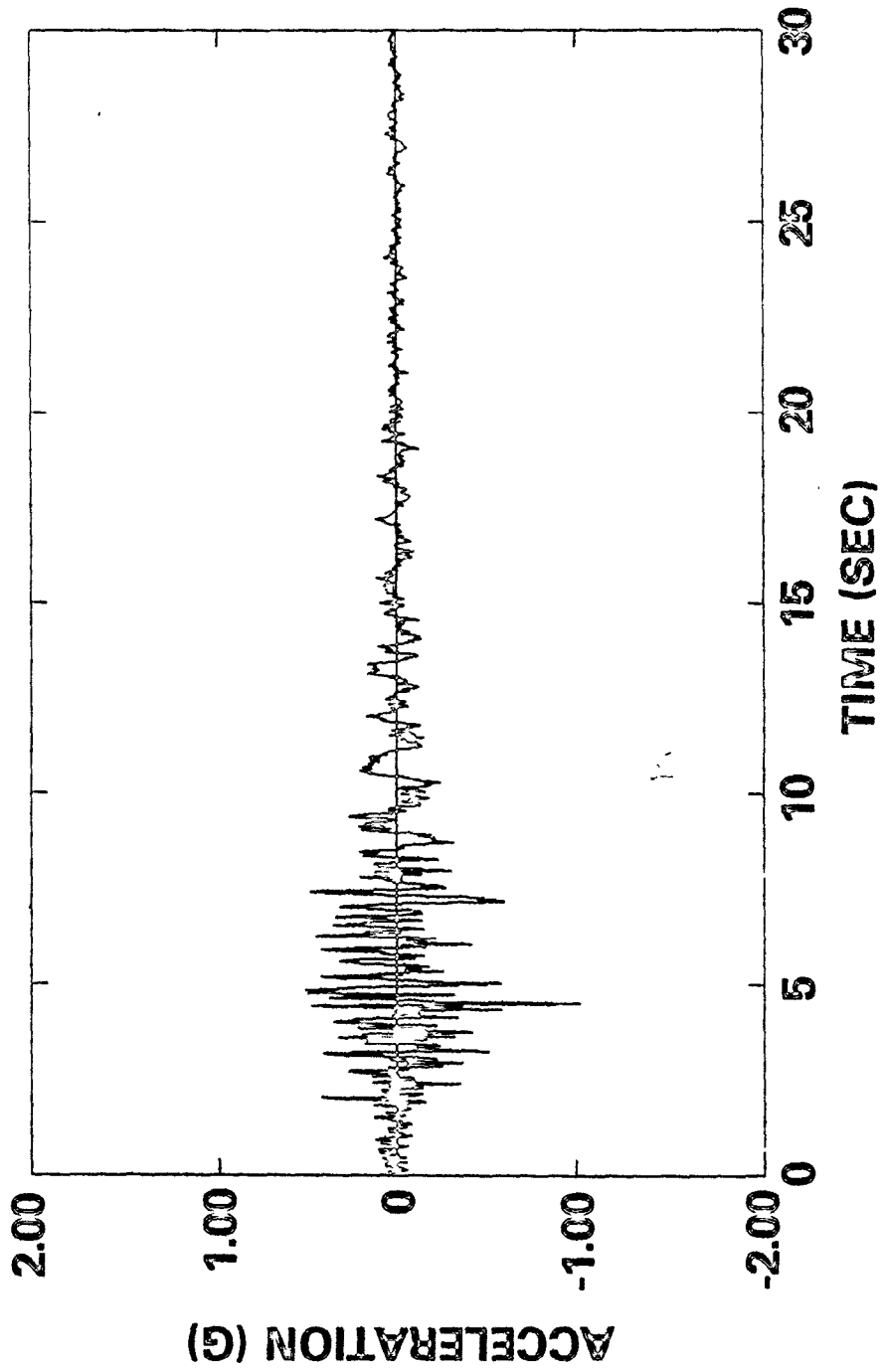
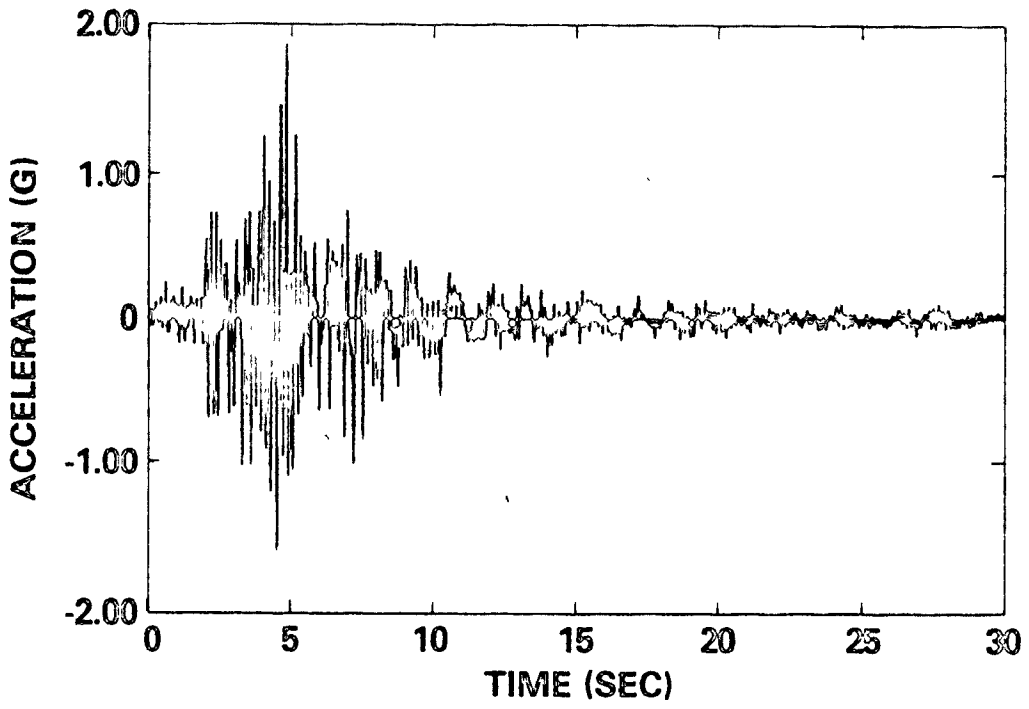


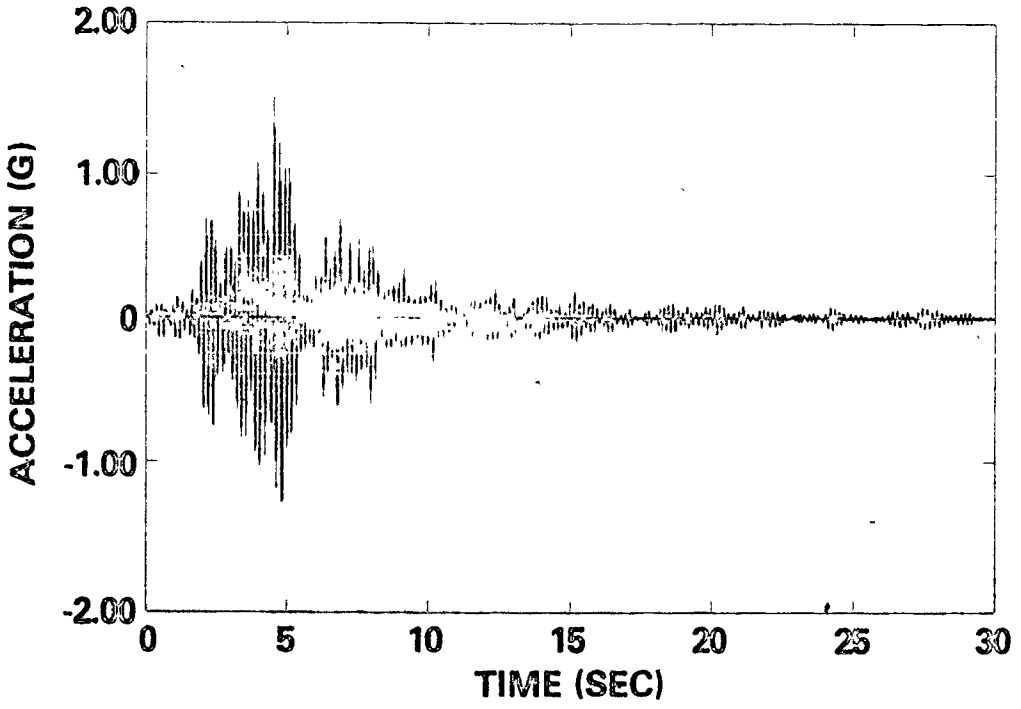
FIG. 5.1b CANDU MASS 4 FLOOR RESPONSE TO ORION RECORD, E-W COMPONENT



**FIG. 5.2 LANKERSHIM N-S GROUND MOTION
SCALED TO 1G**



(a) CANDU Mass 4 Floor Response



(b) 5.83 Hz SDOF Response

FIG. 5.3 COMPARISON OF CANDU AND SDOF RESPONSES FOR THE INTERNAL STRUCTURE (Record; Lankershim N-S)

SDOF model.

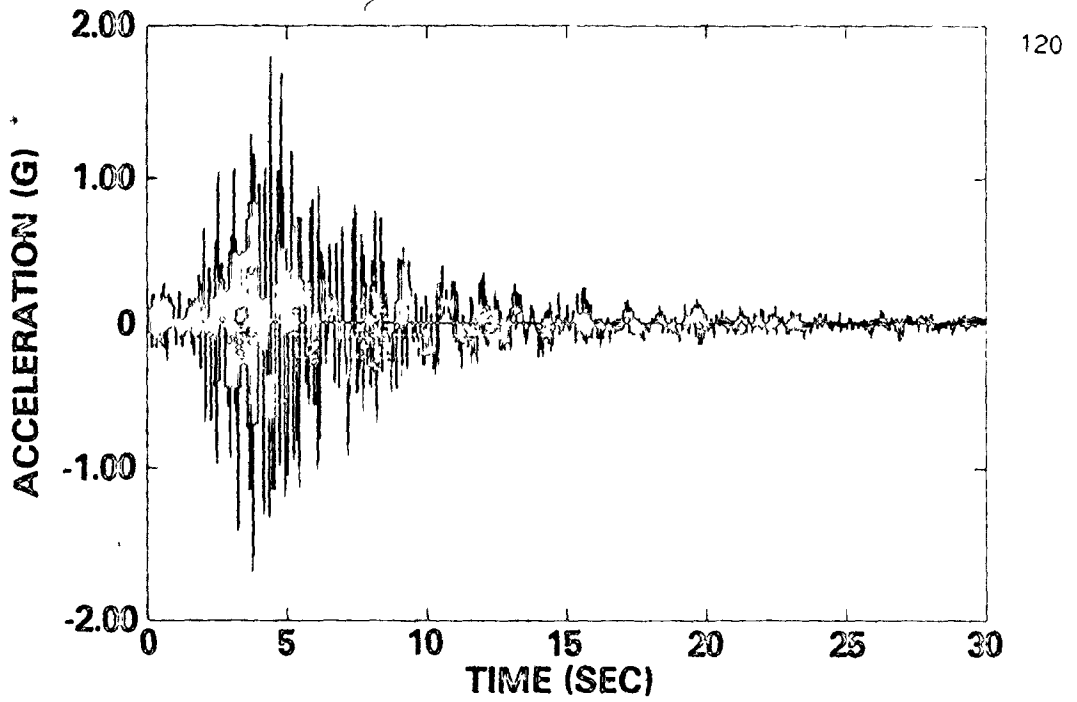
The time-history responses of the CANDU vault at mass 12 and the 10 Hz SDOF system in Fig. 5.4a and 5.4b, respectively, do not exhibit the same agreement as did the previous pair of systems. On rock sites, the amplitude envelopes of both CANDU and SDOF model responses appear quite similar but differences in frequency content of the waveforms is significant in the 15-30 seconds region where the motion of mass 12 was predominantly low frequency.

Greater dissimilarities in CANDU vs. 10 Hz SDOF model response ~~appeared~~ on stiff soil sites where modelling problems posed by high frequency attenuations increased, consequently the SDOF model was only able to simulate the first 10 seconds or so with reasonable accuracy.

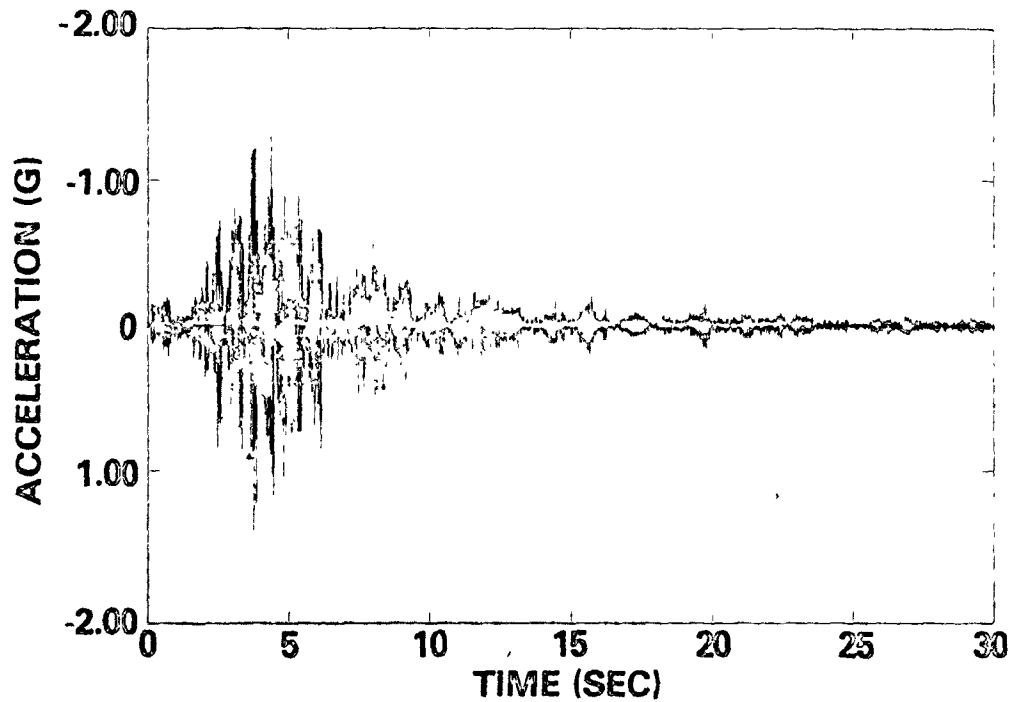
The 10 Hz SDOF model was severely limited in its capability to simulate time dependent responses on deep cohesionless sites. Although amplitude characteristics were generally well modelled in the first 10 seconds the CANDU response showed clear signs of low frequency components over the entire 30 seconds. Consequently, for the last 20 seconds of record on these sites there were few similarities in either amplitude envelope or frequency.

5.3 Response Spectra

Response spectra were calculated for each ground and floor motion time-history, for 1% spectral damping, using an adaptation of Nigam and Jennings' computer program SPECEQ (24). Spectral values were calculated at 35 frequencies ranging from 0.5 Hz to 35 Hz, plus additional points



(a) CANDU Mass 12 Floor Response



(b) 10 Hz SDOF Response

FIG. 5.4 COMPARISON OF CANDU AND SDOF MODEL RESPONSES FOR THE REACTOR VAULT (Record; Lankershim N-S)

at each of the CANDU modal frequencies.

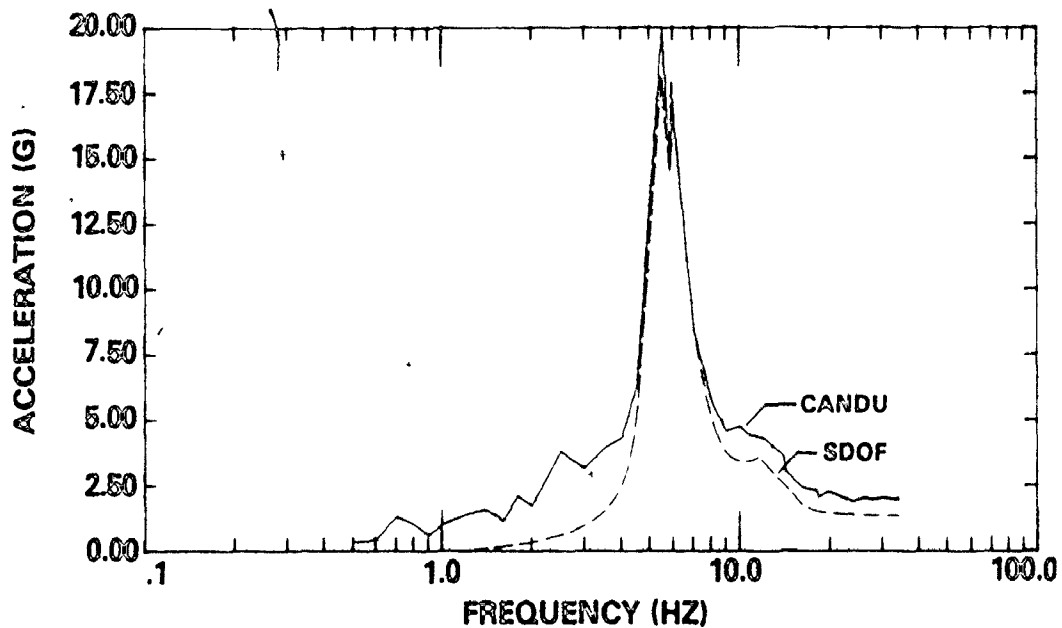
Even though only four records were used in each soil group, distinctive differences were evident in the ground response spectra for each site. At low frequencies (0.5 - 2 Hz) the spectral values for rock and stiff soil sites were less than the spectral levels for deep cohesionless soils and there were also significant differences in the frequency range where the largest spectral amplifications occurred. Peak amplifications on rock tended to occur at slightly higher frequencies than the peak amplifications on stiff soils which in turn were at higher frequencies than peak amplifications on deep cohesionless sites.

Two CANDU floor response spectra (FRS) for the Lankershim rock site are shown in Fig. 5.5a and 5.5b, respectively. The major difference in spectra at these two floor locations was the predominantly single frequency characteristic (at 5.8 Hz) of the internal structure (mass 4) versus the multi-frequency, broadband FRS of the reactor vault (mass 12).

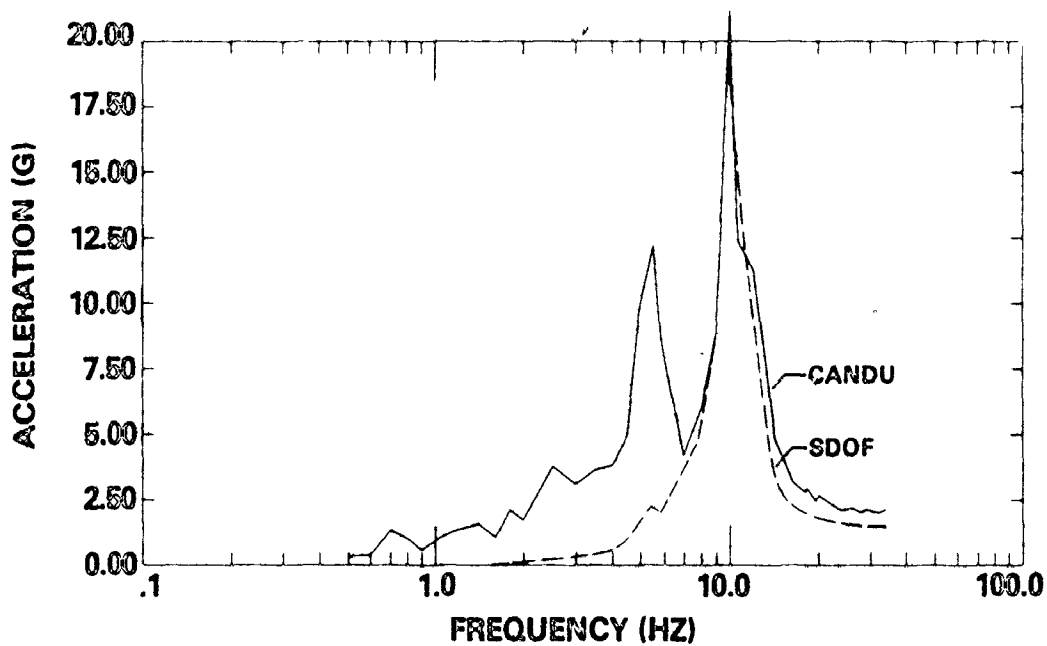
CANDU Mass 4 FRS vs. 5.83 Hz SDOF FRS A common feature for all mass 4 FRS was a predominant peak at the first modal frequency (5.83 Hz) of the internal structure. Table 5.1, summarizing peak FRS values for the SDOF model, indicates that peak CANDU spectrum values were predicted quite accurately by the SDOF model.

TABLE 5.1 MAXIMUM FRF VALUES FOR CANDU MASS 4
AND 5.83 Hz SDOF MODEL

RECORD		CANDU MASS 4 (g)	5.83 Hz SDOF MODEL (g)
Lankershim	NS	19.95	18.90
Lankershim	EW	13.51	11.62
Caltech	EW	13.98	12.74
Caltech	NS	34.34	35.49
El Centro	NS	19.40	21.74
El Centro	EW	15.74	15.97
Hollywood	EW	22.16	20.80
Hollywood	NS	23.73	26.68
Eureka	NE	14.82	15.84
Eureka	NW	16.12	17.21
Orion	NS	15.82	16.70
Orion	EW	15.44	15.01
1% spectral damping			



(a) CANDU Mass 4 and 5.83 Hz SDOF Model



(b) CANDU Mass 12 and 10 Hz SDOF Model

**FIG. 6.5 COMPARISON OF CANDU AND SDOF
MODEL FLOOR RESPONSE SPECTRA
(Record ; Lankershim N-S)**

Figure 5.5a compares a CANDU and a SDOF FRS to show the typical close similarities that were found to exist throughout the peak and high frequency regions. In low frequency regions however, the SDOF FRS tended to drop below the levels of the CANDU FRS. Differences in site soil conditions did not result in any distinctive changes in the mass 4 FRS.

The CANDU dynamic model in Fig. 2.3 shows quite clearly how the internal structure of the reactor building is essentially modelled by a vertical arrangement of lumped masses. In this type of modelling a dominant first mode response can well be expected.

CANDU Mass 12 FRS vs. 10 Hz SDOF FRS Unlike the previous comparisons, few similarities exist between FRS for the reactor vault at mass 12 and for the 10 Hz SDOF model. The multi-frequency response of the vault is immediately noticeable in the spectra of Fig. 5.5b and sharply contrasts with the narrow-banded spectrum of the 10 Hz SDOF model. Considering all soil types, response spectra for mass 12 were broadband across frequencies of 2 - 12 Hz.

One similarity that did appear between the CANDU and SDOF responses was that the peak values at 10 Hz in the CANDU spectra were predicted quite accurately by the SDOF model. These values are compared in Table 5.2.

TABLE 5.2 MAXIMUM FRS VALUES FOR CANDU MASS 12
AND 10 HZ SDOF MODEL

RECORD		CANDU MASS 12 FRS (g)	10 HZ SDOF MODEL FRS (g)
Lankershim	NS	21.17	19.46
Lankershim	EW	8.41	7.67
Caltech	EW	16.39	15.51
Caltech	NS	18.96	17.00
El Centro	NS	20.72	19.37
El Centro	EW	15.07	14.19
Hollywood	EW	32.85	30.31
Hollywood	NS	34.73	28.98
Eureka	NE	8.24	7.59
Eureka	NW	11.33	9.51
Orion	NS	14.99	12.65
Orion	EW	18.86	17.46

1% spectral damping

5.4 Comments on Modelling Time and Frequency Domain Responses

The results in sections 5.2 and 5.3 lead to some general comments on using SDOF systems to simulate the seismic response of CANDU reactor structures.

- (1) Dynamic similitude between a SDOF model and a CANDU structure must consider; (i) the model frequency to be the same as the first mode frequency of the full-scale structure (i.e., CANDU internal structure), (ii) equivalent structure and model damping, (iii) a transformation from the generalized coordinate response of the SDOF model to the coordinate system of the CANDU structure using the appropriate CANDU modal participation factor and mode shape in the product $\Gamma_j \phi_{ji}$.
- (2) Single frequency CANDU structures can be defined as those structures which respond in a predominately single frequency manner (i.e., the 5.83 Hz internal structure) and are not influenced by the response of other sub-structures or components of the CANDU system. The time and frequency domain responses of these structures can be satisfactorily modelled using a SDOF system. Multiple frequency CANDU structures can be defined as those structures having more than one predominant response frequency such as the reactor vault. The multiple frequencies may result from multi-modal response of the structure itself or they may be caused by response feed-back from other structures.

(3) For single frequency CANDU structures:

(i) SDOF floor response time-histories are very similar in shape and amplitude to the responses in CANDU over the 30 seconds of earthquake record.

(ii) A SDOF model provides FRS which are very similar in shape and peak amplitude to the CANDU FRS, however at low frequencies (≤ 2 Hz) the SDOF FRS tend to be somewhat below the CANDU spectra.

(4) For multiple frequency CANDU structures:

(i) SDOF time domain responses are generally reasonably similar to the CANDU responses in the first 10 seconds or so but beyond about 10 seconds the CANDU response may show a significant attenuation of high frequency motions which the SDOF system cannot simulate.

(ii) FRS for the SDOF responses bear little resemblance to the multi-frequency, broadband CANDU FRS. Low frequency spectral amplitudes may be present in the CANDU FRS due to response feed-back from low frequency structural systems, and/or due to the presence of significant levels of low frequency ground motions.

5.5 Maximum Floor Accelerations

Maximum floor accelerations presented in Table 5.3 are the result of a 1 g peak ground acceleration and therefore represent ground-structure amplifications (denoted by $A_{g/s}$) for the CANDU and SDOF

TABLE 5.3 STRUCTURAL AMPLIFICATIONS

RECORD	GROUND MOTION	CANDU RESPONSES		SDOF RESPONSES	
		MASS 4	MASS 12	5.83 Hz	10.0 Hz
Lankershim N-S	1.0	1.87	1.80	1.50	1.38
Lankershim E-W	1.0	1.81	1.65	.92	.72
Caltech E-W	1.0	2.12	2.38	1.47	1.43
Caltech N-S	1.0	3.01	2.33	2.26	1.25
El Centro N-S	1.0	2.02	1.90	1.38	1.36
El Centro E-W	1.0	1.74	1.67	1.16	1.26
Hollywood E-W	1.0	2.38	2.58	1.63	2.16
Hollywood N-S	1.0	1.82	2.80	1.85	2.42
Eureka N79E	1.0	1.44	1.58	1.14	.63
Eureka N11W	1.0	1.48	1.43	1.07	.98
Orion N-S	1.0	1.59	1.53	1.13	1.05
Orion E-W	1.0	1.61	1.84	1.36	1.00
5% structural damping					

systems.

The values for CANDU range from approximately 1.4 to 3 with the higher amplifications occurring on the rock and stiff soil sites. It is interesting to compare these results with other studies of in-structure motion amplification. In a paper by Duff (9) on the development of floor response spectra for nuclear power plant design, an example case calculates an $A_{g/s}$ value of 3 for a 5% damped structure. Another study on seismic floor motions (31) analyzed responses of six multi-story buildings to the 1940 El Centro N-S earthquake and found top floor amplifications of 1.5 to 3.7 with a mean of 2.4. Data recorded during the 1971 San Fernando earthquake (20) have yielded peak upper-story accelerations and peak amplifications. Although the limited data does not allow clear distinctions to be made on the basis of soil conditions or building types, when all the data is lumped together $A_{g/s}$ was found to vary from about 4.5 for 0.1 g ground acceleration, to about 2.2 for 0.3 g maximum ground acceleration. As these relationships are actual field measurements the non-linearities in real structural responses are quite evident. These results, from sources in the literature, provide a measure of confidence on the seismic amplifications calculated using the CANDU model. Additionally, the levels of motion amplification in the CANDU structure do not seem to show appreciable differences from the maximum acceleration amplifications which could occur in non-nuclear multi-story structures.

The amplifications predicted by the SDOF systems are less than the CANDU levels for similar site conditions. This can be attributed to

the contributions of higher CANDU modes and indicates that $A_{g/s}$ could be significantly underestimated by a SDOF model. Alternative procedures are available however for evaluating structural amplifications without resorting to a full time-history analysis. Methods proposed by Duff (9) and by Biggs and Roesset (4) are two possibilities.

5.6 Duration of Strong Motion

The duration of strong motion for each ground motion and structural response are shown in Table 5.4 and are summarized in Table 5.5 for each site category in terms of mean values and standard deviations. Mean durations generally fall within a 4-8 second range, however there does not appear to be definite site dependent trends other than larger standard deviations on deep cohesionless soils.

The individual record data in Table 5.4 is more revealing about characteristics of strong motion duration. For any given earthquake, the difference between duration of strong floor motion and strong ground motion is less than one second. An exception, the two Caltech records show a difference of approximately two seconds. The longest phase of strong ground and floor motion was close to 12 seconds for the Orion event. The calculations showed that the strong motion phase begins within 1.5 - 3 seconds from the start of the event and therefore, in creating artificial earthquake time-histories or in selecting real earthquake records it is reasonable to specify that 15 seconds should be considered as the minimum time of excitation in order to provide reasonable opportunity for the strong motion phase to occur.

TABLE 5.4 DURATIONS OF STRONG MOTION IN SECONDS

RECORD	GROUND MOTION	CANDU RESPONSES		SDOF RESPONSES	
		MASS 4	MASS 12	5.83 Hz	10.0 Hz
Lankershim N-S	5.4	5.5	6.3	5.9	5.9
Lankershim E-W	5.6	5.8	6.5	5.9	6.5
Caltech E-W	4.8	6.8	6.9	6.2	5.0
Caltech N-S	6.9	8.7	8.9	7.1	8.6
El Centro N-S	3.6	3.6	3.5	3.5	3.5
El Centro E-W	10.2	10.1	10.1	13.2	3.3
Hollywood E-W	5.6	6.0	5.9	4.8	3.9
Hollywood N-S	5.7	6.4	6.2	6.4	6.0
Eureka N79E	3.3	3.0	3.9	2.8	3.4
Eureka N11W	3.7	3.6	4.0	5.1	6.0
Orion N-S	11.0	9.5	9.7	9.5	7.0
Orion E-W	11.9	12.0	12.1	10.2	7.7

TABLE 5.5 SITE DEPENDENT DURATIONS OF STRONG MOTION IN SECONDS

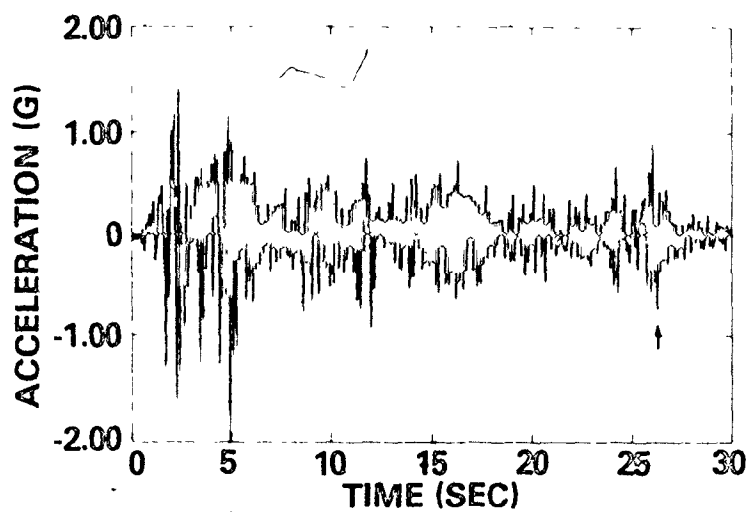
SITE	GROUND MOTION	CANDU		SDOF	
		MASS 4	MASS 12	5.83 Hz	10.0 Hz
Rock	5.7 * (0.9)+	6.7 (1.4)	7.1 (1.2)	6.3 (0.6)	6.5 (1.5)
Stiff Soil	6.3 (2.8)	6.5 (2.7)	6.4 (2.8)	7.0 (4.3)	4.2 (1.3)
Deep Cohesionless	7.5 (4.6)	7.0 (4.4)	7.4 (4.1)	6.9 (3.6)	6.0 (1.9)
All Sites	6.4 (2.9)	6.7 (2.7)	7.0 (2.5)	6.7 (2.9)	5.6 (1.8)

* mean value

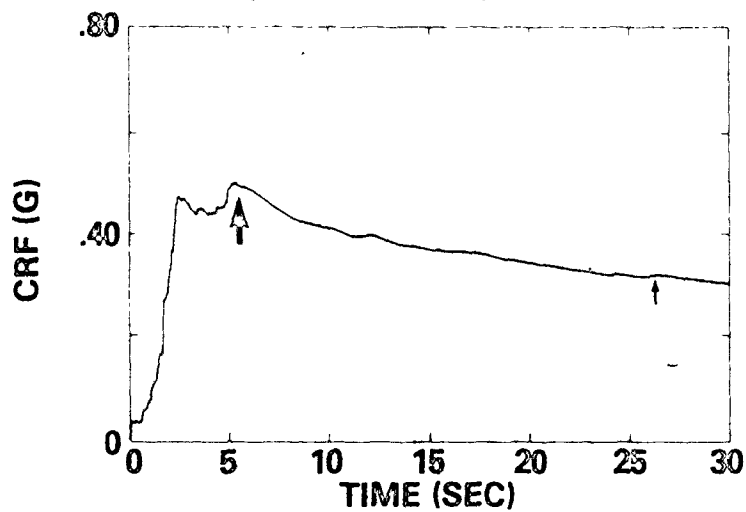
+ standard deviation

Strong motion durations calculated by McCann and Shah (21) indicate that even the smallest positive values of the CRF derivative have been considered as a continuation of the strong motion phase. In adopting the derivative procedure in this study it was felt that some degree of interpretation for each record was required to determine whether the last positive derivative was in fact, a reasonable measure of the end of strong motion. This placed an emphasis on the physical interpretation of the earthquake process for the viewpoint of earthquake engineering rather than simply a mathematical analysis of a time series record.

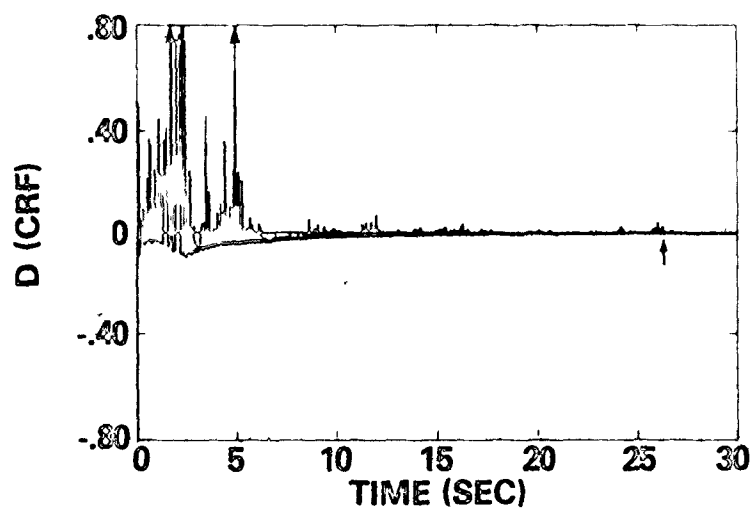
The general shape of the CRF for ground motions has been previously shown (Fig. 3.5) as a curve which rapidly rises to a peak then decays to the end of the record. Some records have a decay portion which smoothly decreases but other records, as in Fig. 5.6, have slight rises past the peak which cause a positive derivative. A computer program to calculate durations which is devised solely on the mathematical theory of the RMS-duration concept will assume that the positive derivative indicates a continuation of the strong motion phase. Physically, although an increase in the CRF indicates an instantaneous power which exceeds the average power, the average power is declining because the RMS process averages over time. As the average RMS declines past the peak, smaller and smaller acceleration peaks will be sufficient to create a positive CRF slope. This is illustrated in Fig. 5.6 where the CRF for the event has a few small "bumps" in the declining segment. The correspondence of points on the CRF with points on the time-history



(a) El Centro N-S, Mass 4



(b) Cumulative RMS Function



(c) Derivative of CRF

FIG. 5.6 INTERPRETING CALCULATIONS OF STRONG MOTION DURATION

and $D(CRF)$ is illustrated, as for example at 26 seconds. In the initial 2-3 seconds the CRF rises steadily and peaks at a time of 5.3 seconds as a result of sustained, high level amplitudes. In contrast, the levels of accelerations which cause rises on the declining segment are very transitory as shown by the time history in Fig. 5.6a, and the short base (time) dimension of the rises in Fig. 5.6c. In a physical interpretation they can be considered to be segments of local strong motion usually lasting only a fraction of a second.

The major peaking in the early stages is therefore, truly representative of a duration of strong motion as it spans several seconds with high levels of excitation. In this study, secondary rises in the declining segment of the CRF have not been considered as contributing to the strong motion phase and the end was deemed to occur when the CRF began its decline after the major peak(s). This is illustrated in Fig. 5.6 where the strong motion duration ends at 5.3 seconds.

Strong motion durations calculated from the SDOF floor motions show promising results. The mean duration times are generally close to those found by a full time-history analysis of CANDU and absent of any definite site-dependent patterns. The capability of a SDOF model to closely simulate the actual strong motion duration is an important feature for future considerations in simplified modelling of the CANDU structure.

Before proceeding to a discussion on RMS acceleration for the strong motion duration, the important overall observation from the above

data is that, for a given earthquake event, the duration of strong motion within the CANDU structure is identical to the duration of strong ground motion. The 12 records included in this study have been intended to be broadly representative of the ground motions that may occur on a wide range of soil conditions at a site approximately 20-40 km from the epicentre of a 6.5 M earthquake. These events indicate that a mean plus one standard deviation value of 12 seconds could be taken as an estimate of the duration of strong shaking.

5.7 RMS Accelerations

Strong motion durations are independent of any acceleration scaling applied to the time-history however, RMS acceleration as the complementary term in the dual parameter measure is affected and its true range of values has been masked by the 1g scaling factor used in this study. To retain information on true RMS accelerations, the ratio A_{rms}/A_m , has been introduced. Data on A_{rms}/A_m , given in Table 5.6 and summarized by site conditions in Table 5.7, indicates that ground and in-structure RMS accelerations generally tend to be greater on less firm soil conditions, and that mean plus one standard deviation ratios for in-structure motions are generally less than the ground motion ratio at the same site.

The SDOF models tend to somewhat overestimate the mean plus one standard deviation ratios (maximum overestimate is approximately 20%) except for the 5.83 Hz system which gives a slight underestimate (by 7%)

TABLE 5.6 RATIOS OF A_{rms}/A_m

RECORD	GROUND MOTION	CANDU RESPONSES		SDOF RESPONSES	
		MASS 4	MASS 12	5.83 Hz	10.0 Hz
Lankershim N-S	.25	.28	.29	.31	.32
Lankershim E-W	.35	.30	.31	.39	.37
Caltech E-W	.32	.24	.22	.29	.31
Caltech N-S	.33	.26	.27	.35	.34
El Centro N-S	.37	.29	.32	.36	.32
El Centro E-W	.32	.30	.28	.37	.28
Hollywood E-W	.36	.28	.32	.40	.40
Hollywood N-S	.35	.37	.31	.37	.34
Eureka N79E	.42	.44	.33	.42	.38
Eureka N11W	.42	.42	.38	.38	.25
Orion N-S	.31	.31	.30	.32	.29
Orion E-W	.38	.35	.30	.32	.39

TABLE 5.7 SITE DEPENDENT RATIOS A_{rms}/A_m

SITE	GROUND MOTION	CANDU		SDOF	
		MASS 4	MASS 12	5.83 Hz	10.0 Hz
Rock	.31* (.04)+	.27 (.03)	.27 (.03)	.34 (.04)	.33 (.03)
Stiff Soil	.35 (.02)	.31 (.04)	.31 (.02)	.37 (.02)	.34 (.05)
Deep Cohesionless	.38 (.05)	.38 (.06)	.33 (.04)	.36 (.05)	.34 (.06)
All Sites	.33 (.06)	.32 (.06)	.30 (.04)	.36 (.04)	.33 (.05)

* mean value

+ standard deviation

on the deep cohesionless site. The higher ratios for SDOF systems can be attributed to quasi-harmonic response whereas CANDU responses are superpositions of several frequency components.

In light of these results it seems reasonable to consider that A_{rms}/A_m for a given ground motion will generally be at least as great as the ratio for the resulting floor motions. The maximum mean plus one standard deviation ratio in Table 5.6 is 0.43 but considering that most ratios for CANDU are considerably less than this value, it is recommended that a ratio of $A_{rms}/A_m = 0.4$ be considered as a likely maximum for both ground motions and in-structure floor motions. Motions which exceed this level would be expected to have very short durations of strong shaking which would tend to offset the effects of higher RMS accelerations, as for example in the case of mass 4 response to the Eureka events (compares Tables 5.4 and 5.6).

5.8 Cumulative Damage Process

The initial reference level used in calculating parameters N_{eq} was the maximum acceleration within each record. Since different bases of normalization can put N_{eq} values into quite different contexts, an accurate interpretation of normalized values requires that the significance of the reference level must always be borne in mind.

To illustrate this point and to present the results from different viewpoints, two reference levels will be used. The basic N_{eq} data values, presented in Table 5.8, are referenced to the maximum acceleration for each case (see Table 5.3 for maximum acceleration data)

and are calculated using Eq. 3-5. For example, N_{eq} for Lankershim N-S, CANDU mass 4, was calculated by summing over i peaks:

$$N_{eq} = \frac{1}{2} \sum_i \left(\frac{R_i}{1.87} \right)^2$$

The spread of N_{eq} values for the CANDU floor responses in Table 5.8 makes it difficult to categorize the results either by site soil conditions or by floor location. Considering the 24 floor motions as one group gives a spread of values from approximately 5.5 to 22 with a mean plus one standard deviation of $N_{eq} = 15$. This value should provide an estimate of the number of equivalent cycles of floor motion which could occur during an earthquake when the peak floor acceleration is considered as the reference level.

A second normalization procedure has been adopted to clearly distinguish between ground and in-structure values. In Table 5.9 appear summaries of the N_{eq} values all normalized to a reference level of 1g (normalized values are denoted by \bar{N}_{eq}). For these results the following statement can be made: When all ground motions and structural responses are compared on the basis of equal maximum amplitudes then it is clear that in-structure floor motions have a significantly greater cyclical response (higher \bar{N}_{eq}) than their respective ground motions. Values of \bar{N}_{eq} in Table 5.9 indicate that in-structure exposures (for say, a piece

TABLE 5.8 CUMULATIVE DAMAGE PARAMETER N_{eq} WITH $\beta = 2$

RECORD	GROUND MOTION	CANDU RESPONSES		SDOF RESPONSES	
		MASS 4	MASS 12	5.83 Hz	10.0 Hz
Lankershim N-S	4.5	6.6	10.9	12.3	8.6
Lankershim E-W	7.0	6.9	10.8	19.9	14.3
Caltech E-W	5.3	5.6	6.2	12.3	7.5
Caltech N-S	9.5	8.0	12.4	19.8	14.2
El Centro N-S	8.4	8.4	13.2	21.7	9.0
El Centro E-W	14.3	18.6	21.6	50.0	9.1
Hollywood E-W	10.9	6.2	11.7	18.5	9.5
Hollywood N-S	9.9	13.5	12.7	19.6	10.0
Eureka N79E	4.1	6.7	5.5	10.8	7.5
Eureka N11W	4.6	7.2	8.5	15.6	5.1
Orion N-S	7.2	10.5	13.6	20.9	8.7
Orion E-W	13.7	17.2	16.9	23.4	17.5

* referenced to the maximum acceleration in each response

TABLE 5.9 SITE DEPENDENT N_{eq} NORMALIZED TO 1g WITH $\beta = 2$

SITE	GROUND MOTION	CANDU		SDOF	
		MASS 4	MASS 12	5.83 Hz	10.0 Hz
Rock	6.6* (2.1)+	35.9 (24.7)	41.9 (17.4)	43.2 (39.2)	15.4 (6.1)
Stiff Soil	10.9 (2.5)	42.7 (10.4)	71.3 (22.5)	55.8 (13.1)	33.4 (21.5)
Deep Cohesionless	7.4 (4.4)	25.1 (14.0)	30.0 (19.7)	24.1 (14.0)	8.7 (6.5)
All Sites	8.3 (3.5)	33.7 (17.8)	47.7 (25.6)	41.0 (26.6)	19.2 (16.3)

* mean value

+ standard deviation

of floor mounted equipment) to repeated cyclic floor motion may be from 3 to 7 times "more severe" than exposures at ground level locations. By "more severe", it is meant that the combined action of the amplitudes and a number of repetitive cycles could cause failure of a floor mounted equipment component (due to a cumulative damage process) sooner than if the component was mounted directly on the ground.

The mean values of \bar{N}_{eq} estimated by the SDOF systems appear to be high for the 5.83 Hz model but low for the 10 Hz model. Some reasonable agreement can be found for a limited number of cases when it is observed that mean \bar{N}_{eq} values for the 5.83 Hz SDOF on rock and stiff soil sites lie somewhere between the mean and mean plus one standard deviation of the CANDU mass 4 responses on the same sites. This relationship is also true when all site records are combined for the 5.83 Hz and mass 4 systems. The exception appears to be on deep cohesionless sites where the SDOF mean \bar{N}_{eq} is almost equivalent to the CANDU mean value. The 10 Hz SDOF system does not model the mass 12 values with any kind of assurance and underestimates all mean values by a factor of 2 to 3.

The agreement of results between SDOF and CANDU systems that can be justified for some cases and not justified in others is based upon the frequency characteristics of the systems. The internal CANDU structure's (mass 4) time-domain characteristics have been modelled quite accurately by a SDOF system whereas the vault structure (mass 12) modelling was not so successful. The multi-frequency response and the large amplitude, low frequency waves do not show up on a SDOF response but these can significantly influence the \bar{N}_{eq} summation.

To conclude, the summary of results indicates a mean plus one standard deviation (84.1% probability of non-exceedence) of $N_{eq} = 15$ can be accepted as a conservative estimate of the cumulative damage parameter for in-structure floor motions for the type of seismic events considered in this study. This value is referenced to the peak floor acceleration and implies a weighting factor of $\beta = 2$.

5.9 Summary

The 5.83 Hz SDOF system has provided a simple and accurate model of the seismic response of the mass 4 level of the CANDU internal structure. The CANDU and model responses were similar in terms of time-history, response spectra, duration of strong motion, RMS acceleration ratio A_{rms}/A_m , and the cumulative damage parameter N_{eq} but the maximum floor acceleration was underestimated by the SDOF model.

The 10 Hz SDOF system did not provide a satisfactory overall model of the reactor vault seismic responses because reasonable similarities existed only in the time-history responses on hard ground and in durations of strong motion.

Numerical values recommended from the outcome of the data analysis were; $A_{rms}/A_m = 0.4$; duration of strong motion = 12 seconds; and $N_{eq} = 15$, normalized to peak floor acceleration and using $\beta = 2$.

CHAPTER 6

SEISMIC QUALIFICATION TESTING

6.1 Introduction

A natural extension to the characterization of seismic motions in CANDU structures, and a major objective of this research program is to examine and make recommendations on the current practice in seismic qualification testing. The basis for the recommendations are the theoretical analysis of some simple test methods in Chapter 4, summaries of real seismic data and the outcome of the parameter studies in Chapter 5, and a measure of practical experience in seismic equipment qualification.

Current standards (6,18) provide some basic guidelines on the selection of either single frequency or multi-frequency methods. Two factors must be considered in this selection, (1) the dynamic characteristics of the seismic floor motion, and (2) the dynamic response characteristics of the equipment test specimen. A very general relationship in Table 6.1, based on floor and equipment frequencies, indicates the conditions when single or multiple frequency test motion may be suitable. Its basic premise is that single frequency tests may be justifiable when the floor motion is predominantly single frequency and/or when the equipment can be shown (by exploratory dynamic testing, say) to have a predominant single frequency response. Under the first condition multi-frequency motions will not reach the equipment and in

the second case, dynamic properties of the equipment do not permit multi-modal responses.

TABLE 6.1 FREQUENCY CHARACTERISTICS

CHARACTERISTIC FLOOR MOTION	CHARACTERISTIC EQUIPMENT RESPONSE	TEST MOTION
SF	SF	SF
SF	MF	SF
MF	SF	SF
MF	MF	MF

SF: single frequency
MF: multiple frequency

The recommendations in this chapter are devoted to single frequency testing. This is not a direct attempt to favour the use of single frequency test methods over multi-frequency methods but rather, to show that single frequency motions have a useful place in seismic qualification because they have the capability to simulate many characteristics of real seismic floor motions. The recommendations comment on the general procedures used in single frequency testing, they examine and rank the usefulness of specific test motions, and finally they propose a set of procedures as a guide in examining equivalencies between different types of test motions.

6.2 Recommendations for Single Frequency Testing

The following characterization parameters deserve consideration in the description and evaluation of single frequency seismic qualification test methods, and are incorporated into the set of recommendations in this section;

- (i) response spectrum
- (ii) ratio, A_{rms}/A_m
- (iii) cumulative damage parameter, N_{eq}
- (iv) cumulative RMS function
- (v) maximum acceleration

6.2.1 Response Spectrum

It is recommended, for single frequency testing, that the frequency response curves for a limited-duration sine, a sine-beat, or a decaying sine (Figs. 4.1, 4.5 and 4.12, respectively) be used to describe the spectrum (referred to hereafter as the test response spectrum, TRS) produced by each single frequency test motion. The complete TRS will tend to be a jagged envelope of peaks and valleys with the peak levels and frequency bandwidth controlled by the number of applied cycles and the spectral damping. For the decaying sine, the decay parameter is also a controlling factor.

Floor responses can be considered to be single frequency when the FRS consists of a single, predominant narrowband peak and spectral amplifications away from the peak are quite low in comparison to the peak value.

Modal frequencies of an equipment response can be considered as well-separated and non-interacting under single frequency excitations if the equipment frequencies are separated by at least one octave since spectral amplification at ± 1 octave from an excitation frequency will be close to unity.

If equipment modes are well separated, and the FRS is single frequency according to the above definitions then single frequency testing should be required only in the regions of floor resonances and equipment resonances. In these regions the TRS should envelope the FRS. Tests at other frequencies would combine low amplifications with non-resonant conditions which would be ineffective in exciting equipment responses. Most regulatory authorities however, require that testing be performed over the complete frequency range to adequately cover any equipment resonances which may not have been detected during low-level exploratory testing.

When the FRS is single frequency and equipment modes are not well defined, or there are multiple equipment resonances then the FRS should be enveloped by the single frequency TRS at all frequencies. This will ensure that SDOF response at all frequencies will be at least as severe as responses described by the FRS.

6.2.2 Test Input Levels

In most testing applications the floor motion time-history is unknown; however, the maximum floor acceleration is known from the zero period acceleration (ZPA) on the FRS. This is interpreted as the

acceleration which a floor mounted rigid body (frequency greater than 33 Hz) would experience during earthquake shaking. Current specifications often require test input motions at each frequency to be at least at the ZPA level except where spectrum values fall below the ZPA, i.e., at low frequencies (ref. (18), section 6.6.1(2)). By this requirement it appears that some unwarranted conservatism may be introduced by applying a maximum seismic force (Seismic Force = specimen mass x ZPA) to the test specimen at each frequency. Furthermore, it is difficult to adequately justify why a single maximum condition at high frequency is imposed across the entire spectrum. Experience shows that forces caused by motion amplification in the low-to-middle frequency range (1-15 Hz) are likely to have a much greater damage potential than rigid body forces at high frequencies. Since energy is involved in the response amplification process it seems a more reasonable approach to consider RMS accelerations in determining test motion input levels.

The procedure which is recommended here is to provide a test motion at each frequency which has an RMS acceleration of 0.4 times the ZPA level of the floor response spectrum. Since the 0.4 parameter has been evaluated in section 5.7 at an 84.1% probability level of non-exceedance for real seismic events, there is a reasonable measure of assurance that the levels of input power will be conservative at each test frequency.

An inherent drawback in this type of procedure is that since the three single frequency test motions all have ratios A_{rms}/A_m greater than 0.4, it will not be possible to simulate both RMS accelerations and peak

accelerations simultaneously. To recognize that a full seismic force could be of consequence to the functional or operational capability of the equipment, the current recommended procedure of CSA N289.4 and IEEE 344-1975 in providing a single ZPA level test at a non-resonant equipment frequency greater than 33 Hz should be retained as part of the single frequency seismic qualification test.

6.2.3 Duration and Number of Tests

Seismic test standards often require "that peak equipment response be reproduced reliably and for a sufficient number of cycles" to provide a simulation of seismic fatigue conditions. A key point in this requirement is that the problem is treated in terms of peak equipment response and not in terms of the seismically induced floor motions. This approach seems quite natural for consideration of equipment fatigue, however difficulties can quickly be encountered in trying to apply this procedure to practical tests cases. For example, two specimens can be selected, a very flexible frame unit with a predominantly single-degree-of-freedom response, and a second specimen, an engine unit with multi-frequency responses owing to the many small attachments and components on the engine block. A question could be posed: If both are tested to the same seismic environment, on what basis does a measurement of peak equipment response indicate the actual fatigue performance of the equipment?

In the case of the flexible frame it may be possible to relate say, weld deterioration, to peak equipment response but for the engine,

fatiguing may occur simultaneously in several components but not at the same rate because each may respond at a different levels for different durations. This is clearly a much more complex situation to evaluate.

Another problem related to repeated cyclic testing is the loosening of nuts, bolts, screws and friction-type fasteners. The rate and times at which these loosen and possibly dislodge may be much more dependent upon the number of cycles of test motion than the amplitude of the equipment response. As most equipment components use many fastening devices in numerous capacities, including fastening the equipment to the floor, a failure of these could produce unexpected and severe results.

The above examples illustrate just a few of the problems that can occur in interpreting and implementing current guidelines on fatigue life simulation. The following recommendations recognize the difficulties associated with defining and simulating a reasonable seismic fatigue environment and propose that the parameter N_{eq} be used as a guide in developing appropriate test motions.

Table 5.8 in section 5.8 has shown that CANDU floor motions may be expected to have an N_{eq} value generally within a range of 7 to 20 when referenced to the peak record response. It is recommended that a mean plus one standard deviation of $N_{eq}^* = 15$ (asterisk denotes recommended value) taken over the ensemble of 24 CANDU floor motions, be considered as the equivalent number of cycles of peak floor motion that are likely to occur during a seismic event. The total number of frequencies and number of cycles of motion applied at each frequency can then be selected to give a cumulative damage parameter equivalent to the

recommended N_{eq}^* value.

For test situations in which the FRS is single frequency (as outlined in section 6.2.1) it is recommended that the total number of tests performed within the narrowband region of the FRS be sufficient to accumulate a total N_{eq} test value at least equivalent to the recommended value, N_{eq}^* . The test motion N_{eq} values must be normalized to the ZPA of the FRS before being compared to $N_{eq}^* = 15$.

When the FRS is broadband, test motions at all frequencies should be considered in accumulating a total N_{eq} test value at least equivalent to the recommended value.

The first recommendation recognizes that narrowband quasi-harmonic floor motions have the potential for imposing severe cyclical loads on equipment hence the concentration of repeated cyclic tests in the narrowband region. The recommendation for testing under broadband FRS conditions however, indicates that cyclic contributions may come from many frequencies and should be sufficient if the total cyclic effect is distributed across the entire spectrum without regard to concentrations at specific frequencies.

Owing to a wide variation in shapes and amplitude levels of the FRS specified for each seismic qualification programme, it is not possible to make firm recommendations on the spacing of adjacent test frequencies. The 1977 draft version of CSA N289.4 (section 4.2.1) and IEEE Standard 344-1975 (section 6.6.2.1) recommend that test frequencies be no further apart than one-half octave intervals and that additional tests be performed at all equipment resonances. Some additional

guidelines can be put forth here to expand on this suggested practice.

To completely envelope the FRS, single frequency peaks of the TRS must overshoot the FRS, as illustrated by Fig. 6.1 where test frequencies are spaced at $\frac{1}{\epsilon}$ -octave intervals to form a TRS which envelopes the flat portion of the spectrum at level S. To minimize the overshoot, the points of overlap between adjacent TRS peaks should just touch the flat spectrum. For a given test frequency f_t , these points of overlap occur at frequencies f_1 and f_2 , above and below f_t where

$$f_{1,2} = f_t (1 \pm (2^{\frac{1}{\epsilon}} - 1)) \quad (6-1)$$

and f_1 and f_2 are indicated in Fig. 6.1. When the spectrum is sloping the exact nature of the enveloping is more difficult to determine since adjacent test frequency spectra do not overlap symmetrically on both sides of a peak. Fig. 6.1 shows how a sloping FRS causes the bandwidth of individual spectra to be extended at frequencies on one side of f_t and shortened at frequencies on the other side. Since the FRS used for seismic qualification may have several sloped segments, a graphical or iterative computer procedure is usually the easiest way to determine the envelope.

The choice of a suitable frequency spacing will depend largely upon the shape of the FRS and the ratio between the maximum FRS value and its ZPA. Generally, the high amplitude, sharply peaked FRS encountered in many test situations may require test frequencies to be spaced closer apart than the $\frac{1}{2}$ -octave intervals previously described in order to obtain a complete enveloping by the TRS. It is recommended

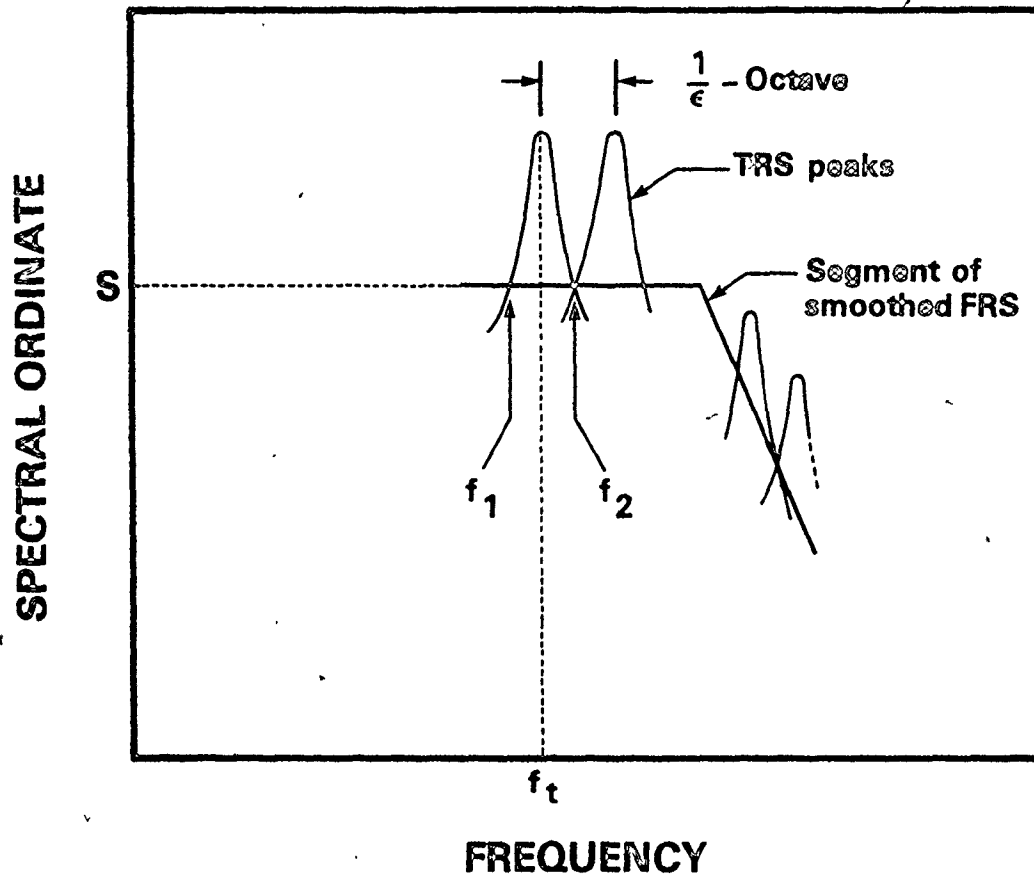


**FIG. 6.1 ENVELOPING THE FLOOR
RESPONSE SPECTRUM**

here that a 1/3-octave interval be considered as a more appropriate requirement for the maximum spacing of adjacent test frequencies. In test applications, this spacing should generally provide adequate capability to envelope most segments of a FRS, except perhaps in limited regions around a FRS peak where spacing at 1/6 or 1/9-octaves may be necessary.

A second recommendation associated with the 1/3-octave limitation is that it should be generally unnecessary to include any additional tests at equipment resonant frequencies. This is in contrast to the CSA and IEEE practices. It is felt that use of 1/3-octave intervals will provide a test input close enough to any equipment resonant frequency to sufficiently excite the equipment in its resonant mode. An additional convenience of this approach is that equipment resonant frequencies do not have to be precisely identified during exploratory tests since they will not be required as test frequencies. Thus, the spectrum enveloping phase of the seismic qualification test program can be developed without an exact evaluation of the equipment's resonant frequencies.

6.2.4 Type of Test Motion

The intent so far in sections 6.2.1 through 6.2.3 has been to outline areas and make recommendations which will allow single frequency testing to simulate some of the characteristics of real seismic motions, independent of the type of test motion used. It is now appropriate to individually examine the realism of each of the three test motions by considering the cumulative RMS function, the shape of the test waveform,

and again, the ratio A_{rms}/A_m . The considerations are as follows:

- (i) The characteristic shape of the CRF for real seismic floor motions has been illustrated in Fig. 5.6 and the smoothed shapes of test motion CRF's are shown in Fig. 6.2. It is readily apparent that distribution of power over time in a real seismic floor motion is simulated reasonably well only by a sine beat motion.
- (ii) The occurrence of the maximum acceleration in a real seismic floor motion is only a transitory phenomenon and this fact should be taken into account in the selection of a single frequency test motion. The brief excursion to maximum amplitude is more realistically simulated using a sine beat or decaying sinusoid rather than the sustained amplitudes of a limited duration sine.
- (iii) A previous recommendation (in section 6.2.2), based input test levels on a ratio $A_{rms}/A_m = 0.4$. While this ratio cannot be achieved by any of the three single frequency methods, the decaying sinusoid and the sine beat provide the closest simulations with ratios of $A_{rms}/A_m = 0.53$ and 0.6 , respectively. These motions maintain a realistic relationship between the levels of average power and the peak amplitudes.

From this study it is concluded that the sine beat motion is capable of providing the most realistic test simulation of seismic floor motion. The second preference would be a decaying sinusoidal motion and the third ranking test, the one which least simulates a real seismic

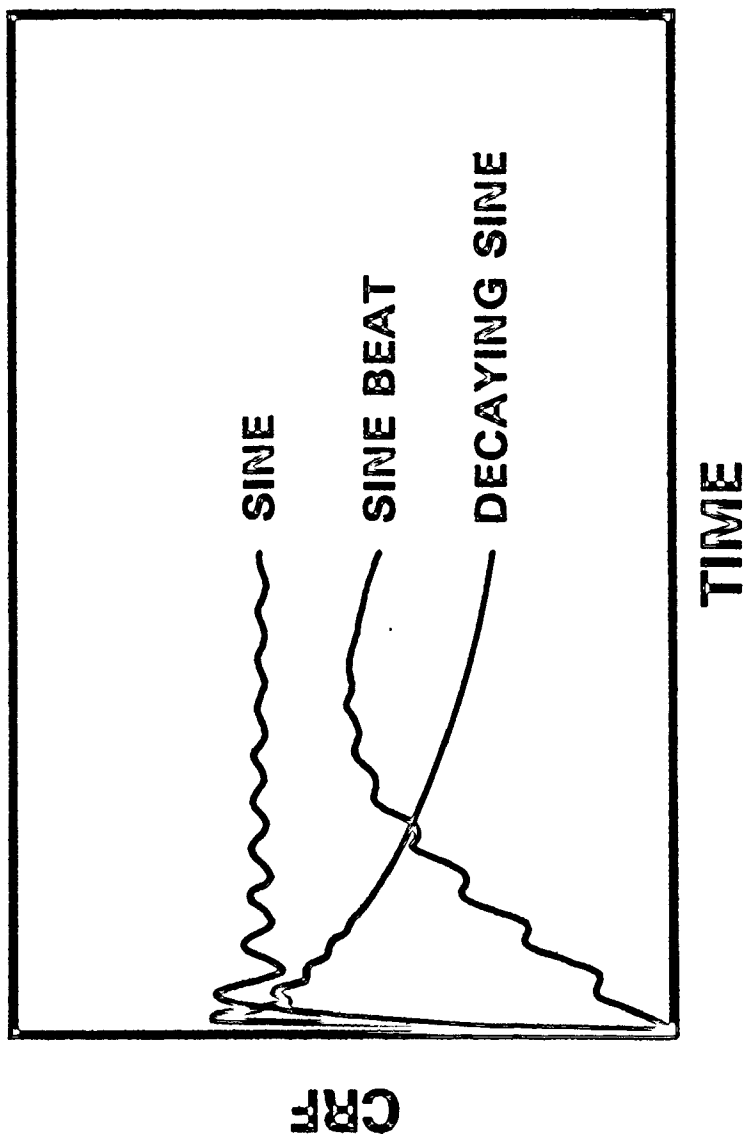


**FIG. 6.2 CUMULATIVE RMS FUNCTIONS OF
SINGLE FREQUENCY MOTIONS**

environment, is the limited-duration constant amplitude sine.

6.3 Equivalency in Single Frequency Tests

A great deal of freedom is generally permitted in the selection of a suitable test procedure. To quote from CSA N289.4, section 1.0, "The test procedures described herein are the common methods currently in use, and do not preclude the use of other equivalent methods, where justified". Again, from section 5.8, "Other tests that conservatively simulate the expected seismic environment ... may be used to seismically qualify components. Such tests must be carefully specified and the basis for equivalency adequately demonstrated before being permitted". A major obstacle is that very little indication is given on what "equivalency" is, or on how it can be established. The theoretical analysis from Chapter 4 has been used in this section to aid in formulating a set of procedures for establishing equivalency in seismic qualification amongst a sine, sine beat and decaying sine test. More precisely, two single frequency tests will be considered equivalent when there is agreement in the following parameters:

- (i) strong phase RMS acceleration
- (ii) duration of strong motion
- (iii) cumulative damage parameter, N_{eq}
- (iv) maximum spectral ordinate at resonance.

Theoretical considerations have shown that RMS acceleration is capable of providing a potentially more useful description of the acceleration levels in an earthquake motion than a single peak value,

especially when amplitudes may fluctuate in a rather random manner. The basis of equivalency is to require that equivalent test motions have equivalent RMS accelerations. Once this is established, equivalency in other parameters can be found.

It is convenient to define a reference sine motion having n cycles of motion at maximum acceleration \tilde{A} to use in developing equivalent sine beat and equivalent decaying sine motions. Therefore, the reference values are, $N_{eq} = n$; $A_{rms} = 0.707\tilde{A}$; duration of strong motion is n cycles, and the spectral ordinate at resonance is $\tilde{S} = \tilde{Q}\tilde{A}$ where \tilde{Q} is evaluated for n cycles and $\zeta\%$ damping.

Procedure for an Equivalent Sine Beat Motion

Step 1: Establish the maximum amplitude A_m of the sine beat motion so that the RMS acceleration is equal to the reference RMS acceleration; thus

$$A_m = \frac{.707}{.6} \tilde{A} = 1.18\tilde{A}$$

Step 2: Evaluate the quasi-resonant amplification Q , for the sine beat which will result in the same spectral ordinate \tilde{S} as in the reference sine motion. Since A_m for the sine beat is greater than \tilde{A} , a lower amplification is required to achieve the \tilde{S} level; thus

$$Q = \frac{\tilde{S}}{1.18}$$

Using this value of Q and 1% damping the required number of cycles per beat N , can be found from Fig. 4.6.

Step 3: The number of cycles of strong sine beat motion is

$$N_{sm} = \frac{2}{3} N$$

Step 4: The cumulative damage parameter is evaluated from Fig. 4.7 and normalized from $A_m = 1.18 \tilde{A}$ to $A_m = \tilde{A}$ for comparison with the original sine motion.

As a numerical example consider a 5-cycle reference sine motion with maximum amplitude 1.0g. For 1% damping $Q = 13.5$ (Eq. 4.14), therefore $S = 13.5g$. The equivalent sine beat will require a maximum amplitude of 1.18g (Step 1). To achieve a response spectrum ordinate of 13.5g requires $Q = 13.5/1.18 = 11.4$. From Fig. 4.7, 7 cycles per beat are required, to give $Q = 11.4$ (Step 2).

The duration of strong motion is $\frac{2}{3}(7) = 5$ cycles (Step 3). From Fig. 4.7, $N_{eq} = 3.5$ for $\beta = 2$, and normalizing to $A_m = 1.0g$ gives $\bar{N}_{eq} = 5$ (Step 4). This completes the derivation of an equivalent sine beat motion. Steps 1 and 2 involved the actual derivations, steps 3 and 4 were checks on the last two parameters. The real importance of this example has been to show that two different motions can be equivalenced with respect to several major parameters with only minor disagreement (18%) in the maximum acceleration.

A similar procedure can be applied to find a decaying sine

equivalent to the reference sine motion.

Procedure for an Equivalent Decaying Sine Motion

Step 1: Establish the maximum amplitude A_m of the decaying sine motion as

$$A_m = \frac{.707\tilde{A}}{.53} = 1.32\tilde{A}$$

Step 2: Evaluate the required quasi-resonant amplification

$$Q = \frac{\tilde{S}}{1.32}$$

with the appropriate spectral damping, and use Fig. 4.13 to find the required decay parameter μ .

Step 3: The number of cycles of strong motion is

$$N_{sm} = \frac{1}{10\mu}$$

where μ is a decimal percentage.

Step 4: Normalize the N_{eq} value for n cycles of sine motion at amplitude \tilde{A} into \bar{N}_{eq} at amplitude $1.32\tilde{A}$. Using this value of \bar{N}_{eq} , and Fig. 4.14 (with μ and β as above) find the number of cycles of decaying sine motion required to be equivalent to the reference number of cycles of sine motion. If \bar{N}_{eq} cannot be achieved by a single decaying sinusoid, the test may be repeated until the sum of the individual \bar{N}_{eq}

values equals the required \bar{N}_{eq} . When repeated tests are used the number of cycles N in each test should be at least equal to N_{sm} in Step 3 so that the strong motion durations of sine and decaying sine are equivalent in each run.

Continuing with the previous example, an equivalent decaying sine motion can be developed. To match the RMS acceleration of the sine motion, the decaying sine must have $A_m = \frac{.707}{.53} \tilde{A} = 1.32\tilde{A}$ (Step 1). To achieve the 13.5g response spectrum ordinate at 1% damping $Q = 13.5/1.32 = 10.2$. The decay parameter for this Q value and 1% structural damping is $\mu = 3\%$ (Step 2). Consequently there will be 3.3 cycles of strong motion (Step 3). Normalizing the 5 cycles of 1g peak sine motion to a peak of 1.32g gives $\bar{N}_{eq} = 5/(1.32)^2 = 2.87$ ($\beta=2$). Interpolating from Fig. 4.14, for $\mu = 3\%$ (i.e., $\mu\beta = 6$), the requirement is 11 cycles of decaying sine motion (Step 4).

The two example motions derived above are summarized in Table 6.2.

As current testing specifications do not provide direct guidance on test equivalences, the above procedures should enable some basic comparisons and evaluations to be made of simple test motions.

TABLE 6.2 EXAMPLES OF EQUIVALENT MOTIONS

CHARACTERISTIC	SINE REFERENCE	SINE BEAT EQUIVALENT	DECAYING SINE EQUIVALENT
No. of cycles	5	7	11
Maximum acceleration	1.0g	1.18g	1.32g
Strong phase RMS acceleration	.707g	.707g ^q	.707g
Response Spectrum ordinate (1% damping)	13.5g	13.5g	13.5g
Duration of Strong, Motion (cycles)	5	5	3.3
N _{eq} (norm. to 1g)	5	5	5

CHAPTER 7

SUMMARY AND CONCLUSIONS

The main purpose of this research program has been to develop parameter characterizations of seismic floor motions and to subsequently apply these parameters to examine single frequency seismic qualification test procedures.

A review of earthquake engineering literature was made to select a set of techniques which could be applied to characterize seismic time-history records. The techniques included measurement of peak accelerations, calculations of response spectra, concepts of cumulative damage processes, root-mean-square acceleration, cumulative RMS functions and durations of strong motion. A theoretical study examined each technique in detail and provided valuable information on the characteristics of some simple forms of harmonic motions. A significant feature in considering harmonic motion was that complete characterizations could be developed by analytical solutions rather than by numerical procedures.

In order that valid and realistic recommendations and conclusions could be drawn, the study relied entirely on real seismic data and incorporated an actual structural dynamic model used in the design of CANDU nuclear power plants. Twelve earthquake ground motion records were selected from western USA events as being broadly representative of the ground shaking which could occur on a wide range of soil conditions

at 20-40 km from the epicentre of a 6.5 magnitude earthquake. These records were input to the CANDU mathematical model to produce an ensemble of floor responses at two floor levels within the structure. Additionally, seismic responses of two single-degree-of-freedom systems were calculated to provide information for some special studies on simplified modelling of parts of the CANDU structure.

An ensemble of seismic motion parameters were obtained by characterizing the ground and floor motion time-histories by each of the techniques obtained in the literature survey. After some graphical comparisons and reviews of this data it was possible to obtain both qualitative and quantitative descriptions of seismic floor motions within a CANDU structure. Qualitative characteristics were appropriate for describing response spectra and cumulative RMS functions since, in the context of this investigation, they were most useful as graphical indications of the frequency and power content, respectively, of the seismic motions. For the other parameters investigated; RMS acceleration (in conjunction with maximum acceleration), cumulative damage processes, and duration of strong motion, it was possible to recommend specific numerical values based upon the statistical data summaries.

In the final stage of the research program, characteristics of both real seismic motions and the harmonic motions were considered together in examining and making recommendations on current procedures for single frequency seismic qualification testing.

Detailed results of the theoretical analyses and seismic motion

characterizations have been presented in Chapters 4 and 5 respectively, and recommendations for testing have been discussed in Chapter 6. The main conclusions pertaining to the overall objectives stated at the outset of this research program are as follows:

- (1) Single parameter descriptions provide only a limited amount of information about seismic motions and are, by themselves, largely inadequate for the complex considerations in seismic equipment qualification. Multi-parameter descriptions have the inherent capability to describe a seismic motion in much greater detail, therefore, by a careful selection of parameters information can be retained which is of direct applicability to seismic qualification testing. Each of the parameters developed in previous stages of this research have demonstrated a validity and usefulness in being included as part of a multi-parameter characterization of seismic floor motions.
- (2) Very little indication is provided in the current seismic qualification test guides on the appropriate uses of different forms of single frequency test motions. Based upon the results of some strong theoretical analyses and comparisons with characteristics of real seismic motions, it is concluded that the sine beat motion can provide a more realistic simulation of actual seismic floor motions than either a decaying sinusoid or a limited-duration constant amplitude sine motion.

(3) Multi-parameter characterization provides a means to develop equivalencies between different types of test motions. By making a basic assumption that equivalent test motions have equivalent RMS accelerations over their respective durations of strong motion, it has been demonstrated that it is generally possible to develop other single frequency test motions with characteristics similar to the original motion.

(4) Despite the fact that real CANDU reactor buildings are complex multi-degree-of-freedom systems, certain parts of their structural system can be simplified into equivalent SDOF systems. This is possible when the displacements of a structural system are primarily restricted to a single shape. The capability of performing parametric studies of seismic floor motions using SDOF systems affords considerable savings and simplicity over having to perform a full time-history analysis each time on a multi-degree-of-freedom CANDU model.

Seismic qualification is a relatively new area of earthquake engineering and the nuclear power industry is placing an increasing emphasis on the need to achieve valid seismic qualification tests both for safety and economic reasons. To the present time, the common practice has been to address problems of seismic qualification using standard and familiar techniques of structural and mechanical engineering, such as the response spectrum. However, the complex

✓

considerations involved with the response of structural and mechanical systems in an earthquake environment demand that more innovative and realistic approaches be taken in the future in order that acceptable solutions may be found. The research program undertaken here is one step in that direction.

REFERENCES

- [1] Applied Technology Council, Tentative Provisions for the Development of Seismic Regulations for Buildings, ATC 3-06 publication, San Francisco, June 1978.
- [2] Arias, A., "A Measure of Earthquake Intensity", Seismic Design of Nuclear Power Plants, R. Hansen (Ed.), MIT Press, Cambridge, Mass., 1970.
- [3] Bathe, K.J., Wilson, E.L. and Peterson, F.E., "SAP IV - A Structural Analysis Program for Static and Dynamic Response of Linear Systems", EERC Report No. 73-11, University of California, Berkeley, June 1973.
- [4] Biggs, J.M. and Roesset, J.M., "Seismic Analysis of Equipment Mounted on a Massive Structure", Seismic Design of Nuclear Power Plants, R.J. Hansen (Ed.), MIT Press, Cambridge, Mass.
- [5] Blume, J.A., "On Instrumental Versus Effective Acceleration and Design Coefficients", Proc. 2nd U.S. National Conf. on Earthquake Engineering, Stanford University, California, Aug. 1979, pp. 868-882.
- [6] Canadian Standards Association, Standard N289.4, Testing Procedures for Seismic Qualification of CANDU Nuclear Power Plants, Draft, Sept. 1977.
- [7] Clough, R.W. and Penzien, J., Dynamics of Structures, McGraw-Hill, Inc., 1975.
- [8] Drenick, R.F., Wang, P.C., Yun, C.B. and Philippacopoulos, A.J., "Critical Seismic Response of Nuclear Reactors", 5th SMIRT Conf., paper K8/4, Berlin, W. Germany, 1979.
- [9] Duff, C.G., "Simplified Method for Development of Earthquake Ground and Floor Response Spectra for Nuclear Power Plant Design", Proc. 2nd Canadian Conf. on Earthquake Engineering, Hamilton, Canada, June 1975.
- [10] Duff, G.C. and Heidebrecht, A.C., "Earthquake Fatigue Effects on CANDU Nuclear Power Plant Equipment", Proc. 3rd Canadian Conf. on Earthquake Engineering, vol. 1, Montreal, Canada, June 1979, pp. 325-335.

- [11] Fackler, W.C., "Equivalence Techniques for Vibration Testing", The Shock and Vibration Information Center, U.S. Dept. of Defense, Monograph 9, 1972.
- [12] Fischer, E.G. and Wolff, F.H., "Comparison of Fatigue Effects in Simulated and Actual Earthquakes", Experimental Mechanics, Dec. 1973, pp. 531-538.
- [13] Hanks, T.C. and Johnson, D.A., "Geophysical Assessment of Peak Accelerations", Bull. Seism. Soc. Am., vol. 66, no. 3, June 1976, pp. 959-968.
- [14] Heidebrecht, A.C. and Tso, W.K., "Evaluation of Seismic Equipment Qualification", Final Report to Atomic Energy Control Board of Canada, McMaster University, Hamilton, Canada, May 1979.
- [15] Housner, G.W., "Measures of Severity of Earthquake Ground Shaking", Proc. First U.S. National Conf. on Earthquake Engineering, Ann Arbor, Michigan, 1975, pp. 25-33.
- [16] Hudson, D.E., Trifunac, M.D. and Brady, A.G., "Analysis of Strong Motion Earthquake Accelerograms, Index Volume", EERL Report 76-02, California Institute of Technology, Aug. 1976.
- [17] Hudson, D.E., Trifunac, M.D. and Brady, A.G., "Analysis of Strong Motion Earthquake Accelerograms", vol. II, Parts A-L, EERL Report 71-50, California Institute of Technology, Sept. 1971.
- [18] Institute of Electrical and Electronics Engineers, Inc., IEEE Standard 344-1975, IEEE Recommended Practices for Seismic Qualification of Class 1E Equipment for Nuclear Power Generating Stations.
- [19] Ishac, M.F., Torsional Coupling in Seismic Response of Reactor Systems, Ph.D. Thesis, McMaster University, Hamilton, Canada, June 1979.
- [20] Liu, S.C., Fagel, L.W. and Dougherty, M.R., "Earthquake-Induced In-Building Motion Criteria", J. of the Structural Division, ASCE, vol. 103, no. ST1, Jan. 1977, pp. 133-152.
- [21] McCann, M.W. and Shah, H.C., "Determining Strong-Motion Duration of Earthquakes", Bull. Seism. Soc. Am., vol. 69, no. 4, Aug. 1979, pp. 1253-1265.
- [22] Miner, M.A., "Cumulative Damage in Fatigue", J. Appl. Mech., series A, vol. 12, no. 1, 1945, pp. 159-164.

- [23] Newmark, N.M., Blume, J.A. and Kapur, K.K., "Seismic Design Spectra for Nuclear Power Plants", J. of the Power Division, ASCE, vol. 99, no. P02, Nov. 1973, pp. 287-303.
- [24] Nigam, N.C. and Jennings, P.C., "Digital Calculation of Response Spectra From Strong-Motion Earthquake Records", NISEE Computer Applications, California Institute of Technology, June 1968.
- [25] Rice, S.O., "Mathematical Analysis of Random Noise", Selected Papers on Noise and Stochastic Processes, Nelson Wax (Ed.), Dover Publications, Inc., New York, 1954, p. 138.
- [26] Roberts, C.W. and Shipway, G.D., "Seismic Qualification - Philosophy and Methods", J. of the Power Division, ASCE, vol. 102, no. P02, Jan. 1976, pp. 113-120.
- [27] Seed, H.B., Murarka, R., Lysmer, J. and Idriss, I.M., "Relationships of Maximum Acceleration, Maximum Velocity, Distance from Source, and Local Site Conditions for Moderately Strong Earthquakes", Bull. Seism. Soc. Am., vol. 66, no. 4, Aug. 1976, pp. 1323-1342.
- [28] Seed, H.B., Ugas, C. and Lysmer, J., "Site-Dependent Spectra for Earthquake-Resistant Design", Bull. Seism. Soc. Am., vol. 66, no. 1, Feb. 1976, pp. 221-243.
- [29] Stoykovich, M., "Seismic Design and Analysis of Nuclear Plant Components", Structural Design of Nuclear Plant Facilities, ASCE, vol. 1, New York, 1973, pp. 1-28.
- [30] Trifunac, M.D. and Brady, A.G., "On the Correlation of Seismic Intensity Scales with the Peaks of Recorded Strong Ground Motion", Bull. Seism. Soc. Am., vol. 65, no. 1, Feb. 1975, pp. 139-162.
- [31] Wilson, J.C., "Earthquake Floor Response and Fatigue of Equipment in Multi-Storey Structures", Proc. 1st International Conf. on Environmental Forces on Engineering Structures, London, England, July 1979, pp. 181-196.
- [32] Wilson, J.C., Tso, W.K. and Heidebrecht, A.C., "Seismic Qualification by Shake Table Testing", Proc. 3rd Canadian Conf. on Earthquake Engineering, vol. 1, Montreal, Canada, June 1979, pp. 493-510.